

AD-A113 428

DEFENCE RESEARCH ESTABLISHMENT OTTAWA (ONTARIO)
FREQUENCY COMPRESSION OF WIDEBAND SIGNALS USING A DISTRIBUTED S-ETC(U)
NOV 81 L J CONWAY

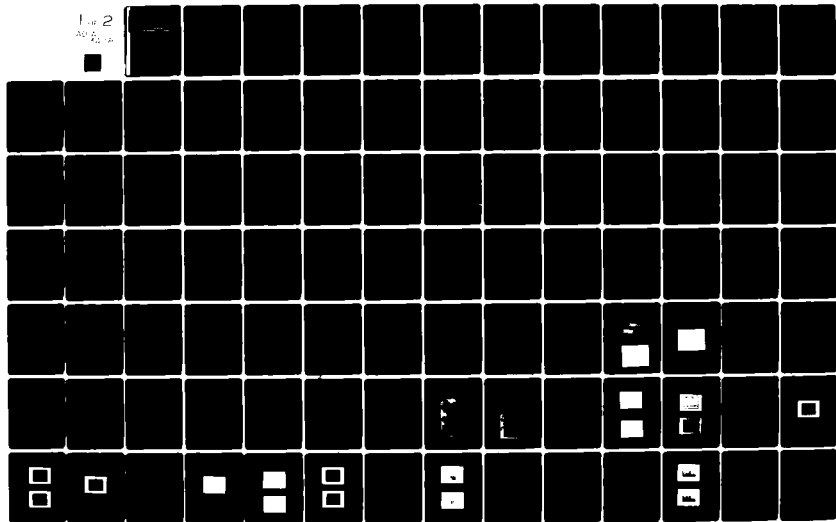
F/8 9/5

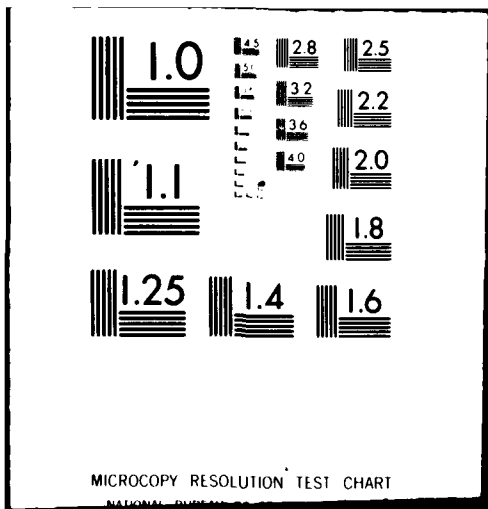
UNCLASSIFIED

NL

1 of 2

AD-A113 428





MICROCOPY RESOLUTION TEST CHART

NATIONAL BUREAU OF STANDARDS

3

AD A113428

RESEARCH AND DEVELOPMENT BRANCH
DEPARTMENT OF NATIONAL DEFENCE
CANADA

DEFENCE RESEARCH ESTABLISHMENT OTTAWA

DREO REPORT NO. 852
DREO R 852

FREQUENCY COMPRESSION OF WIDEBAND SIGNALS USING A DISTRIBUTED SAMPLING TECHNIQUE

by
L.J. Conway



DTIC
ELECTE
APR 14 1982
S D
E

DTIC FILE COPY

PROJECT NO.
31020

This document has been approved
for public release and sale; its
distribution is unlimited.

NOVEMBER 1981
OTTAWA

82 04 14 065

ABSTRACT

Present methods of frequency conversion include heterodyne conversion and harmonic or subharmonic generation. These methods have inherent limitations which restrict their usefulness in a number of applications. A novel frequency compression/expansion system which makes use of sampling techniques is not confined to the same limitations as these conventional frequency conversion systems. The unique integration of delay lines, sampling gates and amplifiers permits frequency compression or expansion as well as amplification of wideband pulsed r.f. signals at frequencies far above the cut-off frequencies of the amplifying devices used.

The theory and design of the frequency compression/expansion system is presented in this report. The theoretical results are compared with those obtained from an experimental system and good agreement is demonstrated.

RÉSUMÉ

Parmi les méthodes actuelles de conversion de fréquence, on compte la conversion par hétérodynage et par production d'harmoniques ou de sous-harmoniques. Les limitations inhérentes à ces méthodes restreignent toutefois leur utilité dans le cas de certaines applications. Un nouveau système de compression/expansion de la fréquence employant des techniques d'échantillonnage ne comporte pas les mêmes limitations que les systèmes classiques de conversion de fréquence. Une technique unique, soit l'utilisation simultanée de lignes à retard, de portes d'échantillonnage et d'amplificateurs, permet la compression et l'expansion de la fréquence, de même que l'amplification de signaux RF pulsés, à large bande, à des fréquences bien supérieures à la fréquence de coupure des dispositifs amplificateurs utilisés.

Le mémoire expose les principes de réalisation du système de compression/expansion de la fréquence. La comparaison entre les prédictions théoriques et les résultats obtenus au moyen d'un système expérimental révèle qu'il existe une corrélation étroite entre ces valeurs.

TABLE OF CONTENTS

	<u>Page</u>
<u>ABSTRACT/RÉSUMÉ</u>	iii
<u>TABLE OF CONTENTS</u>	v
<u>LIST OF ILLUSTRATIONS</u>	ix
<u>LIST OF TABLES</u>	xiii
<u>LIST OF SYMBOLS</u>	xiv
1.0 <u>INTRODUCTION</u>	1
1.1 <u>Background and Objective</u>	1
1.2 <u>Report Organization</u>	2
2.0 <u>THEORETICAL DEVELOPMENT</u>	2
2.1 <u>Introduction</u>	2
2.2 <u>Sampling an Arbitrary Signal $f(t)$</u>	2
2.3 <u>Recovering $f(t)$ from its Samples</u>	7
2.4 <u>Amplification of Samples</u>	9
2.5 <u>Amplification of Wideband Signals</u>	9
2.6 <u>Frequency Scaling of Wideband Signals</u>	9
3.0 <u>PRACTICAL CONSIDERATIONS</u>	14
3.1 <u>Introduction</u>	14
3.2 <u>Practical Filter Considerations</u>	14
3.3 <u>Practical Sampler Considerations</u>	19
3.3.1 <u>Sampler's Finite Pulse Width</u>	19
3.3.2 <u>Losses Due to the Sampler's Non-zero Impedance</u>	23

TABLE OF CONTENTS (CONT'D)

	<u>Page</u>
3.4 <u>Final Output Filter</u>	29
4.0 <u>DESIGN OF AN EXPERIMENTAL FREQUENCY COMPRESSION SYSTEM</u>	30
4.1 <u>Introduction</u>	30
4.2 <u>Experimental Circuit</u>	30
4.3 <u>Delay Line Considerations</u>	33
4.3.1 <u>Introduction</u>	33
4.3.2 <u>Determination of W for a 50 Line</u>	33
4.3.3 <u>Dispersion and Moding Effects</u>	33
4.3.4 <u>Determination of Sampling Interval</u> <u>(T_s) and Other Delay Line Parameters</u>	35
4.3.5 <u>Transmission Line Losses</u>	41
4.4 <u>Sampling Gate</u>	42
4.4.1 <u>Introduction</u>	42
4.4.2 <u>Six-Diode Sampling Gate</u>	42
4.4.3 <u>Drawbacks of the Six-diode Sampling Gate</u>	46
4.5 <u>Amplifier-Filter Selection</u>	47
4.6 <u>Pulse Generation Devices</u>	47
5.0 <u>EXPERIMENTAL RESULTS</u>	51
5.1 <u>Introduction</u>	51
5.2 <u>Subsystem Parameter Measurement</u>	51
5.2.1 <u>Introduction</u>	51
5.2.2 <u>Meander Delay Line Insertion Loss</u>	51
5.2.3 <u>Sampler Characteristics</u>	51

TABLE OF CONTENTS (CONT'D)

	<u>PAGE</u>
5.3 <u>System Measurements</u>	57
5.3.1 <u>Basic Experimental Set-up</u>	57
5.3.2 <u>Sampling Pulse</u>	57
5.3.3 <u>Time Domain and Frequency Domain Responses</u>	57
5.3.4 <u>System Performance Measurements</u>	65
5.3.5 <u>Frequency Compression Factor a</u>	69
5.3.6 <u>Multiple Signal Reconstruction</u>	73
5.3.7 <u>Summary of Results</u>	73
6.0 <u>CONCLUSIONS</u>	80
6.1 <u>Summary and Conclusions</u>	80
6.2 <u>Future Work Areas</u>	80
7.0 <u>REFERENCES</u>	81
APPENDIX A - <u>INPUT AND OUTPUT MEANDER LINE-SAMPLER-AMPLIFIER</u> <u>MODELLING</u>	83
APPENDIX B - <u>MICROSTRIP DESIGN EQUATIONS, PROGRAM</u> <u>LISTING AND DESIGN TABLE</u>	91
APPENDIX C - <u>MICROSTRIP CONDUCTOR LOSS EQUATIONS</u>	95
APPENDIX D - <u>MOTOROLA MC1590G AMPLIFIER SPECIFICATIONS</u>	97
APPENDIX E - <u>SAMPLING GATE VOLTAGE BIAS DERIVATION</u>	103
APPENDIX F - <u>AUTOMATIC INSERTION LOSS AND RETURN</u> <u>LOSS MEASUREMENT PROGRAM DESCRIPTION</u>	109

LIST OF ILLUSTRATIONS

	<u>PAGE</u>
FIGURE 2.1 - SIGNAL $f_s(t)$ PRODUCED BY A SAMPLER	3
FIGURE 2.2 - A SEQUENCE OF UNIFORM EQUIDISTANT IMPULSE FUNCTIONS OF PERIOD T	5
FIGURE 2.3 - FREQUENCY SPECTRUM OF THE SAMPLED FUNCTION $f_s(t)$	6
FIGURE 2.4 - RECONSTRUCTION OF THE SIGNAL $f(t)$ FROM ITS SAMPLES	8
FIGURE 2.5 - AMPLIFICATION OF A SET OF SAMPLES $\phi_s(t)$	10
FIGURE 2.6 - DISTRIBUTED SAMPLING/AMPLIFICATION SYSTEM	11
FIGURE 2.7 - FREQUENCY COMPRESSION SYSTEM	13
FIGURE 2.8 - A MULTIPLE MEMORY FREQUENCY COMPRESSION SYSTEM	15
FIGURE 3.1 - RECONSTRUCTION OF THE SIGNAL $f(t)$ FROM ITS SAMPLES	16
FIGURE 3.2 - A PRACTICAL FILTER WITH CUTOFF FREQUENCY ω_n	18
FIGURE 3.3 - IMPULSE RESPONSE OF A PRACTICAL SAMPLER	20
FIGURE 3.4 - PRACTICAL SAMPLER REPRESENTATION	21
FIGURE 3.5 - FILTER COMPENSATION RESULTING FROM THE FINITE SAMPLER PULSE WIDTH	22
FIGURE 3.6 - INPUT MEANDER DELAY LINE-SAMPLER-AMPLIFIER MODEL	24
FIGURE 3.7 - SIMPLIFIED MODEL OF THE INPUT MEANDER DELAY LINE CONFIGURATION DURING THE SAMPLER'S "ON" STATE	26
FIGURE 3.8 - MODEL OF THE OUTPUT AMPLIFIER-SAMPLER- MEANDER LINE CONFIGURATION	27
FIGURE 3.9 - MODEL OF THE OUTPUT NETWORK FOR THE SAMPLER'S (a) "OFF" CONDITION AND (b) "ON" CONDITION	28
FIGURE 3.10 - SPECTRUM OF THE RECONSTRUCTED SIGNAL AS PRODUCED BY A SAMPLING RATE HIGHER THAN THE NYQUIST RATE	31
FIGURE 4.1 - PROTOTYPE FREQUENCY COMPRESSION SYSTEM	32

LIST OF ILLUSTRATIONS (CONT'D)

	<u>PAGE</u>
FIGURE 4.2 - MICROSTRIP TRANSMISSION LINE	34
FIGURER 4.3 - MEANDER DELAY LINE OF DELAY TIME T' SECONDS	36
FIGURE 4.4 - EFFECTS OF THE PROPAGATION DELAY IN THE PULSE LINE ON THE MENADER LINE'S DELAY TIME BETWEEN ADJACENT CHANNELS	38
FIGURE 4.5 - PHYSICAL LAYOUT OF THE INPUT SIDE OF THE PROTOTYPE CIRCUIT	39
FIGURE 4.6 - CALCULATED INSERTION LOSS FOR THE INPUT MEANDER DELAY LINE	43
FIGURE 4.7 - CALCULATED INSERTION LOSS FOR THE OUTPUT MEANDER DELAY LINE	44
FIGURE 4.8 - DIODE SAMPLING GATE	45
FIGURE 4.9 - VIDEO AMPLIFIER CIRCUIT	48
FIGURE 4.10 - PICOSECOND PULSE DEVICES	49
FIGURE 4.11 - TYPICAL PULSE GENERATOR OUTPUT WAVEFORMS	49
FIGURE 4.12 - COMPLEMENTARY OUTPUTS PRODUCED BY A POWER SPLITTER	50
FIGURE 5.1 - INSERTION LOSS AND RETURN LOSS MEASUREMENTS OF THE INPUT MEANDER DELAY LINE FOR THE UNASSEMBLED BOARD	52
FIGURE 5.2 - INSERTION LOSS AND RETURN LOSS MEASUREMENTS OF THE OUTPUT MEANDER DELAY LINE FOR THE UNASSEMBLED BOARD	53
FIGURE 5.3 - INSERTION LOSS MEASUREMENT OF THE INPUT MEANDER DELAY LINE FOR THE ASSEMBLED BOARD	54
FIGURE 5.4 - INSERTION LOSS MEASUREMENT OF THE OUTPUT MEANDER DELAY LINE FOR THE ASSEMBLED BOARD	55
FIGURE 5.5 - INSERTION LOSS MEASUREMENT OF THE SAMPLER UNIT UNDER A FORWARD BIAS (ON) CONDITION	56
FIGURE 5.6 - INSERTION LOSS MEASUREMENT OF THE SAMPLER UNIT UNDER A REVERSE BIAS (OFF) CONDITION	58
FIGURE 5.7 - EXPERIMENTAL SET-UP FOR MEASURING THE SAMPLER'S ON RESISTANCE IN THE PULSED MODE	59

LIST OF ILLUSTRATIONS (CONT'D)

	<u>PAGE</u>
FIGURE 5.8 - EXPERIMENTAL FREQUENCY COMPRESSION CIRCUIT	60
FIGURE 5.9 - COMPONENT SIDE OF THE EXPERIMENTAL FREQUENCY COMPRESSION CIRCUIT	61
FIGURE 5.10 - BASIC EXPERIMENTAL SET-UP	62
FIGURE 5.11 - INPUT SAMPLING PULSE	63
FIGURE 5.12 - OUTPUT SAMPLING PULSE	63
FIGURE 5.13 - (a) INPUT AND OUTPUT TIME DOMAIN WAVEFORMS	64
(b) OUTPUT TIME DOMAIN AND FREQUENCY DOMAIN WAVEFORMS ..	64
FIGURE 5.14 - FREQUENCY SPECTRUM OF THE INPUT CW SIGNAL ($f_{in} = 357\text{MHz}$) AND OUTPUT PULSE SIGNAL (CENTERED ABOUT 193 MHz)	66
FIGURE 5.15 - (a) OUTPUT COMPRESSED SIGNAL	67
(b) OUTPUT NOISE FREQUENCY SPECTRUM	67
FIGURE 5.16 - UNFILTERED OUTPUT FREQUENCY SPECTRUM	68
FIGURE 5.17 - OUTPUT FREQUENCY RESPONSE FOR AN OUTPUT SAMPLING PULSE WIDTH OF 950 psec	70
FIGURE 5.18 - OUTPUT FREQUENCY RESPONSE FOR AN OUTPUT SAMPLING PULSE WIDTH OF (a) 1.25 nsec AND (b) 1.5 nsec	71
FIGURE 5.19 - (a) INPUT CW SIGNAL WITH 1 KHz 73% AM MODULATION	72
(b) OUTPUT CONVERTED PULSE SIGNAL	72
FIGURE 5.20 - (a) USUAL AND DESIRED $(\sin x)/x$ SPECTRUM	74
(b) ATYPICAL $(\sin x)/x$ SPECTRUM	74
FIGURE 5.21 - (a) CONTINUOUS OUTPUT PHASE FOR A GIVEN INPUT FREQUENCY	76
(b) DISCONTINUOUS OUTPUT PHASE FOR A GIVEN INPUT FREQUENCY	76
FIGURE 5.22 - (a) UNFILTERED OUTPUT FOR A SINGLE INPUT SIGNAL	78
(b) UNFILTERED OUTPUT FOR TWO INPUT SIGNAL	78

LIST OF ILLUSTRATIONS (CONT'D)

	<u>PAGE</u>
FIGURE A-1 - MODEL OF THE INPUT MEANDER LINE-SWITCH-AMPLIFIER NETWORK DURING THE SAMPLER'S BIAS ON CONDITION	85
FIGURE A-2 - MODEL OF THE OUTPUT AMPLIFIER-SWITCH-MEANDER LINE CONFIGURATION FOR THE (a) OFF CONDITION AND (b) ON CONDITION	88
FIGURE E-1 - (a) SIX-DIODE SAMPLING GATE	105
(b) CURRENT CONDUCTION DUE TO THE BIAS VOLTAGE	105
(c) CURRENT CONDUCTION DUE TO THE INPUT SIGNAL	105
FIGURE F-1 - AUTOMATIC INSERTION LOSS AND RETURN LOSS MEASUREMENT SET-UP	113

LIST OF TABLES

	<u>PAGE</u>
TABLE 5.1 - EXPERIMENTAL INPUT AND OUTPUT FREQUENCIES FOR THE USUAL AND DESIRED OUTPUT $(\sin x)/x$ SPECTRUM	75
TABLE 5.2 - THEORETICAL INPUT AND OUTPUT FREQUENCIES FOR A CONTINUOUS PHASE RELATIONSHIP FOR A COMPRESSION FACTOR OF .5191 AND A PRF OF 10 MHz	77
TABLE 5.3 - SUMMARY OF RESULTS	79

LIST OF SYMBOLS

a	compression factor
B	bandwidth
c	speed of light (3×10^{10} cm/sec)
C	input intrinsic capacitance of the amplifier
C_d	distributed load capacitance along the meander line
C_o	output intrinsic capacitance of the amplifier
C_T	intrinsic line capacitance
D.U.T.	device under test
f	frequency
f_o	frequency below which dispersion effects may be neglected
f_T	frequency below which significant coupling occurs between the quasi-TEM mode and the lowest order surface wave mode in microstrip
$f_{i_{max}}$	maximum input frequency
$f_{o_{max}}$	maximum output frequency
f_{in}	input frequency
f_{out}	output frequency
$f(t), g(t)$	continuous time functions
$f_s(t), p_s(t)$	sampled time functions
$F(\omega), G(\omega)..$	frequency spectrum of continuous time functions
$F_s(\omega), P_s(\omega)$	frequency spectrum of sampled time functions
$G_{2\omega_n}(\omega), K_{2\omega_n}(\omega)$	frequency spectrum of continuous time functions having radian cutoff frequency ω_n
G	overall system gain for $a = 1$

LIST OF SYMBOLS (CONT'D)

G_o	final output filter gain
G_n	amplifier-filter network gain
G_c	overall system gain for $a < 1$
h	microstrip dielectric substrate thickness
$k_1(t)$	ideal filter impulse response
$k_2(t)$	portion of a practical filter impulse response
$k_{2\omega_n}(t)$	practical filter impulse response
$K_{2\omega_n/N}(\omega)$	frequency spectrum of a continuous time function having radian cutoff frequency ω_n/N
M	integer constant
N	number of parallel channels
R_{si}	resistance of the input sampling gate under a forward bias (ON) condition
R_{in}	input resistance of the amplifier
R_m	real part of Z_m
R_o	series source resistance in the amplifier's output model network
R_l	output load resistance
R_{so}	resistance of the output sampling gate under a forward bias (ON) condition
R_l'	parallel combination of the output load resistance (R_l) and $R_m/2$
R_s	diode's forward bias resistance
R_b	sampling gate's bias resistance

LIST OF SYMBOLS (CONT'D)

R_L	effective load resistance which the sampling gate sees
S_{r_1}, S_{r_2}	input and output sampling rates
S^*	input sensitivity level
T	sampling period
T_1	meander line propagation delay time between input adjacent channels
T_2	meander line propagation delay time between output adjacent channels
t	microstrip strip conductor thickness
T_s	meander line propagation delay time between adjacent channels
T'	total meander line propagation delay time between the 1st and Nth channel
T'_{se}	effective meander line propagation delay time between adjacent channels
t_p	pulse line propagation delay time between adjacent channels.
t_λ	propagation delay time per unit length in microstrip
$\tan\delta$	dielectric loss tangent
V_b	sampling gate bias voltage
V_s	input r.f. voltage
V_o	output r.f. voltage
W	microstrip strip conductor width
W_e	microstrip effective strip conductor width
Z_j	impedance as seen from the jth channel
Z_m	meander line impedance

LIST OF SYMBOLS (CONT'D)

Z_0	characteristic impedance
ϵ_r	dielectric constant
ϵ_{eff}	effective dielectric constant
$\delta(t)$	impulse time function
$\delta_T(t)$	a sequence of impulse time functions of period T
$\delta_{\omega_0}(\omega)$	frequency spectrum of $\delta_T(t)$
\mathcal{F}	Fourier transform
\mathcal{F}^{-1}	Inverse Fourier transform
τ	sampling pulse width
τ_1, τ_2	input and output sampling pulse widths
τ_{eff}	effective output signal pulse width
ω_n	radian cutoff frequency
α	total dissipative losses in microstrip
α_d	substrate dielectric loss
α_c	microstrip conductor loss
α_L	pulse desensitization factor
Ω	ohms
σ	conductivity of the material
μ_0	free space permeability
ν	mhos
λ_0	free space wavelength
*	convolution

LIST OF SYMBOLS (CONT'D)

$\phi(m/2B)$

set of uniform samples sampled at a
rate of $2B$ samples/second

1.0 INTRODUCTION

A particular Electronic Warfare requirement is to receive and analyze microwave signals. It is thus often necessary to instantaneously down-convert microwave signals into frequency regimes associated with the operation of processing devices [1]-[3]. Present methods of converting r.f. signals upward or downward in frequency involve either heterodyne conversion, which relies on mixing a local oscillator signal with the input r.f. signal, or by harmonic or sub-harmonic generation using electrically non-linear devices [4]-[5].

One problem with the heterodyne conversion process is that the absolute bandwidth remains unchanged. For instance, an input band of $(f_1 - f_2)$ with centre frequency f_0 will retain a bandwidth of $(f_2 - f_1)$ even though the centre frequency has been reduced by n to f_0/n or increased by n to nf_0 . In the down conversion process this limits the ultimate instantaneous bandwidth. In harmonic or sub-harmonic signal generation the converted signal can only be an integral multiple or sub-multiple of the input frequency. Also, both heterodyne and harmonic/sub-harmonic conversion are non-linear processes which create harmonic signals and intermodulation products or multiple signals.

In this report, a novel solution to the above problem is presented. The solution provides a new approach to the design of frequency conversion systems.

In section 1.1, the background and objective of the report are presented in greater detail, while the report organization is described in section 1.2.

1.1 Background and Objective

Sampling techniques which permit amplification of wideband signals using lowpass narrowband amplifiers were first reported by Lathi [6] and subsequently by Tucker, Conway and Bouchard [7]. These techniques allow the acquisition, amplification and reconstruction of wideband signals.

An extension of the above is found in carrying out frequency compression/expansion of pulsed r.f. signals. The input is converted by sampling the voltage of a wave distributed along a delay line at a number of points along the line. These sampled voltages are subsequently amplified by amplifier circuits with the new waveform being constructed by the reverse process of applying the amplified voltage samples to an output delay line which is unlike the input delay line.

Although in general limited to pulse systems in the case of frequency compression, this type of approach offers several advantages over conventional frequency conversion systems. It is extremely wideband and is capable of converting signals over an infinite number of conversion factors with gain. As well, this device is a linear device thus allowing the processing of a multitude of signals simultaneously without the generation of intermodulation products.

The objective of this report is to develop a mathematical model describing the frequency compression/expansion concept and to demonstrate the feasibility of carrying out frequency compression of wideband signals in an experimental device.

1.2 Report Organization

Section 2 of this report deals with the theoretical development of the proposed frequency compression/expansion system. Practical considerations based on the theories developed are subsequently introduced in Section 3. The design of an experimental frequency compression system is described in detail in Section 4. Results of the overall experimental system performance are reported and compared to theoretical values in Section 5. Finally, the conclusions and recommendations for future work are presented in Section 6.

2.0 THEORETICAL DEVELOPMENT

2.1 Introduction

This section is concerned with the concepts and theories that are relevant to the design of the proposed system. A review of the basic principles of signal sampling, signal reconstruction and sample amplification is presented. A novel method of amplifying wideband signals using narrowband amplifiers is subsequently introduced. This approach relies on the principle of undersampling a signal and amplifying the narrowband signals generated by several parallel sets of undersamples of the signal. This scheme in turn suggests a method for carrying out wideband frequency compression (or expansion) of pulsed r.f. signals.

2.2 Sampling an Arbitrary Signal $f(t)$

Consider a signal $f_s(t)$ which is composed of narrow samples that may be treated as impulse samples of $f(t)$. As suggested from Fig. 2.1, any sample $f_m = f(mT)$ can be obtained by multiplying $f(t)$ by the appropriate unit impulse function, $\delta(t-mT)$. The sample train $f_s(t)$ is then composed of the entire set $\{8\}$, that is,

$$f_s(t) = f(t) \sum_{m=-\infty}^{\infty} \delta(t-mT) \quad (2-1)$$

$$= \sum_{m=-\infty}^{\infty} f(mT) \delta(t-mT) \quad (2-2)$$

To determine the frequency spectrum of $f_s(t)$, the Fourier transform of

$f(t)$ and $\sum_{m=-\infty}^{\infty} \delta(t-mT)$ must first be determined.

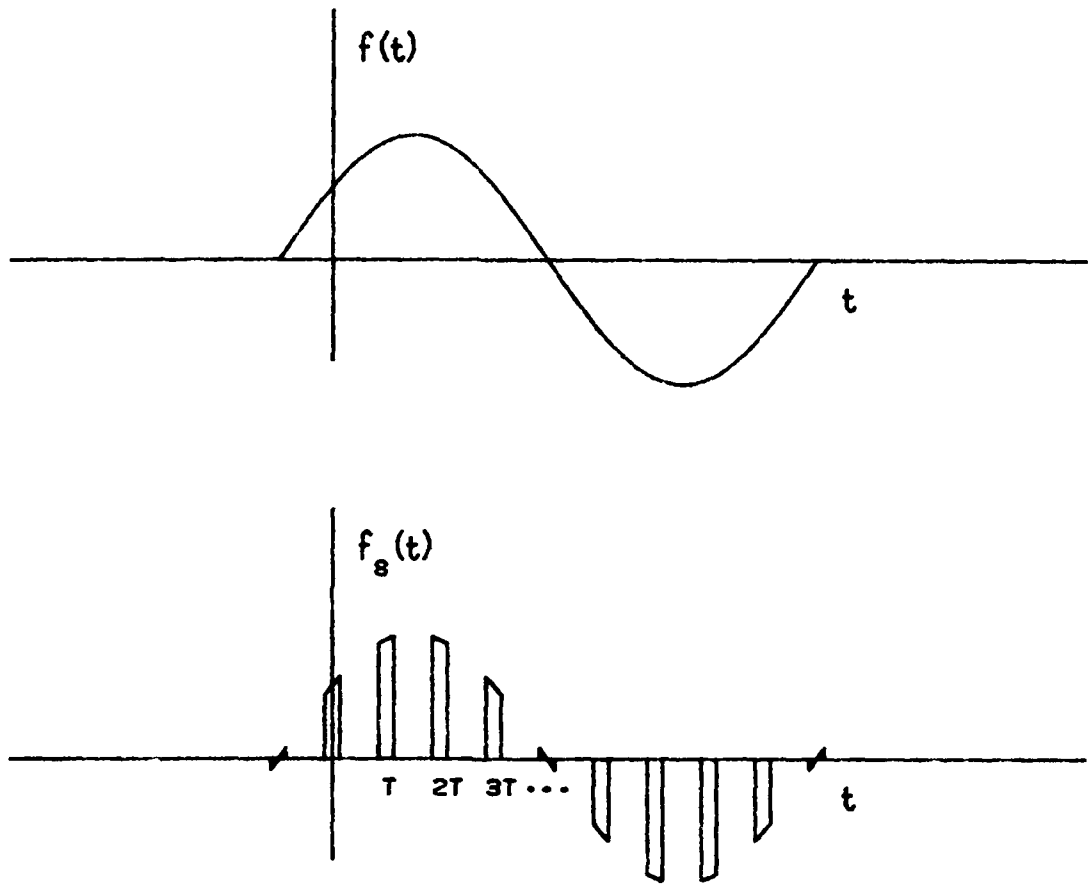


FIGURE 2.1 - SIGNAL $f_s(t)$ PRODUCED BY A SAMPLER

The Fourier transform of $f(t)$ is simply $F(\omega)$. The sampling function

$$\delta_T(t) = \sum_{m=-\infty}^{\infty} \delta(t-mT) \quad (2-3)$$

is a sequence of a uniform equidistant impulse functions of period T (Fig. 2.2). The Fourier transform of this periodic function is given by [9],

$$\mathcal{F}[\delta_T(t)] = \frac{2\pi}{T} \sum_{m=-\infty}^{\infty} \delta(\omega - m\omega_0), \quad (2-4)$$

$$= \omega_0 \delta_{\omega_0}(\omega), \quad (2-5)$$

where

$$\omega_0 = 2\pi/T.$$

Multiplication of two functions in the time domain corresponds to convolution in the frequency domain [9], that is,

$$q_1(t) q_2(t) \leftrightarrow \frac{1}{2\pi} [Q_1(\omega) * Q_2(\omega)] \quad (2-6)$$

The frequency spectrum of $f_s(t)$ is therefore

$$f_s(t) \leftrightarrow F_S(\omega) = \frac{1}{2\pi} [F(\omega) * \frac{2\pi}{T} \sum_{m=-\infty}^{\infty} \delta(\omega - m\omega_0)]. \quad (2-7)$$

This reduces to

$$F_S(\omega) = \frac{1}{T} \sum_{m=-\infty}^{\infty} F(\omega - m\omega_0). \quad (2-8)$$

Therefore, apart from the multiplicative constant $1/T$, the convolution of $F(\omega)$ and $\delta_{\omega_0}(\omega)$ causes $F(\omega)$, the spectrum of $f(t)$, to be reproduced every ω_0 radians (Fig. 2.3). $F(\omega)$ will repeat periodically without overlapping as long as

$$\omega_0 > 2\omega_k \quad (2-9)$$

or

$$\frac{1}{T} > 2B,$$

where B is the upper bandwidth of the signal and is equal to $\omega_k/2\pi$, and $1/T$ represents the sampling rate. This is the well known Nyquist sampling theorem which states that any $2B$ independent samples per second will completely characterize a band-limited signal [11].

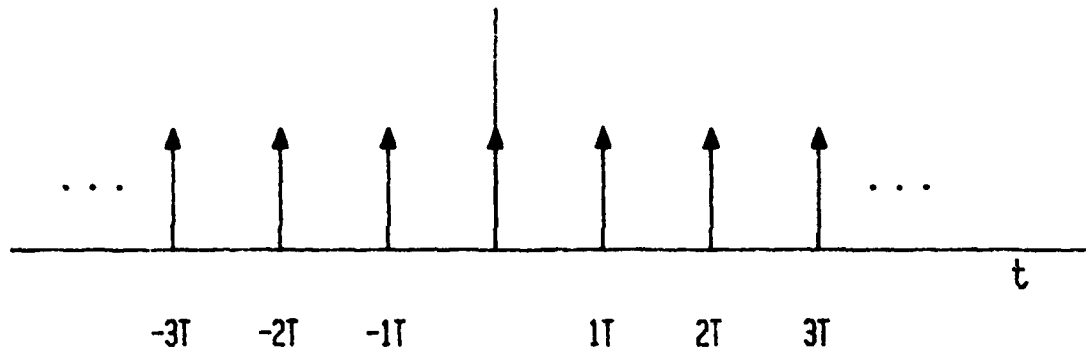


FIGURE 2.2 - A SEQUENCE OF UNIFORM EQUIDISTANT
IMPULSE FUNCTIONS OF PERIOD T

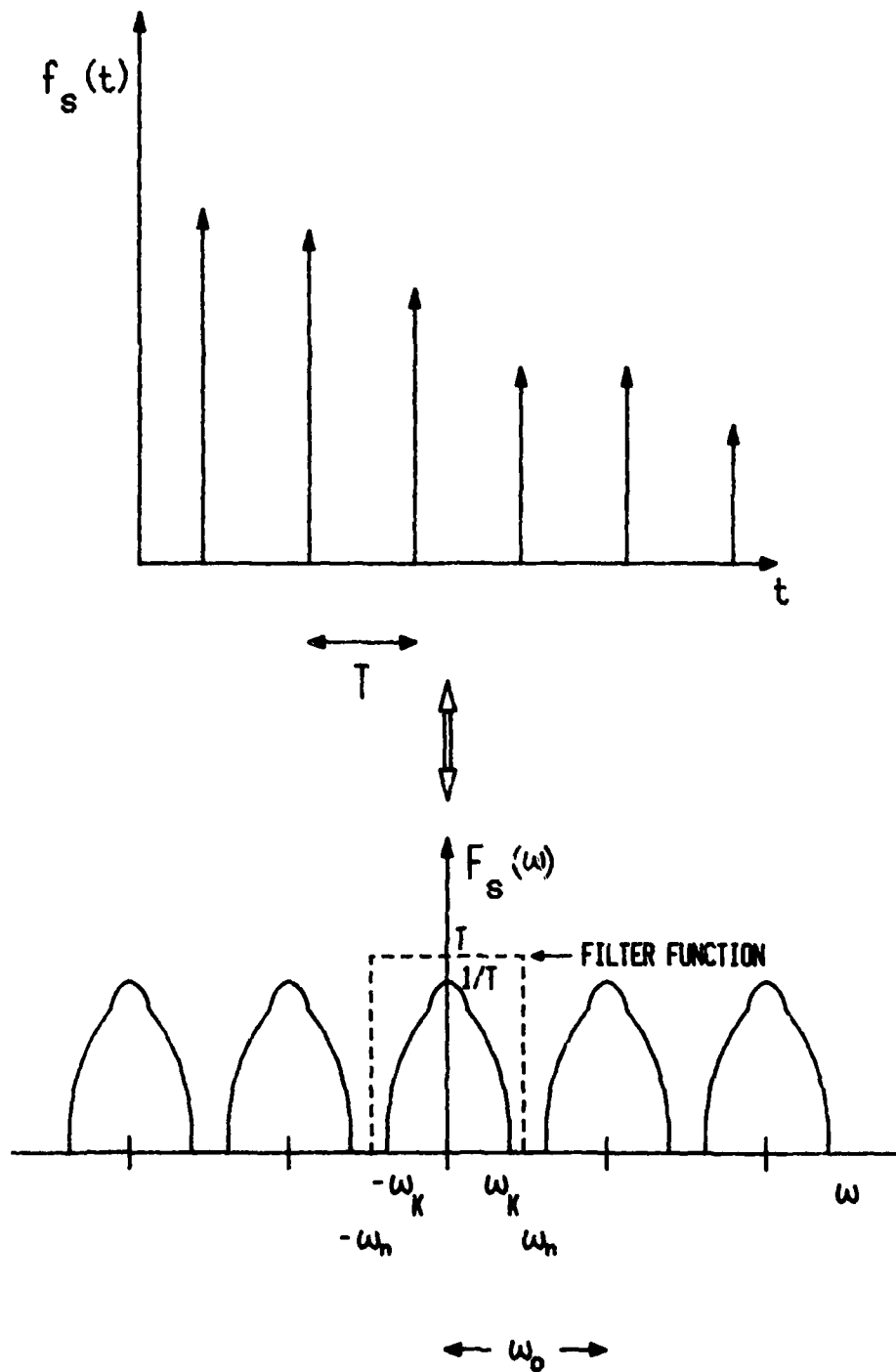


FIGURE 2.3 - FREQUENCY SPECTRUM OF THE SAMPLED FUNCTION $f_s(t)$

2.3 Recovering $f(t)$ From its Samples

The signal $f(t)$ can be recovered from $f_s(t)$ (a Nyquist sample set) by passing the latter through a low pass filter of gain T (Fig. 2.3). This low pass filter can be represented by a transfer function $T G_{2\omega_n}(\omega)$ where $\omega_k < \omega_n < \omega_o - \omega_k$ and $G_{2\omega_n}(\omega)$ represents an ideal low pass filter of cutoff radian frequency ω_n . Thus,

$$F(\omega) = T F_s(\omega) G_{2\omega_n}(\omega). \quad (2-11)$$

Multiplication in the frequency domain corresponds to convolution in the time domain [9], that is,

$$Q_1(\omega) Q_2(\omega) = q_1(t) * q_2(t) \quad (2-12)$$

From the table of Fourier transforms [6]

$$\mathcal{F}^{-1} [F_s(\omega)] = f_s(t) \quad (2-13)$$

and

$$\mathcal{F}^{-1} [G_{2\omega_n}(\omega)] = \frac{\omega_n}{\pi} \frac{\sin \omega_n t}{\omega_n t} = g(t). \quad (2-14)$$

Therefore,

$$f(t) = T f_s(t) * g(t) \quad (2-15)$$

$$\begin{aligned} &= T f_s(t) * \frac{\omega_n}{\pi} \frac{\sin \omega_n t}{\omega_n t}, \\ &= \frac{\omega_n T}{\pi} \sum_{m=-\infty}^{\infty} f(mt) \delta(t-mT) * \frac{\sin \omega_n t}{\omega_n t}, \\ &= \frac{\omega_n T}{\pi} \sum_{m=-\infty}^{\infty} f(mT) \frac{\sin [\omega_n(t-mT)]}{\omega_n(t-mT)}. \end{aligned} \quad (2-16)$$

For the case $\omega_n = 2\pi B = \pi/T$

$$f(t) = \sum_{m=-\infty}^{\infty} f(m/2B) \frac{\sin [2\pi B(t-m/B)]}{2\pi B(t-m/2B)}. \quad (2-17)$$

Equation 2-17 is known as Whittakers' cardinal function and is a general form for reconstructing a function from a set of samples [8]. This function shows a method of reconstructing $f(t)$ from its samples. Each sample $f(mT)$ is multiplied by a sampling function of the form $\sin x/x$ with the resulting waveforms being summed to obtain $f(t)$ (Fig. 2.4). Note that at the sampling point $t = m/2B$ (or $t = mT$) only one term is contributed in the summation, all other terms being zero at this point.

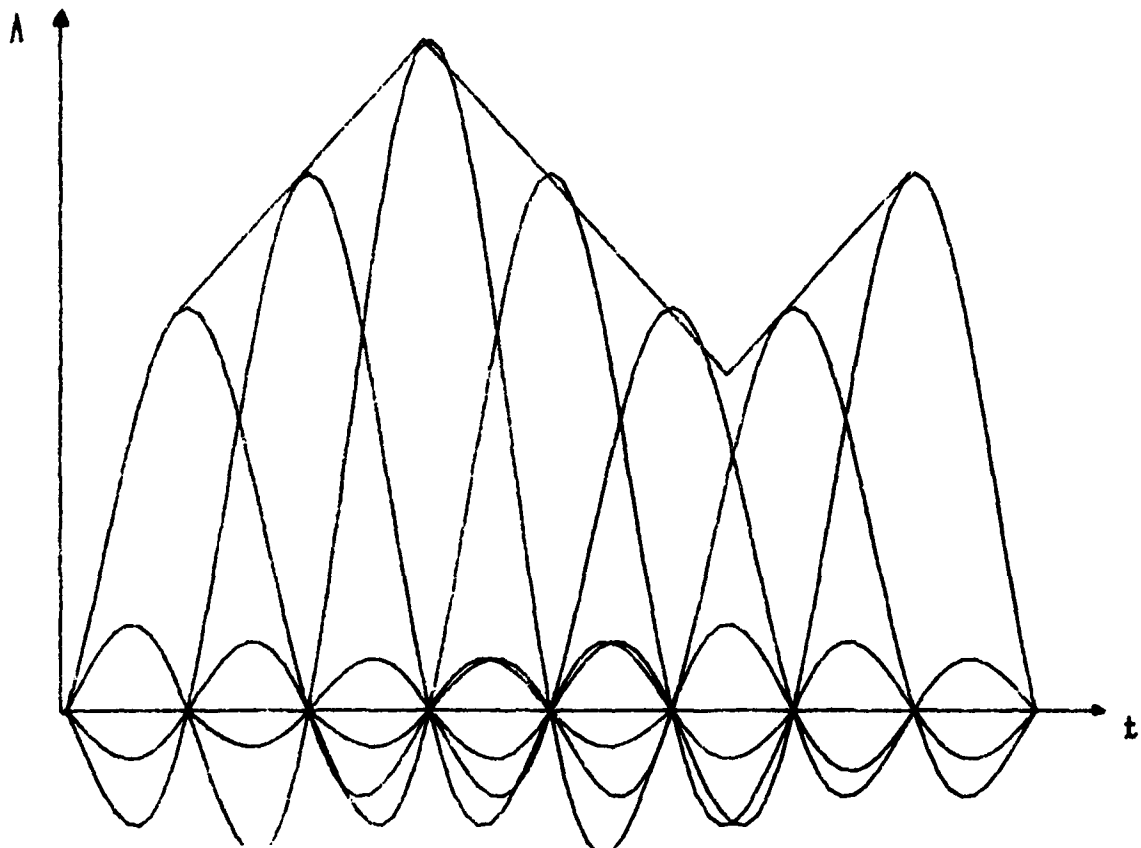


FIGURE 2.4 - RECONSTRUCTION OF THE SIGNAL $f(t)$ FROM ITS SAMPLES

Thus if the Nyquist samples of $f(t)$, sampled at a rate of $2B$ samples/second, are passed through an ideal low pass filter of cutoff frequency B and gain $T = 1/2B$ the output is $f(t)$. If the ideal low-pass filter had a gain of unity instead of T , the output would be $1/T f(t)$ or $2Bf(t)$.

2.4 Amplification of Samples

The result in the previous section suggests a method of amplifying a set of samples. A set of uniform samples of the form $\phi(m/2B) \delta(t - m/2B)$ (sampled at a rate of $2B$ samples/second) when passed through an ideal low pass filter of bandwidth B Hz and gain G gives the output $2BG\phi(t)$. The output of this filter when sampled by an ideal sampler at a rate of $2B$ samples/second will yield the original set of samples amplified by a factor of $2BG$ (Fig. 2.5).

2.5 Amplification of Wideband Signals

Now consider spatially distributing the points at which samples of the signal are taken. This may be accomplished by distributing a signal $\phi(t)$ along an input meander delay line as shown in Fig. 2.6. If there are N sampling points along the meander delay line, the sampling rate at each point must be $2B/N$. Consequently, the subset of samples from each sampling point may be amplified using low-pass filters of gain G_n and cutoff frequency B/N , resulting in a gain of $G(2B/N)$ for each sample. When the amplified subsets are now summed in the same sequence as they were subdivided the original sample set is obtained at an amplified level. When the last filter operation is carried out an additional gain of $G_o(2B)$ is introduced, resulting in an overall gain of

$$G_n(2B/N) G_o(2B). \quad (2-18)$$

Consequently, the present scheme allows amplification of wideband signals using narrowband amplifiers. The nature of amplification is essentially additive as each of the N amplifiers amplifies a spectrum of B/N Hz, however, this spectrum is not an easily identifiable portion of the original spectrum B Hz.

2.6 Frequency Scaling of Wideband Signals

The scheme presented in the previous section can be extended to include wideband frequency compression (or expansion) of pulsed r.f. signals. If a set of uniform samples of the form

$$p(t) = \sum_{m=-\infty}^{\infty} p(mT_1),$$

is multiplied by an impulse train of the form

$$\sum_{m=-\infty}^{\infty} \delta(t - mT_2),$$

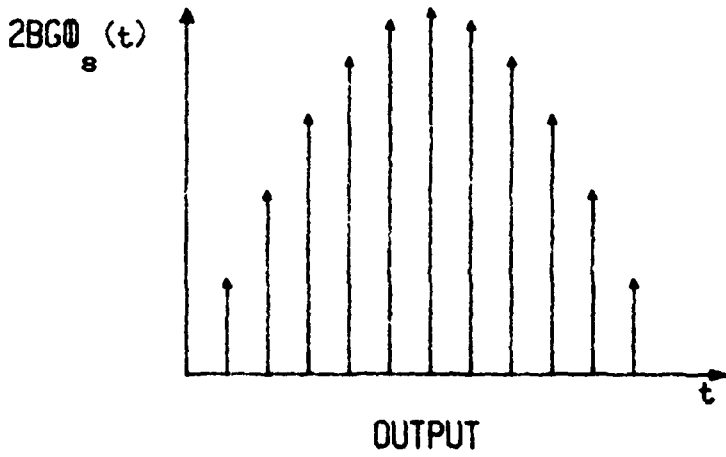
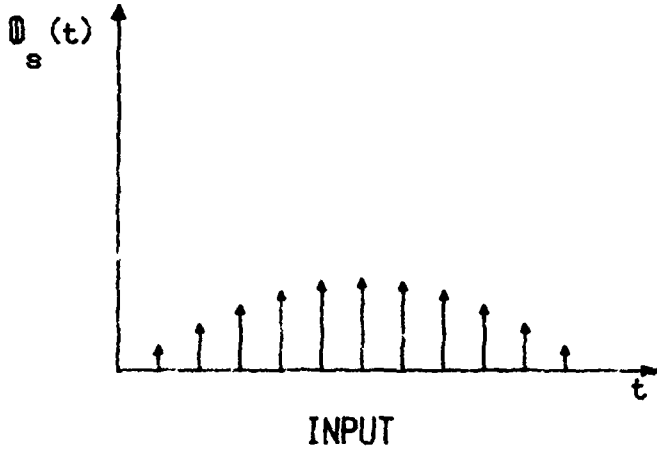
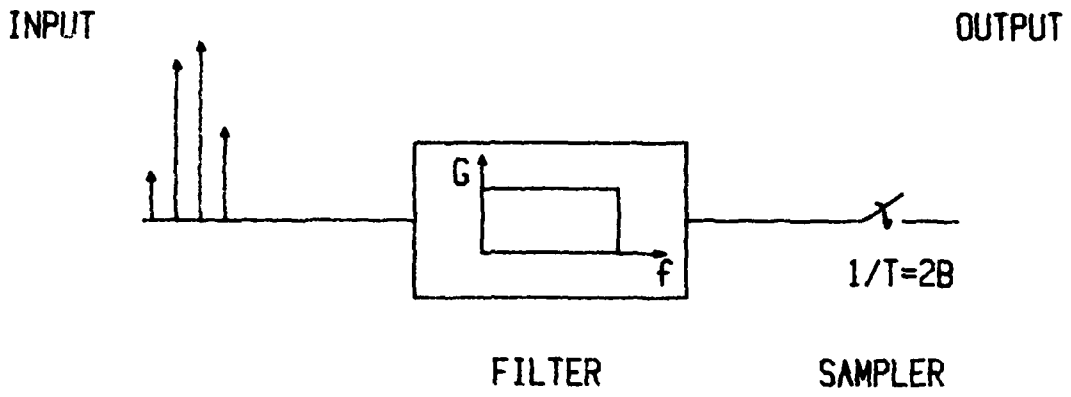


FIGURE 2.5 - AMPLIFICATION OF A SET OF SAMPLES $\phi_s(t)$

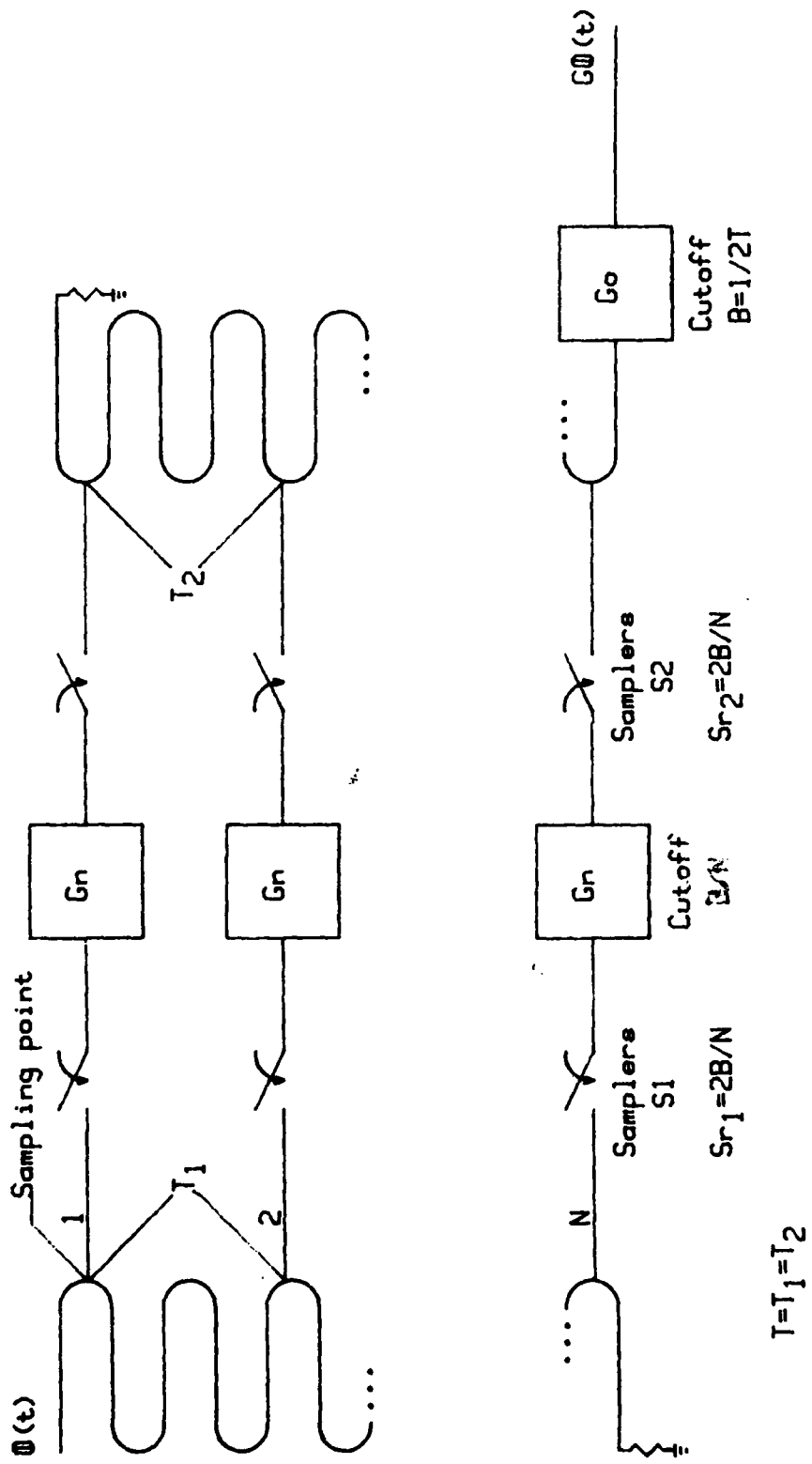


FIGURE 2.6 - DISTRIBUTED SAMPLING/AMPLIFICATION SYSTEM

where $T_1 = aT_2$, a new function $p_s(t)$ is created. Thus,

$$p_s(t) = \sum_{m=-\infty}^{\infty} p(mT_1) \delta(t-mT_2) \quad (20-19)$$

$$= \sum_{m=-\infty}^{\infty} p(maT_2) \delta(t-mT_2)$$

$$= p(at) \sum_{m=-\infty}^{\infty} \delta(t-mT_2). \quad (2-20)$$

The function $p_s(t)$ represents an impulse train of the function $p(t)$ compressed (expanded) in the time scale by a factor of a , for $a > 1$ ($a < 1$).

To obtain the frequency spectrum of $p_s(t)$, the Fourier transform of $p(at)$ and $\sum_{m=-\infty}^{\infty} \delta(t-mT_2)$ must be determined. From the

scaling property [10], the Fourier transform of $p(at)$ is given by

$$p(at) \leftrightarrow \frac{1}{a} P(\omega/a). \quad (2-21)$$

The Fourier transform of $\delta_{T_2}(t)$ is given by

$$\delta_{T_2}(t) \leftrightarrow \omega_2 \delta_{\omega_2}(\omega), \quad (2-22)$$

where $\omega_2 = \frac{2\pi}{T_2}$. Thus, the frequency spectrum of $p_s(t)$ is

$$\begin{aligned} p_s(t) \leftrightarrow P_s(\omega) &= \frac{1}{2\pi} \left[\frac{1}{a} P(\omega/a) * \frac{2\pi}{T_2} \sum_{m=-\infty}^{\infty} \delta(\omega - m\omega_2) \right] \\ &= \frac{1}{aT_2} \sum_{m=-\infty}^{\infty} P(\omega/a - m\omega_2) \end{aligned} \quad (2-23)$$

Therefore, apart from the multiplicative constant $\frac{1}{aT_2}$, the function

$P_s(\omega)$ represents a function $P(\omega)$ expanded (compressed) in the frequency domain by a factor of a , for $a > 1$ ($a < 1$), reproduced at every ω_2 radians. Thus from the scaling property, expansion in the time domain is equivalent to compression in the frequency domain and vice-versa.

A system for carrying out wideband frequency compression is proposed in Fig. 2.7. Although similar to the Distributed Sampling/Amplification System, this system has an output meander delay line which is longer than the input meander delay line. This corresponds to having $T_1 < T_2$, thus allowing frequency compression of the input signal.

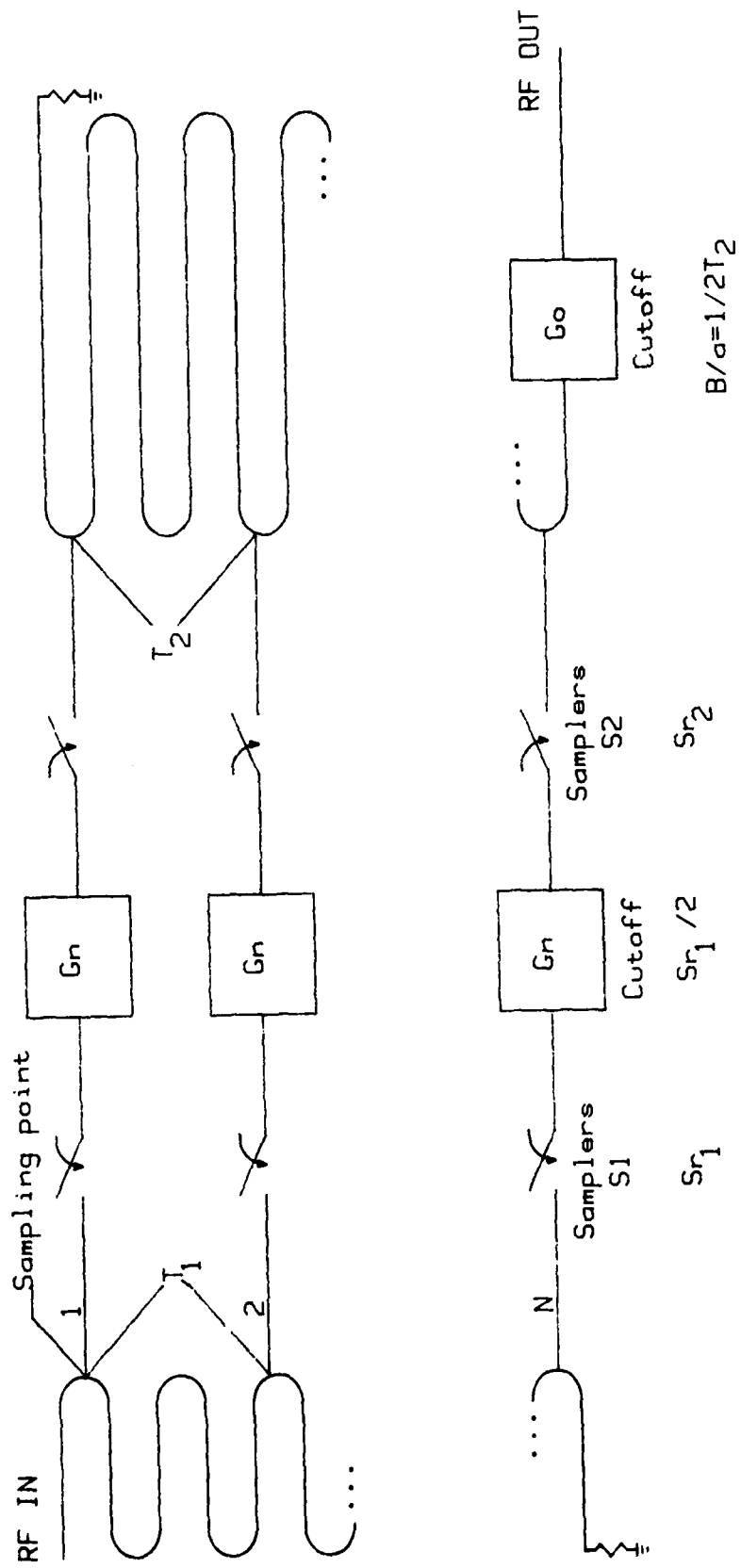


FIGURE 2.7 - FREQUENCY COMPRESSION SYSTEM

A limitation of this system, and in that case of any realizable system, is that only pulsed signals may be totally compressed or expanded in frequency. This results from the time expansion (or compression) of the signal, making frequency compression (or expansion) of cw signals physically unrealizable. Nevertheless, in many applications only a portion of signal need be analyzed.

The complete process involves the acquisition of a sample set having specified time delays between each sample element and the re-distribution of this sample set having different time delays between successive sample elements from that of the input set. This process has an infinite number of frequency compression (or expansion) factor possibilities. As an example, if the input meander line has a specified time delay T_1 between successive channels, and the output meander line has a specified time delay $2T_1$ between successive channels, then frequency compression by a factor of 2 is obtained. To achieve total frequency compression of the input pulsed r.f. signal, the input meander line must have a total delay at least as long as the duration of the r.f. pulse. An alternative method is to have an array of analog memories as suggested in Fig. 2.8. An analysis will not be carried out here, however, it is easily recognized that such a system can be implemented. In this case, the reduction in length of the input meander delay line is at the expense of increased circuit complexity and amplifier cutoff frequency.

If the input signal is completely processed, the overall gain for the system of Fig. 2.7 may be evaluated. Under this condition, the gain of the system is given by

$$G_C = \frac{1}{a} G, \quad a < 1 \quad (2-24)$$

where G is the gain for the system of Fig. 2.6.

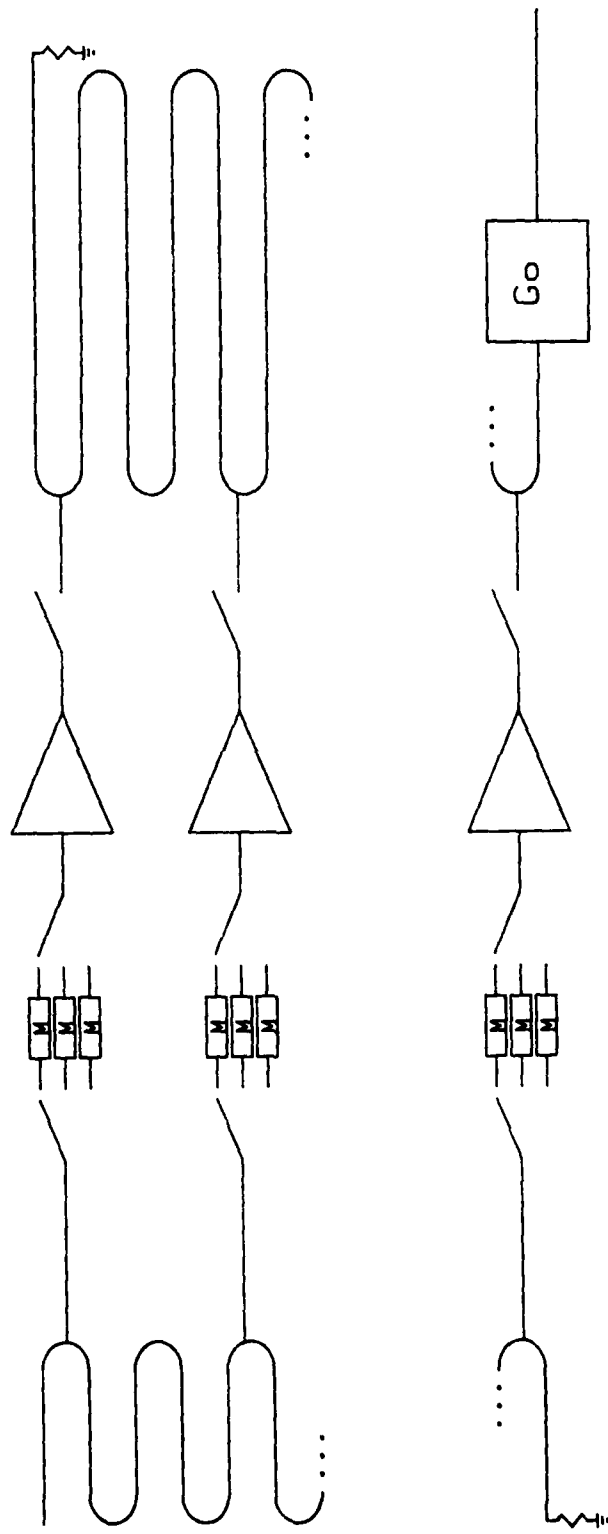
3.0 PRACTICAL CONSIDERATIONS

3.1 Introduction

In the previous section it was assumed that both sampler and filter had ideal characteristics. The filters (amplifiers) were assumed to have an ideal cutoff characteristic while the samplers were assumed to have an ideal impulse response of the form $\delta(t)$. Such characteristics are physically unrealizable and it is therefore necessary to substitute for these physically realizable elements. In this section the effects on the theoretical results due to introducing practical filter and sampler functions will be examined.

3.2 Practical Filter Considerations

Fig. 3.1 shows the output response of an ideal low pass filter to a set of samples. The output at the sampling instant $t = mT$ is the result only of the input sample at the instant mT . No interference from other input samples is contributed at this instant in time. As a result,



M-ANALOG MEMORY

FIGURE 2.8 - A MULTIPLE MEMORY FREQUENCY COMPRESSION SYSTEM

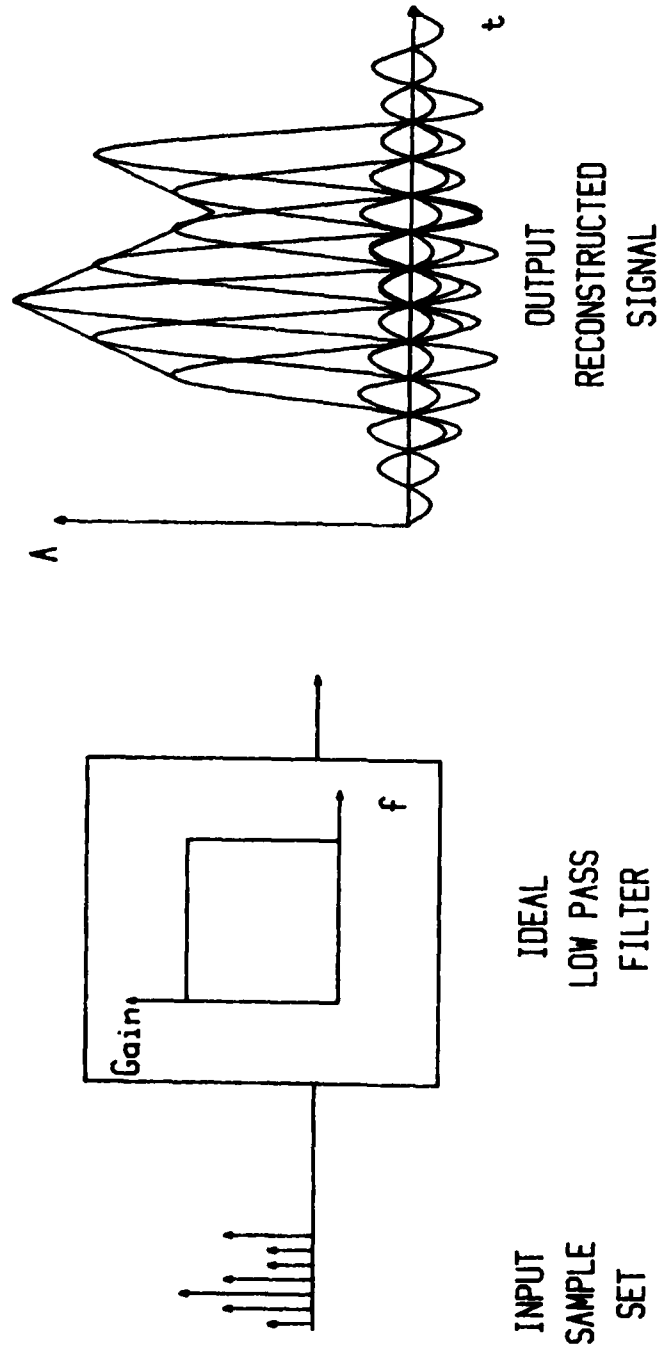


FIGURE 3.1 - RECONSTRUCTION OF THE SIGNAL $f(t)$ FROM ITS SAMPLES

when the filter output is sampled again we obtain the same impulse train at the output within a multiplicative constant. This is what makes amplification of samples possible. Consequently, any other filter satisfying this property will also amplify samples in the same manner. Hence, the only condition that a filter impulse response must satisfy is

$$\begin{aligned} k_{2\omega_n}(t) &= C & t = 0 \\ &= 0 & t = mT, m = \pm 1, \pm 2 \dots \end{aligned} \quad (3-1)$$

A practical filter is shown in Fig. 3.2a. The practical filter's transfer function $K_{2\omega_n}(\omega)$ can be described by the two functions $K_1(\omega)$ and $K_2(\omega)$ as

$$K_{2\omega_n}(\omega) = K_1(\omega) + K_2(\omega). \quad (3-2)$$

Hence, the impulse response $k_{2\omega_n}(t)$ of the practical filter is the sum of the impulse responses for $k_1(t)$ and $k_2(t)$ thus,

$$k_{2\omega_n}(t) = k_1(t) + k_2(t). \quad (3-3)$$

The impulse response of the ideal filter $k_1(t)$ is given by

$$k_1(t) = \frac{\omega_n}{\pi} \frac{\sin \omega_n t}{\omega_n t}. \quad (3-4)$$

In order to obtain $k_2(t)$, let us consider the function $G(f)$ of Fig. 3.2d. If,

$$g(t) \leftrightarrow G(\omega), \quad (3-5)$$

and from the modulation theorem [10]

$$2jf(t) \sin \omega_0 t \leftrightarrow [F(\omega - \omega_0) - F(\omega + \omega_0)], \quad (3-6)$$

then,

$$2jg(t) \sin \omega_n t \leftrightarrow [G(\omega - \omega_n) - G(\omega + \omega_n)]. \quad (3-7)$$

The right hand side of (3-7) is just $K_2(\omega)$. Therefore,

$$k_2(t) = 2jg(t) \sin \omega_n t \quad (3-8)$$

and [9],

$$k_{2\omega_n}(t) = \left[\frac{\omega_n}{\pi} + j2g(t) \sin \omega_n t \right] \frac{\sin \omega_n t}{\omega_n t}. \quad (3-9)$$

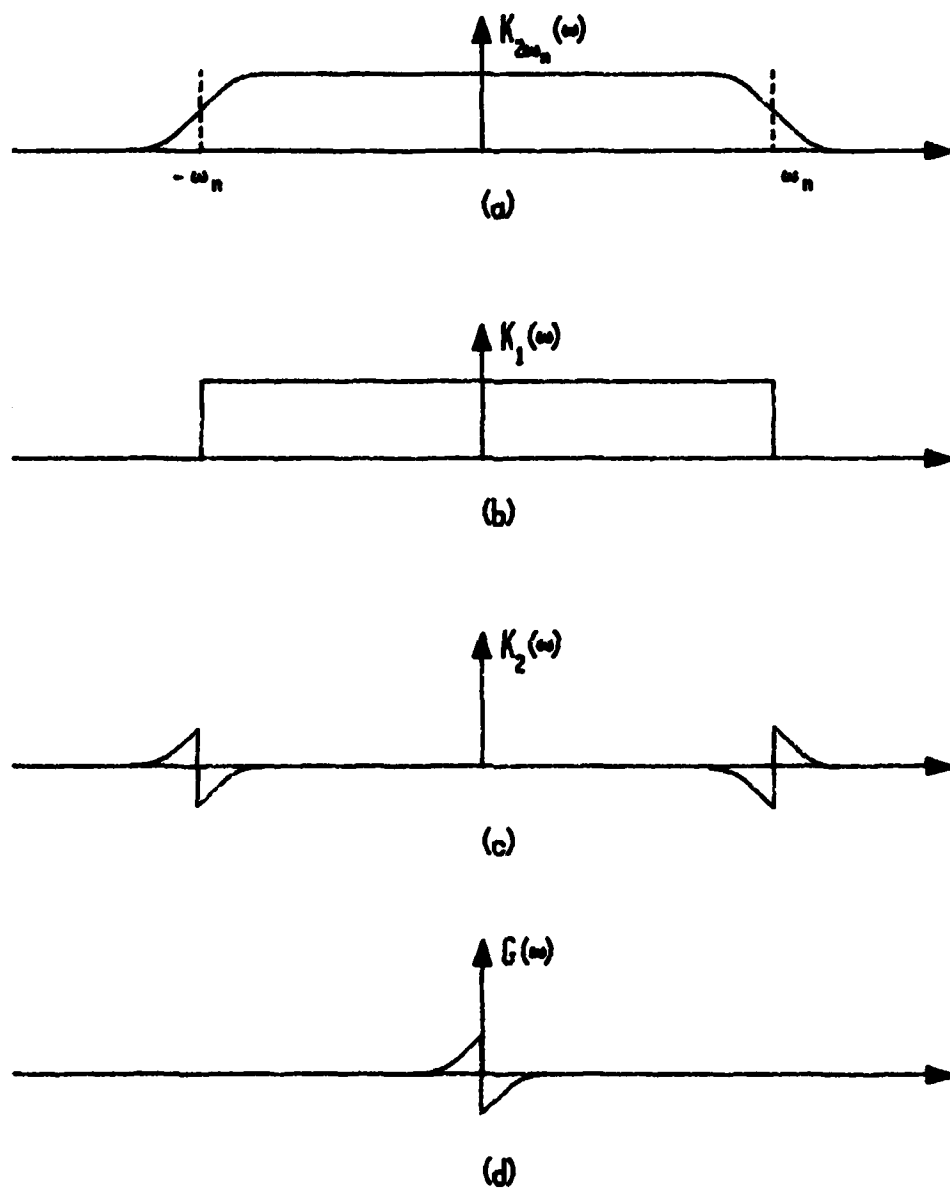


FIGURE 7.8 - A PRACTICAL FILTER WITH CUTOFF FREQUENCY ω_n

It can be seen that $k_{2\omega_n}(t)$ has zeros at $t = m\pi/\omega_n$ for $m = \pm 1, \pm 2, \dots$, exactly at the same points as the ideal filter $k_1(t)$, also $k_{2\omega_n}(0) = \omega_n/\pi = k_1(0)$. This practical filter therefore satisfies the condition of (3-1). Indeed each of the N filter-amplifiers with gain G_n of Fig. 2.6 and Fig. 2.7 may be replaced by practical filters of the form

$$G_n K_{2\omega_n/N}(\omega) \quad (3-10)$$

having cutoff frequency ω_n/N .

It is worth noting that even if ideal filters were physically realizable they would be undesirable, since these filters would have an

impulse response of the form $\frac{\sin \omega_n t}{\omega_n t}$. Any small deviation in sampling

rate, filter cutoff frequency or sampling instant would produce failure because of interference from overlapping pulse tails due to adjacent pulses. The oscillatory nature of the pulse tails is reduced in the case of a gradual cutoff filter [6].

3.3 Practical Sampler Considerations

3.3.1 Sampler's Finite Pulse Width

Unlike an ideal sampler, a practical sampler has some finite pulse width τ (Fig. 3.3). The Fourier transform of $k(t)$ is given by [9]

$$k(t) \leftrightarrow K(\omega) = \tau \frac{\sin \omega\tau/2}{\omega\tau/2} \quad (3-11)$$

Thus, a practical sampler is equivalent to an ideal sampler followed by a gain τ and a filter $K_p(\omega)$ (Fig. 3.4) given by

$$K_p(\omega) = \frac{\sin \omega\tau/2}{\omega\tau/2} \quad (3-12)$$

This finite pulse width causes a loss at higher frequencies. This loss may be compensated by placing in series an inverse filter of the form [6]

$$K_i(\omega) = \frac{\omega\tau/2}{\sin \omega\tau/2} \quad (3-13)$$

This inverse filter may be lumped with the filter which follows the sampler. The compensation factor has the effect of increasing the filter's bandwidth (Fig. 3.5). Thus, samplers S_1 and S_2 of Fig. 2.6 and Fig. 2.7 may be replaced by practical samplers with pulse widths τ_1 and τ_2 , respectively. This introduces additional multiplication factors in the gain equation. The overall gain is now

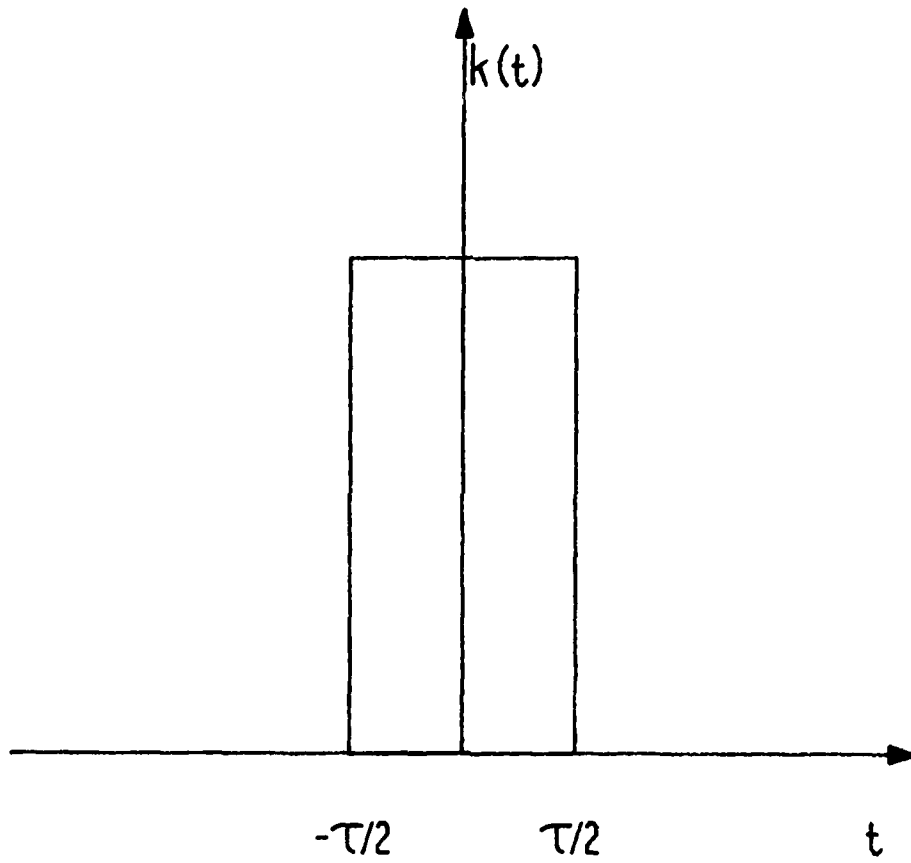


FIGURE 3.3 - IMPULSE RESPONSE OF A PRACTICAL SAMPLER

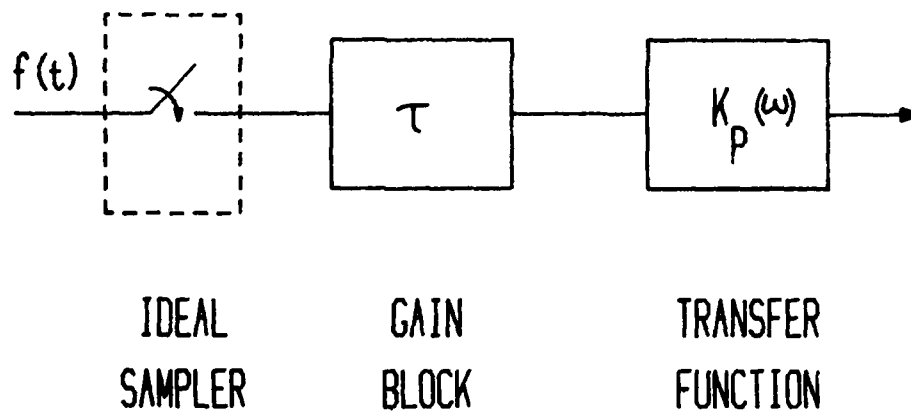


FIGURE 3.4 - PRACTICAL SAMPLER REPRESENTATION

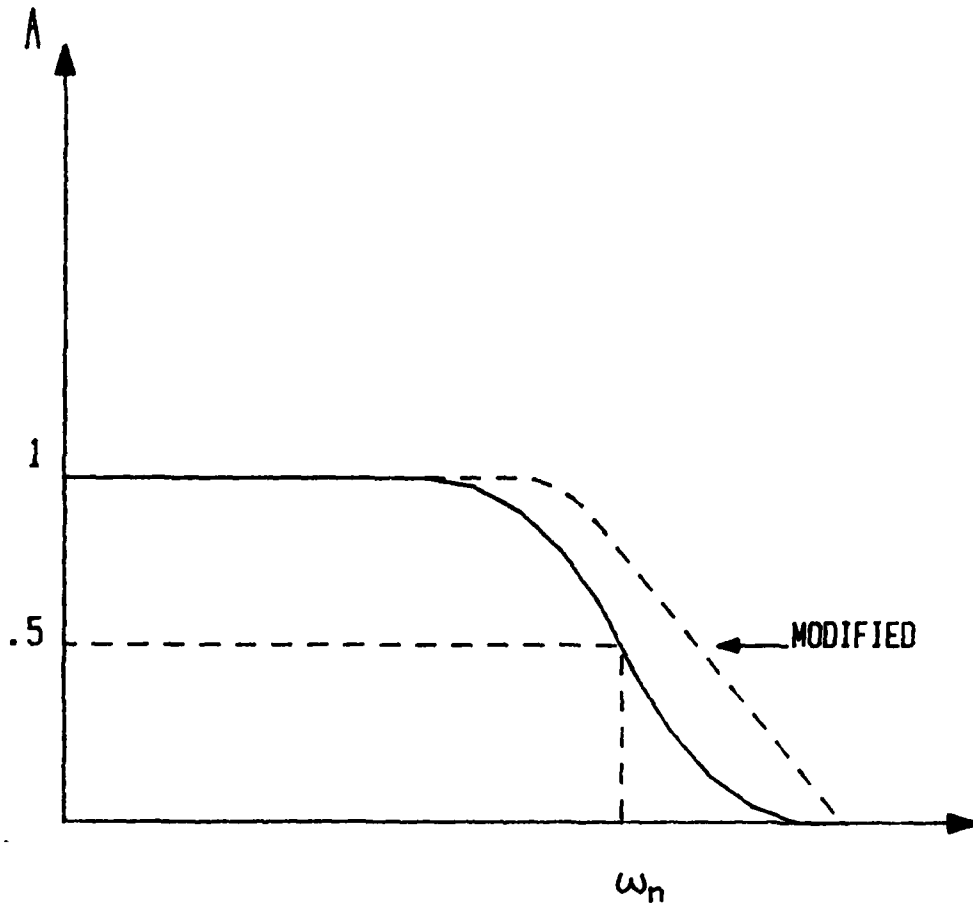


FIGURE 3.5 - FILTER COMPENSATION RESULTING FROM THE FINITE SAMPLER PULSE WIDTH

$$G = G_n(2B/N) G_o(2B) \tau_1 \tau_2,$$

$$\text{and } G_c = \frac{1}{a} G. \quad (3-14)$$

Clearly increasing τ_1 and τ_2 increases the overall gain. The maximum possible pulse width is equal to the sampling interval. The interval between successive samples presented to the same filter of Fig. 2.6 is $N/2B$ ($1/Sr_1$) seconds. Consequently, we can stretch the samples of the sampler S_1 to a maximum value of

$$(\tau_1)_{\max} = \frac{N}{2B}. \quad (3-15)$$

The samples at the output sampler S_2 are separated by $1/2B$ seconds. Therefore,

$$(\tau_2)_{\max} = \frac{1}{2B} = T_2. \quad (3-16)$$

Thus, the overall maximum gain of the system in Fig. 2.6 is [6]

$$G_{\max} = \frac{4B^2 G_o G_n (\tau_1)_{\max} (\tau_2)_{\max}}{N} = G_o G_n. \quad (3-17)$$

For the system of Fig. 2.7

$$G_{c_{\max}} = \frac{1}{a} G_{\max} = \frac{1}{a} G_o G_n. \quad (3-18)$$

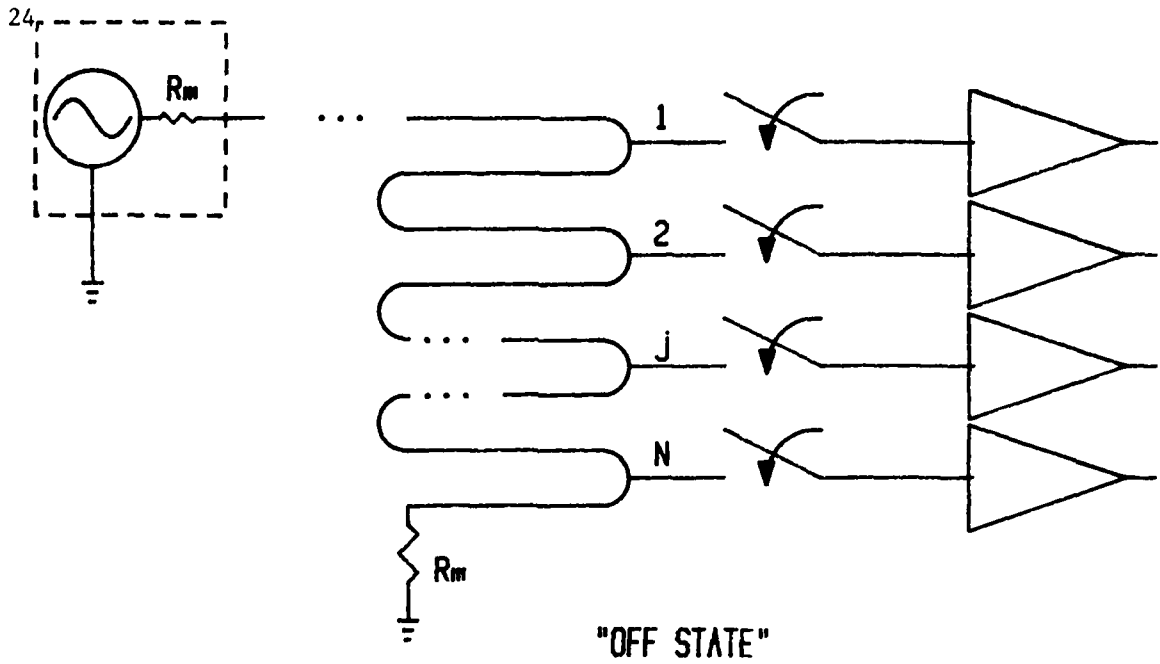
The upper limit on the bandwidth that can be amplified is determined by the pulse width of the sampling pulses. Hence from equation 3-16,

$$B_{\max} = 1/2\tau_2$$

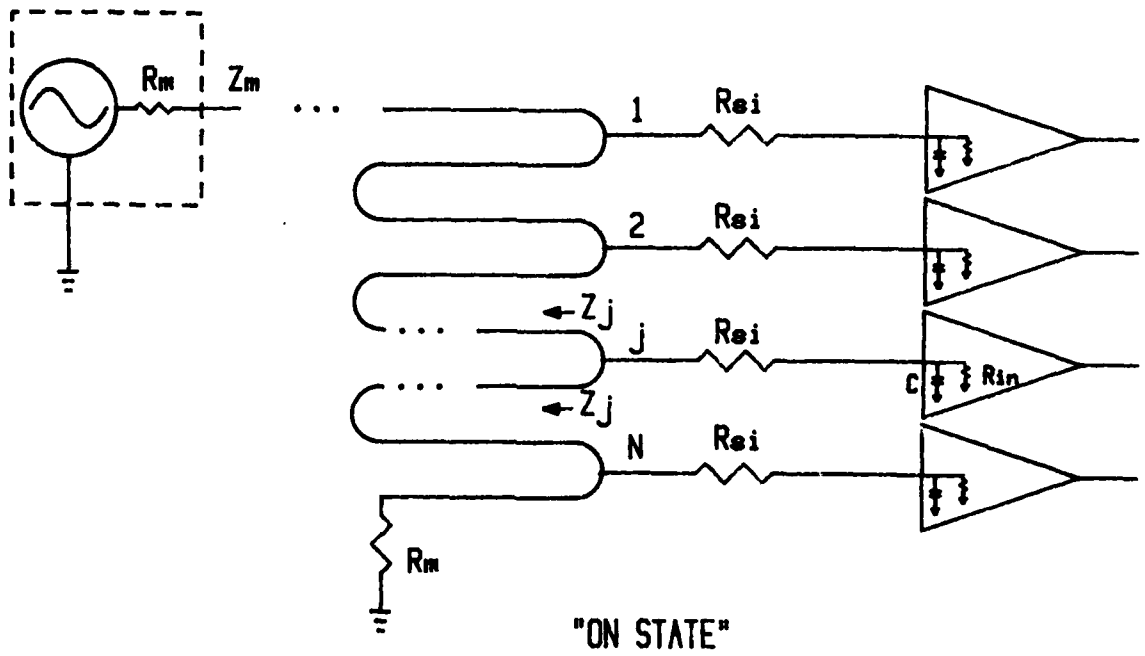
3.3.2 Losses Due To The Sampler's Non-zero Impedance

In considering the practical sampler, the effect of the sampler's non-zero impedance during the on-state must be examined. The non-zero impedance of the sampling gate (in conjunction with the amplifier parameters) introduces a loss factor into the gain formula. Both input and output sampler-amplifier networks contribute to overall system loss.

The loss due to the input meander delay line-sampler-amplifier configuration may be calculated by modelling this structure as a switched-capacitor network as shown in Fig. 3.6. The resistance R_{si} represents the on resistance of the input sampling gate under a forward bias condition and C and R_{in} are the intrinsic capacitance and input resistance of the amplifier circuit. In general, the loss factor must include the loading effect due to adjacent channels. Thus, if the sampling pulse width is greater than the propagation delay time between adjacent channels, the impedance as seen by the j^{th} channel (Z_j) will change as a function of time. Conversely, if the sampling pulse width is



(a)



(b)

FIGURE 3.6 - INPUT MEANDER DELAY LINE-SAMPLER-AMPLIFIER MODEL

less than or equal to the propagation delay time between adjacent channels, the model is simplified as the impedance Z_j reduces to the line impedance Z_m (Fig. 3.7). Since sufficiently narrow sampling pulses may be realized, only the loss factor for the simplified model need be derived.

Thus from Fig. 3.7, the voltage v_{ji} appearing at the input of the amplifier-filter network as a function of the applied open circuit voltage v as derived in Appendix A is given by

$$[V(o) - K_1 v]e^{-K_2 \tau_1} + K_1 v, \quad (3-20)$$

where $V(o)$ represents the voltage appearing at the input to the amplifier immediately before the switch is turned "on", τ_1 is the "on" time of the sampling gate and

$$K_1 = \frac{R_{in}}{2R_{si} + 2R_{in} + R_m}$$

$$\text{and} \quad K_2 = \frac{1}{K_1(2R_{si} + R_m)C}.$$

If the capacitor is completely discharged before the next sample is acquired, equation 3-20 reduces to

$$\frac{v_{ji}}{v} = K_1 [1 - e^{-K_2 \tau_1}]. \quad (3-21)$$

In terms of the maximum available voltage v_1 , equation 3-21 becomes

$$\frac{v_{ji}}{v_1} = 2K_1 [1 - e^{-K_2 \tau_1}]. \quad (3-22)$$

The output amplifier-sampler-meander line configuration is modelled in Fig. 3.8. Again, if the sampling pulse width is less than or equal to the propagation delay time between adjacent output channels, the impedance Z_j as seen from the point j is simply R_m . The output amplifier network may be modelled by an ideal voltage source having an open circuit voltage v_{oc} , a series source resistance R_o , an intrinsic output shunt capacitance C_o and an output load resistance R_l as shown in Fig. 3.9. (The load resistance R_l is necessary to insure stability of the amplifier when the switch is "off".) Thus, the output voltage v_{jo} impressed on the output meander delay line as a function of the open circuit voltage v_{oc} as derived in Appendix A is given by

$$v_{jo} = \{ [V_o(o) - K_5 v_{oc}] \exp(-K_6 \tau_2) + K_5 v_{oc} \}, \quad (3-23)$$

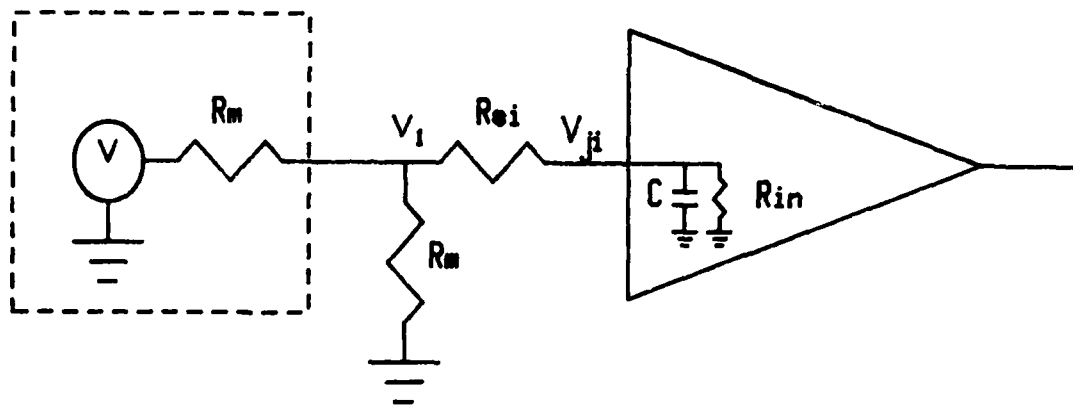
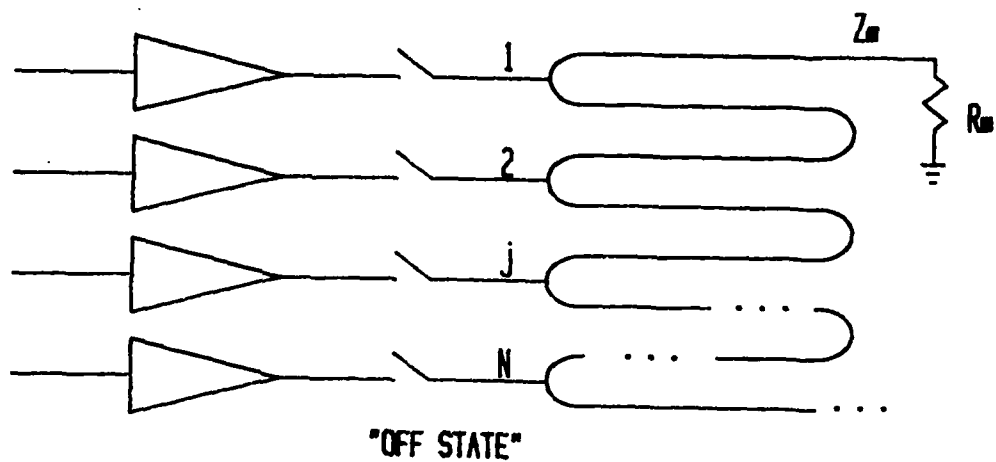
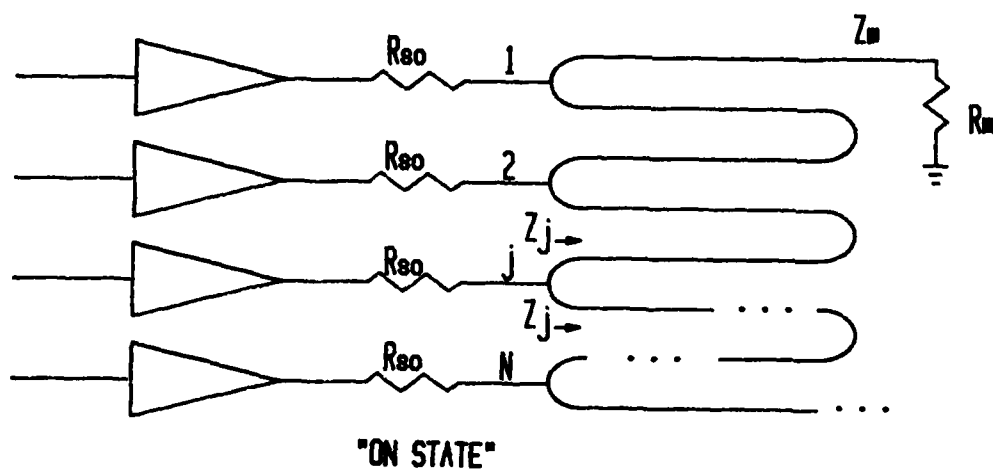


FIGURE 3.7 - SIMPLIFIED MODEL OF THE INPUT MEANDER DELAY LINE CONFIGURATION DURING THE SAMPLER'S "ON" STATE



(a)



(b)

FIGURE 3.8 - MODEL OF THE OUTPUT AMPLIFIER-SAMPLER-MEANDER LINE CONFIGURATION

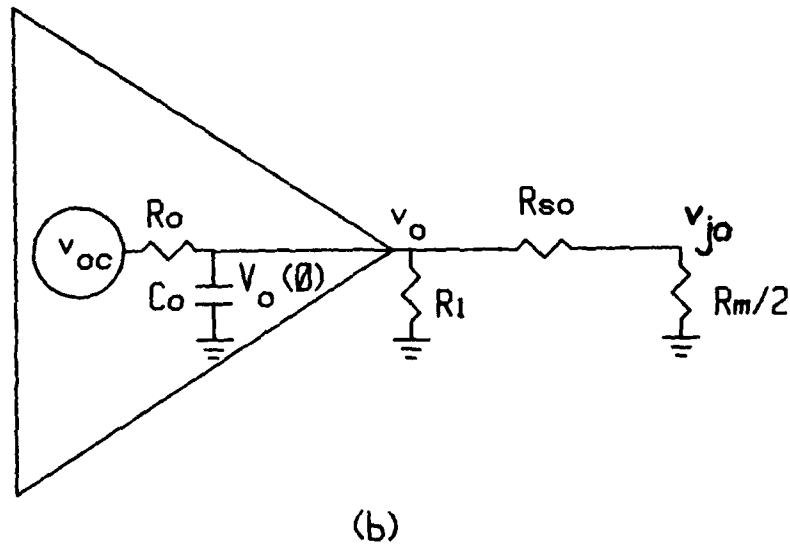
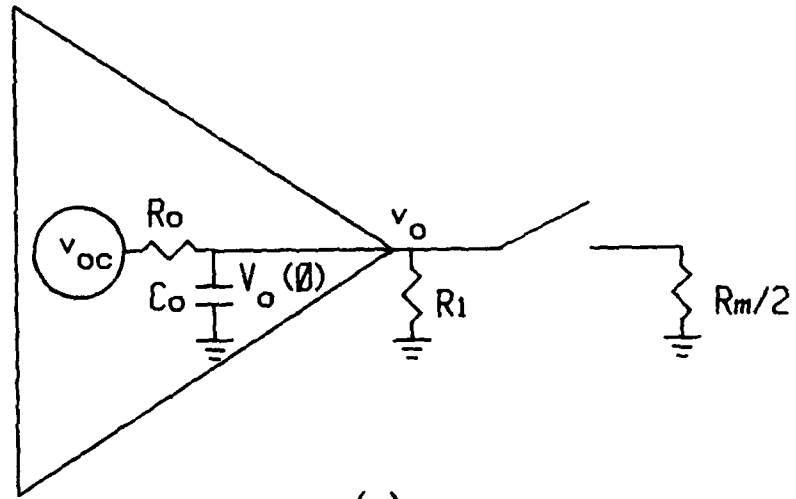


FIGURE 3.9 - MODEL OF THE OUTPUT NETWORK FOR THE SAMPLER'S
 (a) "OFF" CONDITION AND
 (b) "ON" CONDITION

where $V_o(o)$ represents the voltage appearing at the output of the amplifier immediately before the switch is turned "on", τ_2 is the "on" time of the sampling gate and

$$K_3 = \frac{R_m}{2R_{so} + R_m},$$

$$K_5 = \frac{R'_1}{R_o + R'_1},$$

$$K_6 = \frac{R'_1 + R_o}{R'_1 R_o C_o},$$

and
$$R'_1 = R_1 \parallel (R_{so} + (R_m/2)).$$

If the capacitor is completely charged before the output sampling gate is switched "on", equation 3-23 reduces to

$$\frac{v_{jo}}{v_{oc}} = K_3 \{ [K_4 - K_5] \exp(-K_6 \tau_2) + K_5 \}, \quad (3-24)$$

where
$$K_4 = \frac{R_1}{R_o + R_1}.$$

Therefore, the overall gain for the systems of Fig. 2.6 and Fig. 2.7 now becomes

$$G = G_n(2B/N)G_o(2B)\tau_1\tau_2 \{ 2K_1 [1 - e^{-K_2 \tau_1}] K_3 [(K_4 - K_5)e^{-K_6 \tau_2} + K_5] \}$$

and

$$G_c = \frac{1}{a} G. \quad (3-25)$$

In addition to the losses described, the insertion loss of the transmission media must be considered. The insertion loss for a microstrip configuration is examined in the next section.

3.4 Final Output Filter

The final output filter will be a practical filter modified by a compensation factor

$$\frac{\omega \tau_2 / 2}{\sin(\omega \tau_2 / 2)}$$

This compensation factor increases the cutoff frequency. In order to avoid spectral overlapping due to the wider filter bandwidth and the non-ideal filter characteristic, a sampling rate higher than the Nyquist rate is used. This causes the spectrum of the reconstructed signal on the output

meander delay line to have guard bands (Fig. 3.10). This increased sampling rate however requires that the N filter-amplifier elements have increased cutoff frequencies. The final filter need not require any gain, as all the gain may be realized in the low frequency amplifiers. Thus, the final filter may be a passive filter.

4.0 DESIGN OF AN EXPERIMENTAL FREQUENCY COMPRESSION SYSTEM

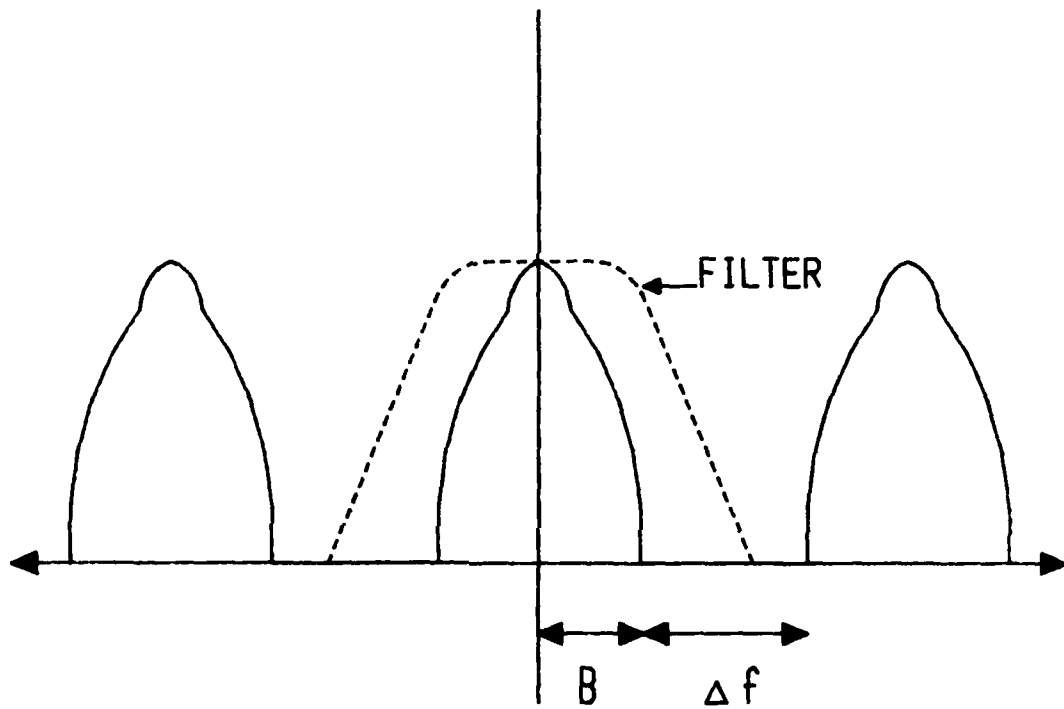
4.1 Introduction

To demonstrate the concept of frequency compression of wideband signals experimentally, a prototype device was developed. The physical characteristics of the proposed system and its design goals are introduced in this section. Considerations on the design of the the input and output meander delay lines, the sampling gate and the amplifier-filter network are described. The selection of suitable pulse generation units is also examined.

4.2 Experimental Circuit

The physical characteristics of the prototype circuit are shown in Fig. 4.1. Regions (1), (4)-(7), (12)-(15) and (18) are constructed in microstrip on a G-10 fiber-glass epoxy substrate of 0.058 inch thickness. Line (1) carries the input signal to be sampled. Element (2) serves to terminate the input meander delay line. When a sampling pulse is generated at the input to transformer (10) complementary pulses are produced at the output of the transformer. These complementary pulses travel down line (4) and (5) to "turn-on" the sampling gates (3) for a brief period of time. The inductors (8) and capacitors (9) serve to d.c. shift the output sampling pulses to aid in voltage biasing the sampling gates. Lines (6) and (7) also provide voltage bias for proper operation of the sampling gates. Once the input signal is sampled, the sampled waveforms are amplified by the amplifier circuits (11). These amplified waveforms are subsequently applied to the output delay line (18) through the output diode switch (16) at predetermined positions which are unlike the input tap positions. This newly constructed wave then propagates down the delay line (18) to its output. Element (17) is a termination resistor for the output delay line. Lines (12) and (13) correspond to the output pulse lines and lines (14) and (15) provide the voltage bias lines for the output sampler units. The transformer (21) provides the complementary output sampling pulses when triggered by a sample pulse.

The design goals for the prototype circuit were selected on the basis of a number of factors including the availability of pulse generation devices, the size of the prototype circuit and the standard impedance for microwave circuits. Design goals satisfying these requirements are given as follows:



B-BANDWIDTH
 Δf -GUARD BAND

FIGURE 3.10 - SPECTRUM OF THE RECONSTRUCTED SIGNAL AS PRODUCED BY A SAMPLING RATE HIGHER THAN THE NYQUIST RATE

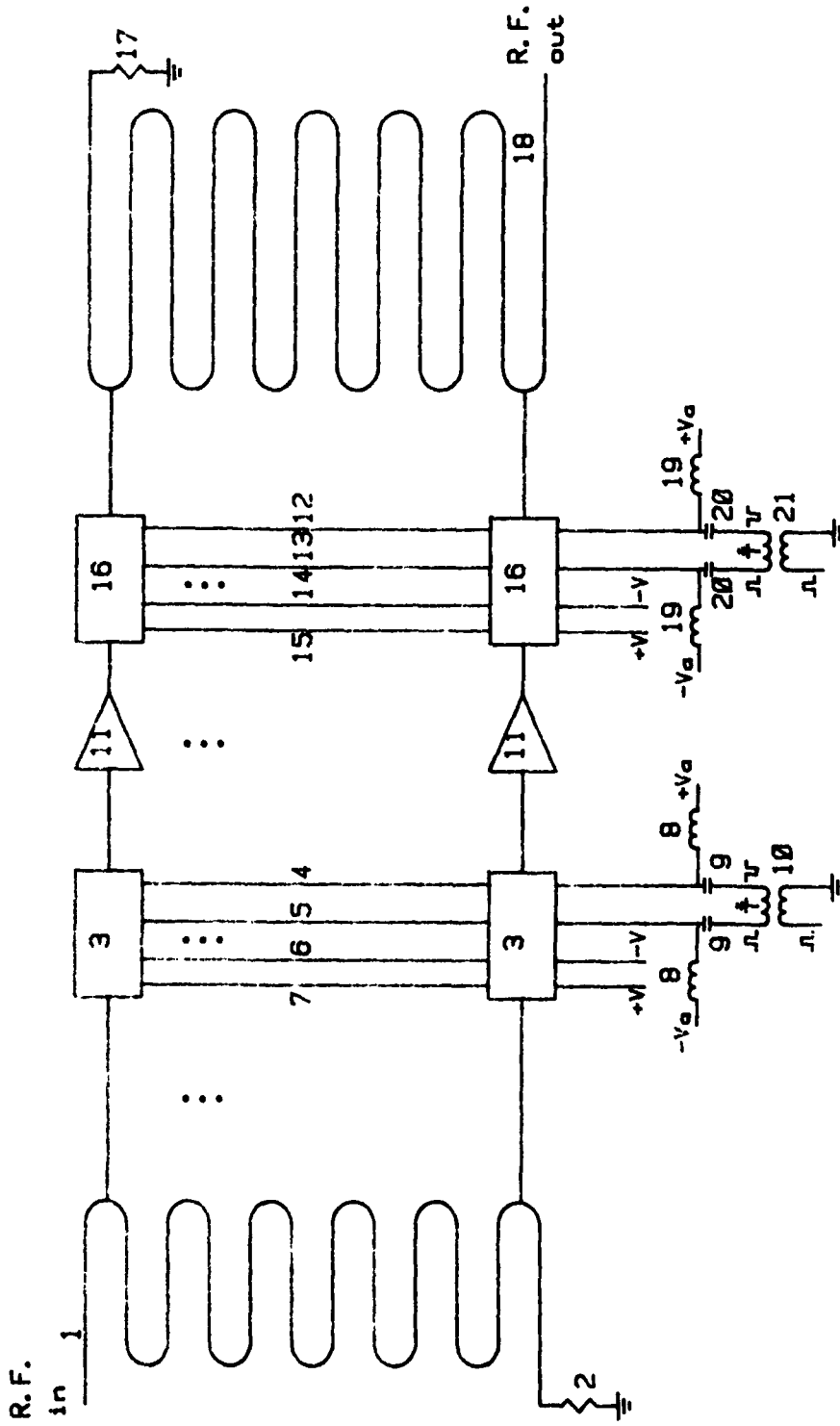


FIGURE 4.1 - PROTOTYPE FREQUENCY COMPRESSION SYSTEM

Input bandwidth	0-1 GHz
Input impedance	50 Ω
Input sampling rate	10 MHz
Frequency compression factor a	$\sim .5$
Output bandwidth	$\sim 0-500$ MHz
Output impedance	50 Ω
Output sampling rate	10 MHz
Number of parallel channels	20

A 20 channel prototype device was selected in order to verify the concept experimentally. In practical systems, this parameter may vary and is largely dependent on the application.

4.3 Delay Line Considerations

4.3.1 Introduction

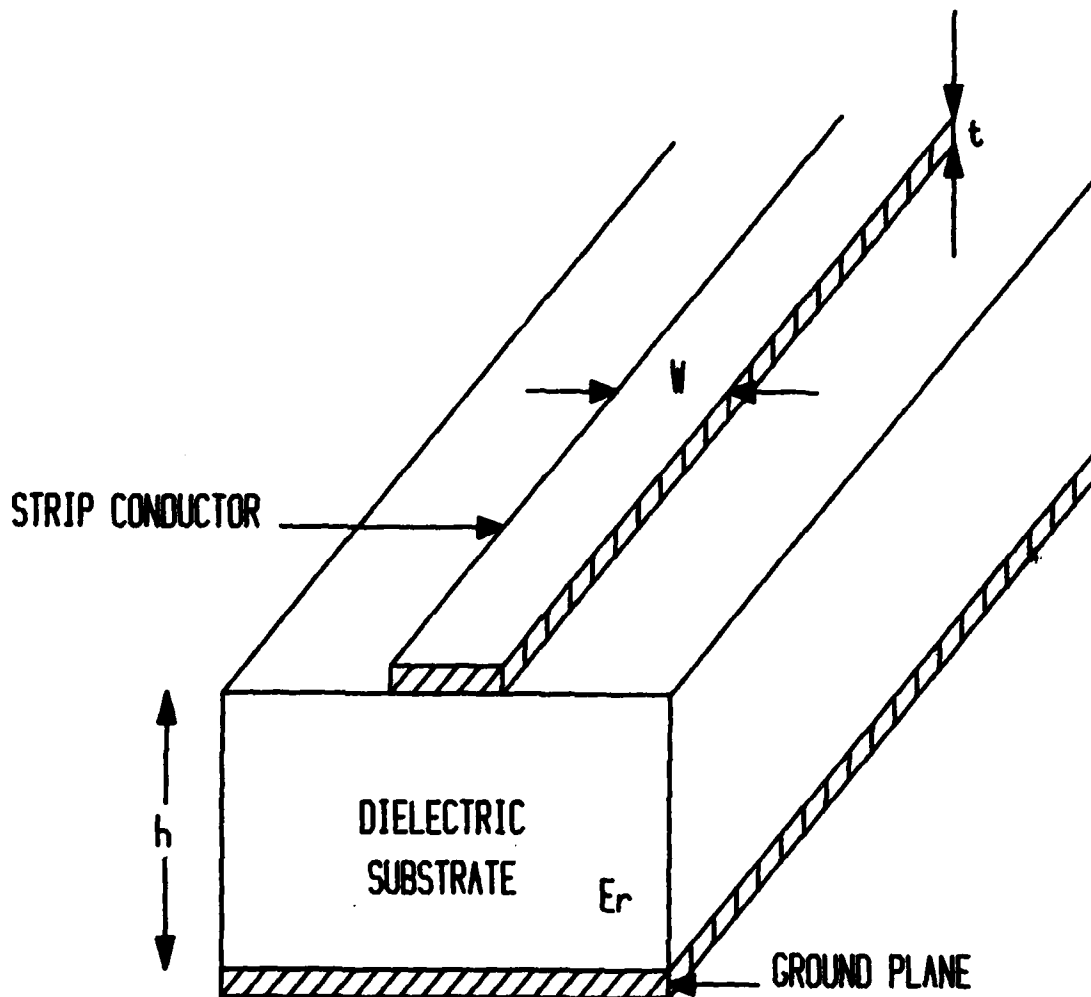
The delay lines were fabricated of microstrip using G-10 fiber-glass epoxy substrate. The ease for implementing circuits in microstrip was the primary reason for its selection. This section discusses a number of delay line considerations and parameters. This includes the determination of the strip width of the microstrip conductor for 50 Ω lines, dispersion and moding effects in microstrip, the determination of the required sampling interval (T_s) between adjacent channels and its corresponding microstrip length and finally a calculation of transmission line losses and their effects on the operation of the circuit.

4.3.2 Determination of W for a 50 Ω line

Hammerstad [12] has characterized the microstrip geometry of Fig. 4.2 for given characteristic impedances. His expressions include useful relationships which define both characteristic impedance (Z_0) and effective dielectric constant (ϵ_{eff}). The equations are expressed in terms of the dielectric constant of the material (ϵ_r), the substrate thickness (h), the strip conductor thickness (t) and the strip conductor width (W). These expressions are outlined in Appendix B. A computer program, also given in Appendix B, determines the value of Z_0 for specified W/h values. For h = 58 mils, t = 1.5 mils and $\epsilon_r = 4.7$, a strip conductor width (W) of about 104 mils is required for the 50 Ω delay lines (printout in Appendix B).

4.3.3 Dispersion and moding Effects

The formulas for characteristic impedance and effective dielectric constant are based on a quasi-TEM mode of propagation. However, at high frequency the effective dielectric constant and characteristic impedance of a microstrip line begin to change with frequency, making the transmission line dispersive. In the case of broadband operation it is



- h : SUBSTRATE THICKNESS
- t : STRIP CONDUCTOR THICKNESS
- W : STRIP CONDUCTOR WIDTH
- ϵ_r : DIELECTRIC CONSTANT

FIGURE 4.2 - MICROSTRIP TRANSMISSION LINE

therefore necessary to examine the effects of dispersion as a function of frequency. The frequency below which dispersion effects may be neglected is given by the expression [13]

$$f_0 \text{ (Ghz)} = 0.3 \sqrt{\frac{Z_0}{h\sqrt{\epsilon_r - 1}}}, \quad (4-1)$$

where h is in cm. Thus, for $Z_0 = 50\Omega$, $h = .147$ cm and $\epsilon_r = 4.7$

$$f_0 \cong 4.0 \text{ Ghz.}$$

Consequently, dispersion effects may be ignored in the prototype circuit.

Another effect which limits high frequency operation in microstrip is the excitation of spurious modes in the form of surface waves and transverse resonances. Surface waves are TM and TE modes which propagate across a dielectric substrate with ground plane. The frequency at which significant coupling occurs between the quasi-TEM mode and the lowest order surface wave mode is given by [13]

$$f_T = \frac{c}{2\pi h} \sqrt{\frac{2}{\epsilon_r - 1}} \cdot \tan^{-1}(\epsilon_r), \quad (4-2)$$

where c is the speed of light, h is the substrate thickness and ϵ_r is the dielectric constant. Therefore, for $c = 3 \times 10^{10}$ cm/sec, $h = .147$ cm and $\epsilon_r = 4.7$

$$f_T \cong 1.8 \times 10^3 \text{ Ghz}$$

Hence, moding effects are negligible in the prototype circuit.

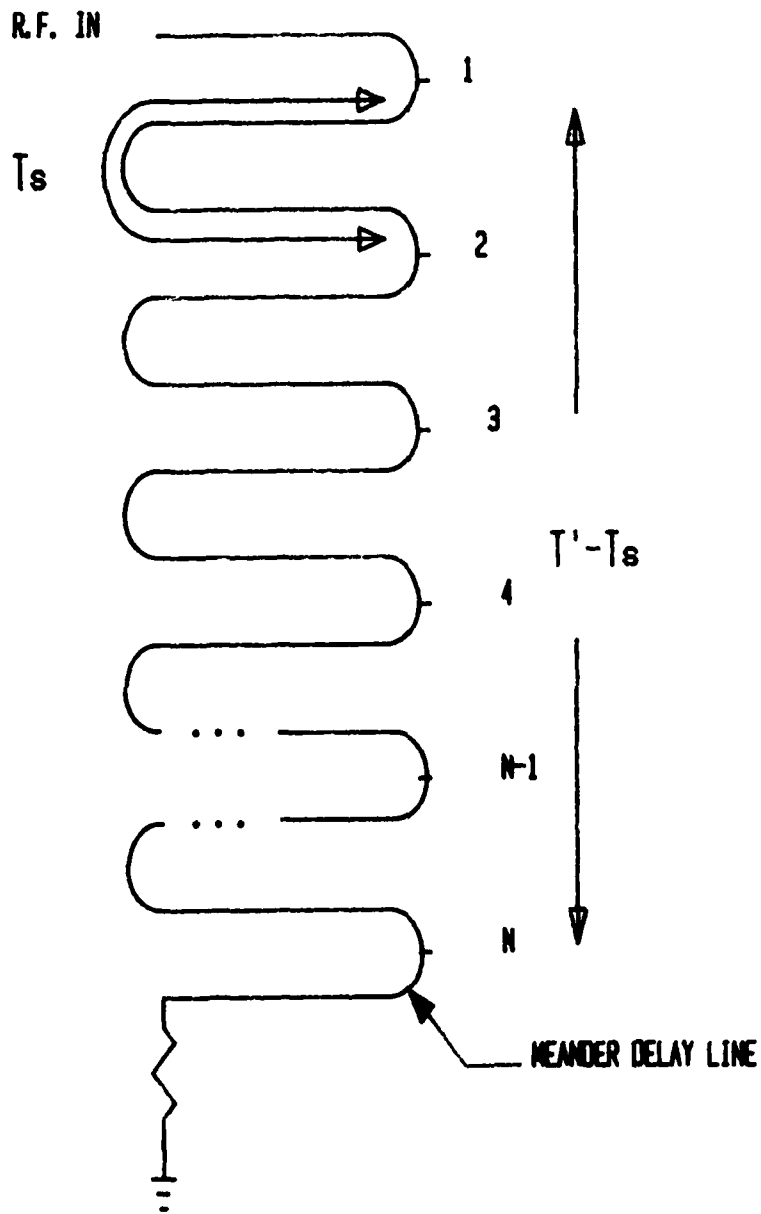
4.3.4 Determination of Sampling Interval (T_s) and Other Delay Line Parameters

The well known Nyquist sampling theorem which relates to the periodic sampling of a band-limited signal can be generalized to any group of independent samples. The more general Nyquist theorem states that any $2B$ independent samples per second will completely characterize a signal band-limited to B Hz. Alternatively, any $2BT'$ unique (independent) uniformly distributed pieces of information are needed to completely specify a signal over an interval T' seconds long [11]. Thus for the meander delay line of Fig. 4.3,

$$N = 2BT' = 2BNT_s$$

and

$$B = 1/2T_s, \quad (4-3)$$



$$T' = (N-1)T_s + T_s = NT_s$$

FIGURE 4.3 - MEANDER DELAY LINE OF DELAY TIME T' SECONDS

where N is the number of independent samples and T_s is the sampling interval (or correspondingly the propagation delay) between adjacent channels. Consequently, if all samplers are activated simultaneously, the delay between adjacent channels, T_s , completely defines the upper frequency for which a Nyquist sample set exists. Any frequency component(s) existing above this upper frequency limit will cause aliasing [8].

Under the condition of non-simultaneous sampling, T_s is modified to reflect the effective time delay (T_{se}) between adjacent channels. In the prototype device there is some finite time difference between activation of each of the sampler units. This results from the propagation delay of the sampling pulse as it travels along a pulse line. Fig. 4.4 indicates two possible conditions which influence the effective delay between adjacent channels. In the first case, when the sampling pulse propagates in the same direction as the incoming signal, the effective time delay between adjacent channels is given by

$$T_{se} = T_s - t_p, \quad (4-4)$$

where t_p represents the propagation delay time of the pulse line between adjacent channels. The opposite condition (Fig. 4.4) gives

$$T_{se} = T_s + t_p. \quad (4-5)$$

Thus for non-simultaneous sampling, the appropriate effective time delay (T_{se}) replaces T_s in equation 4-3.

The physical layout of the input side of the prototype frequency compression system is illustrated in Fig. 4.5. The spacing between adjacent channels (l_1) was set to .8 inches allowing for easy assembly of components. The input signal and sampling pulses were chosen to propagate in the same direction. Thus,

$$T_{se} = T_s - t_p.$$

For an upper frequency limit of 1 GHz

$$T_{se} = \frac{1}{2B} = 500 \text{ psec.}$$

Assuming the quasi-TEM mode of propagation, the propagation delay in microstrip is given by [13]

$$t_\lambda = \frac{1}{V_p} = \frac{\sqrt{\epsilon_{eff}}}{c}. \quad (4-6)$$

From the computer printout in Appendix B

$$\epsilon_{eff} \cong 3.525.$$

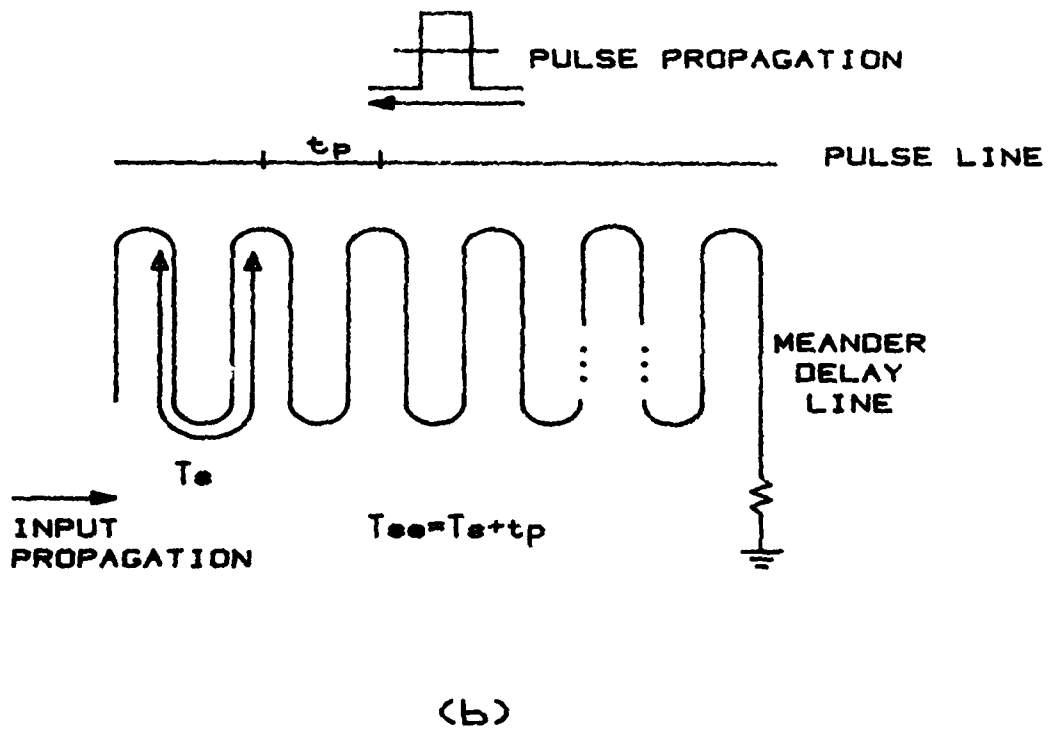
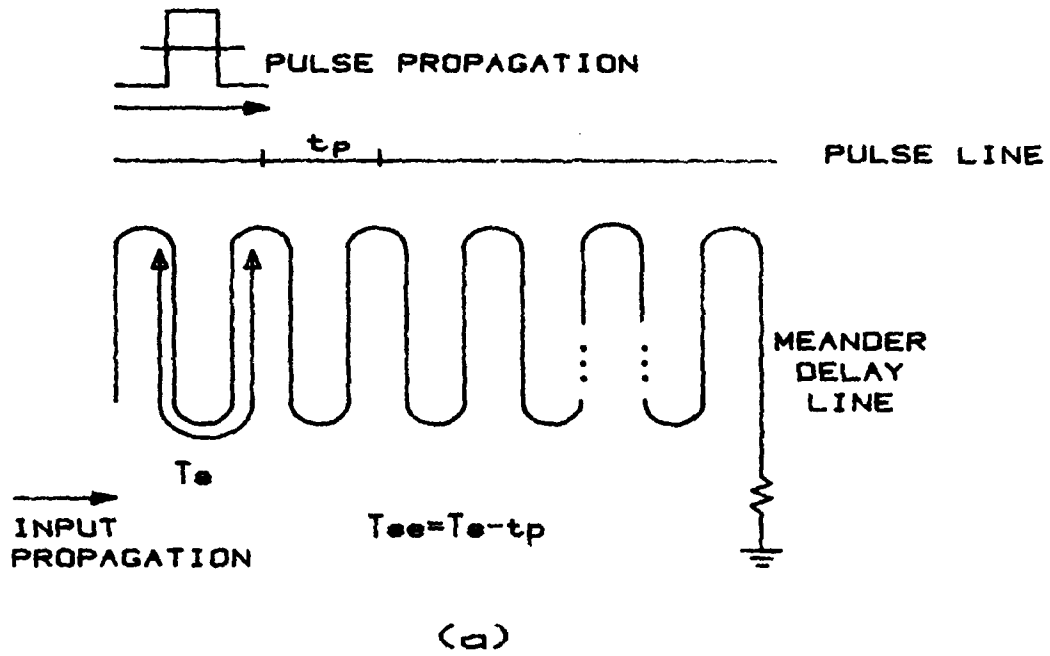
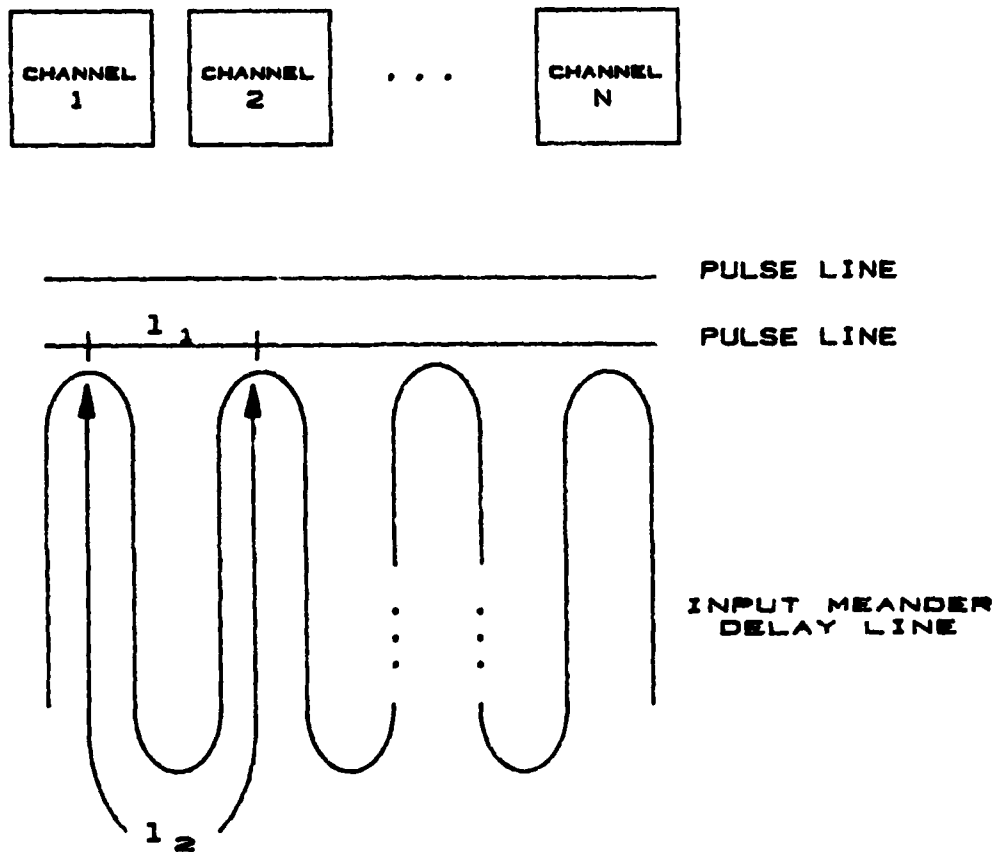


FIGURE 4.4 - EFFECTS OF THE PROPAGATION DELAY IN THE PULSE LINE ON THE MEANDER LINE'S DELAY TIME BETWEEN ADJACENT CHANNELS



l_1 - PHYSICAL LENGTH OF THE PULSE LINE BETWEEN ADJACENT CHANNELS

l_2 - PHYSICAL LENGTH OF THE MEANDER LINE BETWEEN ADJACENT CHANNELS

FIGURE 4.5 - PHYSICAL LAYOUT OF THE INPUT SIDE OF THE PROTOTYPE CIRCUIT

Thus,

$$t_{\lambda} = 62.58 \text{ psec/cm} = 158.96 \text{ psec/in.}$$

Given

$$\begin{aligned} \ell_1 &= .8 \text{ inches,} \\ t_p &= t_{\lambda} \cdot \ell_1 = 127.2 \text{ psec.} \end{aligned}$$

Therefore,

$$T_s = T_{se} + t_p = 627.2 \text{ psec}$$

and

$$\ell_2 = \frac{T_s}{t_{\lambda}} = 3.946 \text{ inches.}$$

Hence, a maximum delay line of 3.946 inches is required between adjacent taps in order to carry out frequency compression of input signals to 1 GHz. In the prototype circuit ℓ_2 was set to 3.648 inches, allowing for the acquisition of a Nyquist sample set up to a maximum input frequency (f_{imax}) of 1.105 GHz.

The output delay line was set to 6.284 inches between adjacent taps, corresponding to an output maximum frequency (f_{omax}) of 573.6 MHz.

Consequently, the compression ratio a is equal to

$$a = \frac{f_{omax}}{f_{imax}} = \frac{573.6 \times 10^6}{1.105 \times 10^9} = .5191.$$

This derivation assumes that no capacitive effects (loading) exist along the delay line. In the case of the prototype circuit this is valid at low frequencies but may not apply at higher frequencies as a result of the diode sampling gates being tapped along the line. The effect of load capacitances on signal propagation delay t_{λ} and characteristic impedance are governed by the following relationships [14]

$$t'_{\lambda} = t_{\lambda} \sqrt{1 + \frac{C_d}{C_T}} \quad (4-7)$$

and

$$Z'_o = \frac{Z_o}{\sqrt{1 + \frac{C_d}{C_T}}} \quad (4-8)$$

where C_d is the distributed load capacitance and C_T is the intrinsic line capacitance. Consequently, capacitive loading has the effect of increasing the signal propagation delay thereby lowering the upper frequency of operation and lowering the characteristic impedance.

The mask for the prototype circuit was obtained from a specialized computer-generated artwork facility available at the Communications Research Centre (CRC) Ottawa. Resolution to less than 1 mil was achieved on the mask layout.

4.3.5 Transmission Line Losses

There are two sources of dissipative losses in a microstrip circuit: conductor loss (α_c) and substrate dielectric loss (α_d). The total loss can be expressed as

$$\alpha = \alpha_c + \alpha_d \quad \text{dB/unit length.} \quad (4-9)$$

Expressions for the conductor loss derived by Pucel [15] account for the nonuniform current distribution on the conductor. These relationships, given in Appendix C, are expressed in terms of the characteristic impedance Z_0 , the dielectric substrate thickness h , the conductor and effective conductor strip width W and W_e , the conductor strip thickness t , the free space permeability μ_0 , the conductivity of the material σ and the frequency f . For a fixed characteristic impedance, conductor loss decreases inversely with substrate thickness and increases with the square root of the frequency.

In the prototype circuit, where $W/h \approx 1.80$ (Appendix B), the conductor loss is given by

$$\alpha_c = \frac{8.68 R_s}{2\pi Z_0 h} \left[1 - \left(\frac{W_e}{4h} \right)^2 \right] \left\{ 1 + \frac{h}{W_e} + \frac{h}{\pi W_e} \right. \\ \left. \left[\ln \left(\frac{2h}{t} - \frac{t}{h} \right) \right] \right\} \text{dB/cm,} \quad (4-10)$$

where R_s is the surface resistivity for the conductor and is given by

$$R_s = \sqrt{\frac{\pi f \mu_0}{\sigma}}. \quad (4-11)$$

Thus, for $Z_0 = 50\Omega$, $h = .147$ cm, $W/h = 1.844$ (Appendix B), $t = .0038$ cm, $\mu_0 = 4\pi \times 10^{-7}$ H/m, $\sigma = 5.80 \times 10^7$ u/m (copper conductor)

$$\alpha_c = 8.191 \times 10^{-8} \sqrt{f} \text{ dB/cm.}$$

Welch and Pratt [16] and Schneider [17] have derived the expression for the attenuation constant for a dielectric. The equation given by

$$\alpha_d = 27.3 \frac{\epsilon_r}{(\epsilon_{\text{eff}})^{\frac{1}{2}}} \cdot \frac{\epsilon_{\text{eff}}^{-1}}{\epsilon_r^{-1}} \cdot \frac{\tan \delta}{\lambda_0} \text{ dB/cm} \quad (4-12)$$

is expressed in terms of the dielectric constant ϵ_r , the effective dielectric constant ϵ_{eff} , the loss tangent (or dissipation factor) $\tan \delta$, and the free space wavelength λ_0 . Thus, for $\epsilon_r = 4.7$, $\epsilon_{\text{eff}} = 3.525$ (Appendix B), and $\tan \delta = .02$ (manufacturer's specification)

$$\alpha_d = \frac{0.9328}{\lambda_0} = 3.109 \times 10^{-11} f \text{ dB/cm.}$$

Consequently, the total loss is

$$\alpha = \alpha_c + \alpha_d = 8.191 \times 10^{-8} \sqrt{f} + 3.109 \times 10^{-11} f \text{ dB/cm.}$$

Plots of the total loss as a function of frequency for the input and output meander delay lines having total lengths (l) of 74.4 and 126.0 inches respectively, are given in Fig. 4.6 and Fig. 4.7.

Dielectric losses are normally very small compared with conductor losses for dielectric substrate [13]. However, in G-10 fiber-glass epoxy substrate the dielectric loss is predominant. The total loss thus increases linearly with frequency. The loss in this substrate is quite large. This will significantly reduce the frequency response, gain, output power level and efficiency. Nevertheless, it is possible to evaluate the system by de-embedding the meander delay lines. Equally, since the loss increases linearly, the overall system will remain substantially linear. This results from the fact that the signal sample which is attenuated the most at the input is attenuated the least at the output and vice-versa. The effect on the total loss by increasing the line length at the output is counterbalanced by a corresponding decrease in frequency. Consequently, linearity is preserved.

4.4 Sampling Gate

4.4.1 Introduction

Basic considerations in the selection of a sampler unit are input-to-output offset, input-to-output feedthrough in the "off" state and sample pulse feedthrough onto the output line. In a conventional discrete circuit, the commonest configuration uses a ring of Schottky diodes driven by a transformer which has the advantages of a high "on" to "off" ratio, reasonably low offset with selected devices and a degree of sample pulse feedthrough cancellation due to the balanced drive to the circuit [18]. A six-Schottky-barrier-diode arrangement was thus selected and is shown in Fig. 4.8. Each of the sampler units in the experimental device is formed of six HP 5082-2815 Schottky barrier diodes having picosecond switching times [20].

4.4.2 Six-diode Sampling Gate

When the gate of Fig. 4.8 transmits no signal, diodes D5 and D6 are conducting and acting as clamps while all other diodes are open. During signal transmission, diodes D5 and D6 are reverse biased while diodes D1 through D4 conduct.

If the points P_1 and P_2 are clamped at a voltage $V_n - V_d$ and $-V_n + V_d$ respectively, where V_d is the forward diode drop, then none of the transmission diodes (D1-D4) will conduct until V_s exceeds V_n . Therefore,

$$(V_n)_{\min} = V_s \quad (4-13)$$

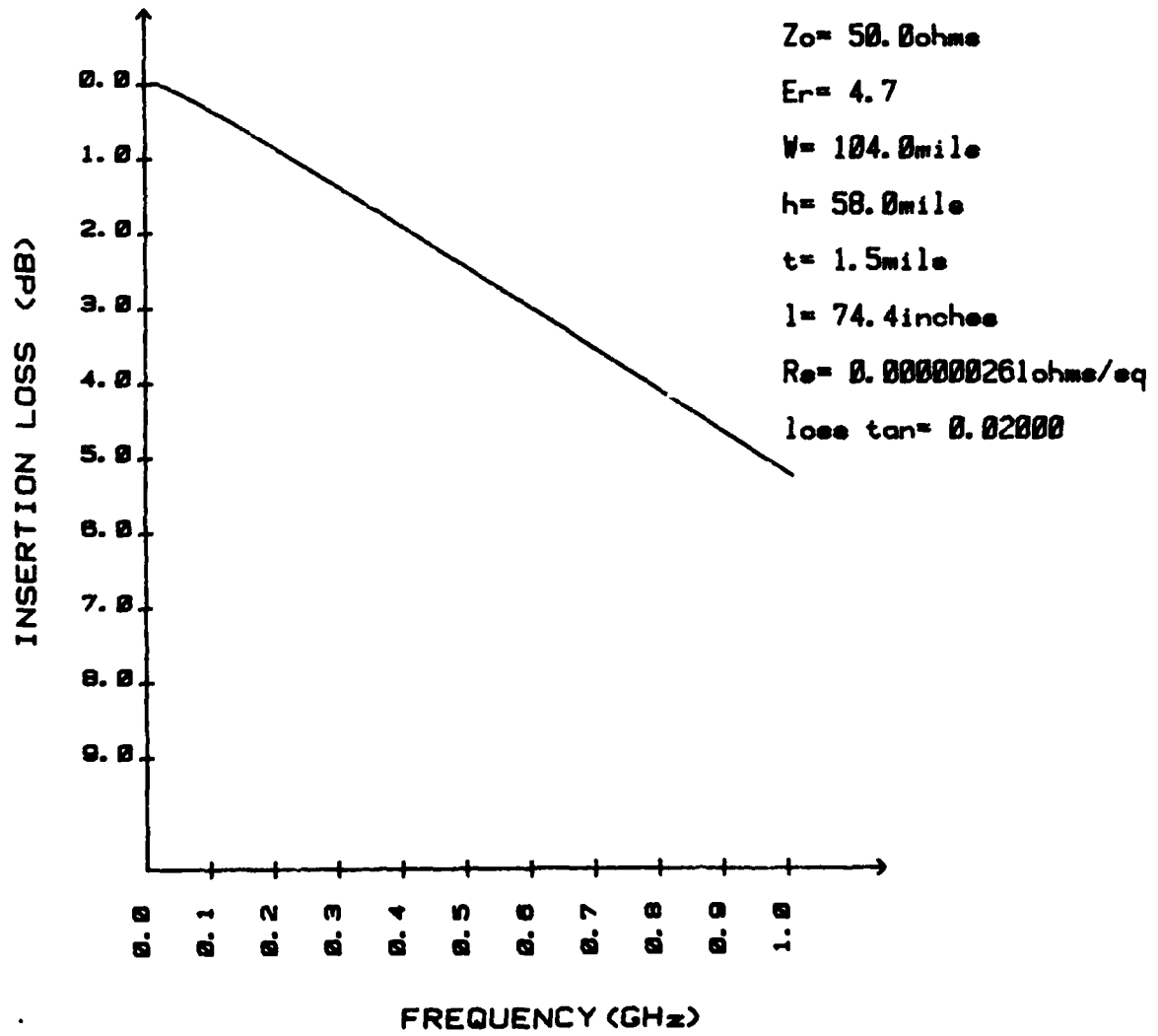


FIGURE 4.6 - CALCULATED INSERTION LOSS FOR THE INPUT MEANDER DELAY LINE

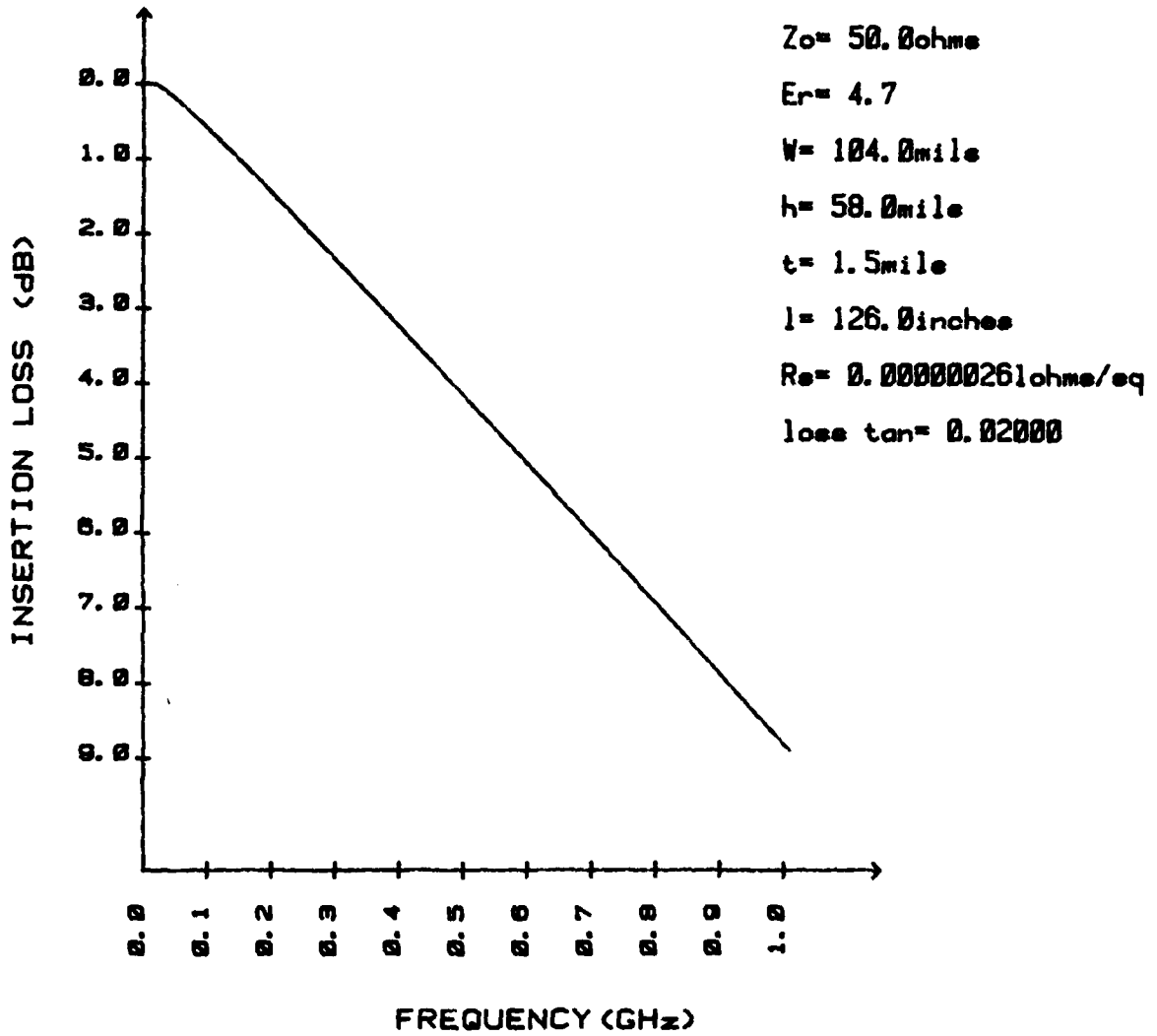


FIGURE 4.7 - CALCULATED INSERTION LOSS FOR THE OUTPUT MEANDER DELAY LINE

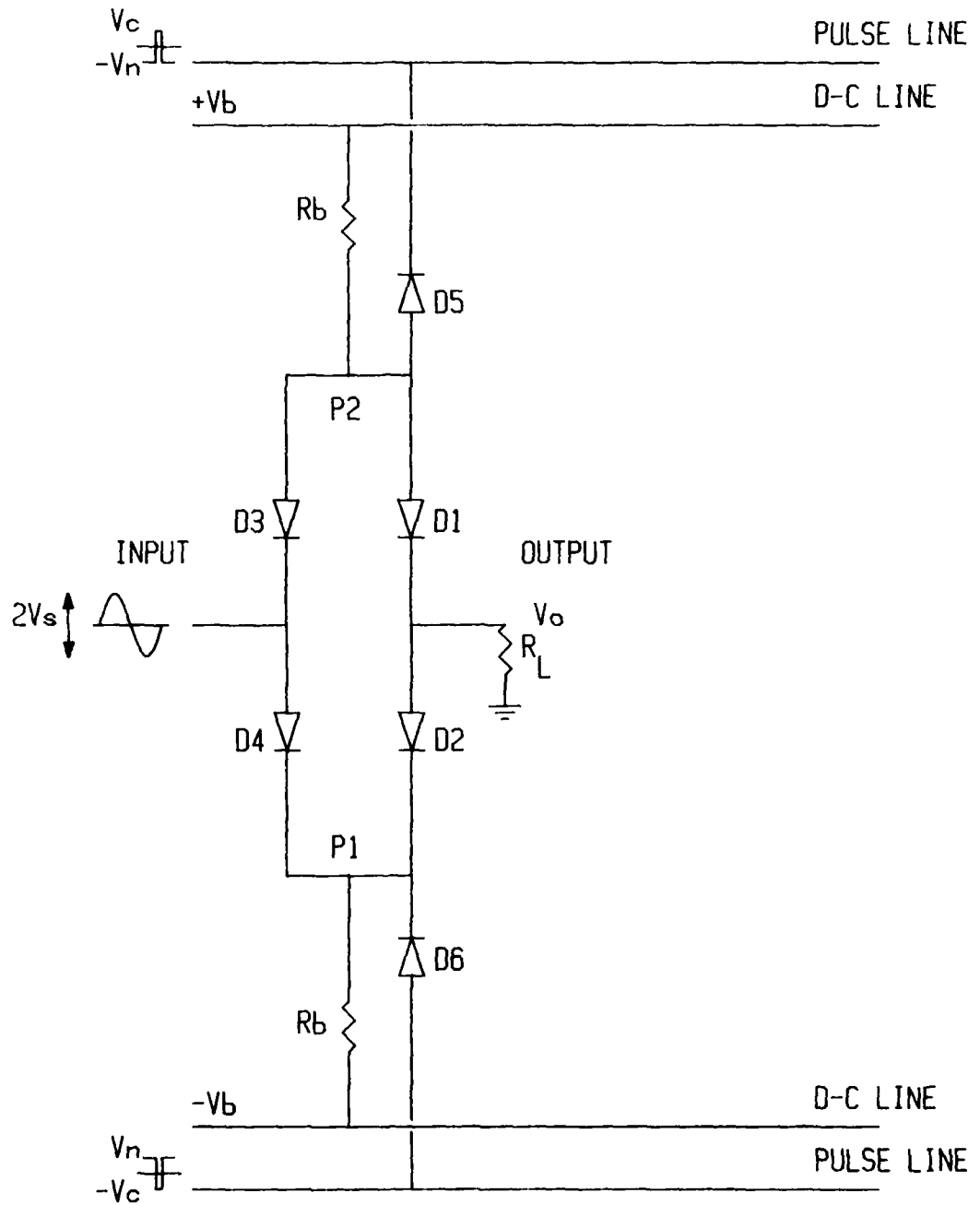


FIGURE 4.8 - DIODE SAMPLING GATE

Conversely, if the clamping diodes D5 and D6 are to remain reverse-biased for a signal amplitude V_s , then

$$(V_c)_{\min} = V_s \cdot \quad (4-14)$$

Furthermore, the required voltages V_b and $-V_b$ depend on the amplitude of the input signal V_s and are determined by the condition that the current conduction be in the forward direction for all four diodes D1 through D4. The derivation of the d.c. bias voltages is carried out in Appendix D and is given by

$$(V_b)_{\min} = \frac{2R_b + R_s}{R_s} \left[1 - \frac{R_b(R_s + 2R_L)}{(R_s + 2R_L)(R_s + 2R_b) - 2R_L R_b} \right] V_s, \quad (4-15)$$

where R_s is the forward diode resistance.

The maximum output voltage $(V_o)_{\max}$ in terms of V_b , R_b , R_L and R_s is derived in Appendix D and is given by

$$(V_o)_{\max} = \frac{2R_s R_L R_b}{(2R_b + R_s)[(R_s + 2R_L)(R_s + R_b) - 2R_L R_b]} V_b. \quad (4-16)$$

The above equations assume that the forward diode resistance R_s in all four conducting diodes are approximately equal.

4.4.3 Drawbacks of the six-diode Sampling Gate

The six-diode switch configuration, although providing picosecond sampling capability, requires a low impedance driving source. Since the diode sampling gate is largely current dependent, sufficient pulse drive is necessary to enable sampling of large signal amplitudes. When 20 samples are driven in parallel the situation is even more critical. To ease the drive requirements a relatively large resistance R_b was necessary.

Consequently, the experimental device is limited to relatively small output power levels.

A second difficulty occurs when the diodes (D1-D4) are reverse-biased in that their associated shunt and junction capacitances and lead inductances begin to limit "on" to "off" ratio of the sampling gate at higher frequencies [21]. This will limit the frequency of operation for the device.

For a maximum sampling pulse amplitude of approximately 4 volts the following design values were found suitable for the input and output sampler units in the experimental device.

$$V_n \approx V_c \approx 2V$$

$$\pm V_b = 12V$$

$$R_b = 3.9k\Omega$$

4.5 Amplifier-Filter Selection

The amplifier-filter unit was selected on the basis of the minimum bandwidth requirement. Thus, for a sampling rate of 10 MHz an amplifier bandwidth of about 5-10 MHz is required. The Motorola MC 1590G satisfies this requirement and was chosen as a result of its high gain characteristic. The layout for the amplifier network as recommended by the manufacturer [22] is shown in Fig. 4.9. From the specifications outlined in Appendix E the following parameter values are obtained:

$$C = 6.4 \text{ pf,}$$

$$R_{in} = 2500 \ \Omega,$$

$$C_o = 2.7 \text{ pf,}$$

$$R_o = 20 \text{ k}\Omega,$$

and

$$G_n = 3328$$

where G_n is the open circuit gain of the amplifier.

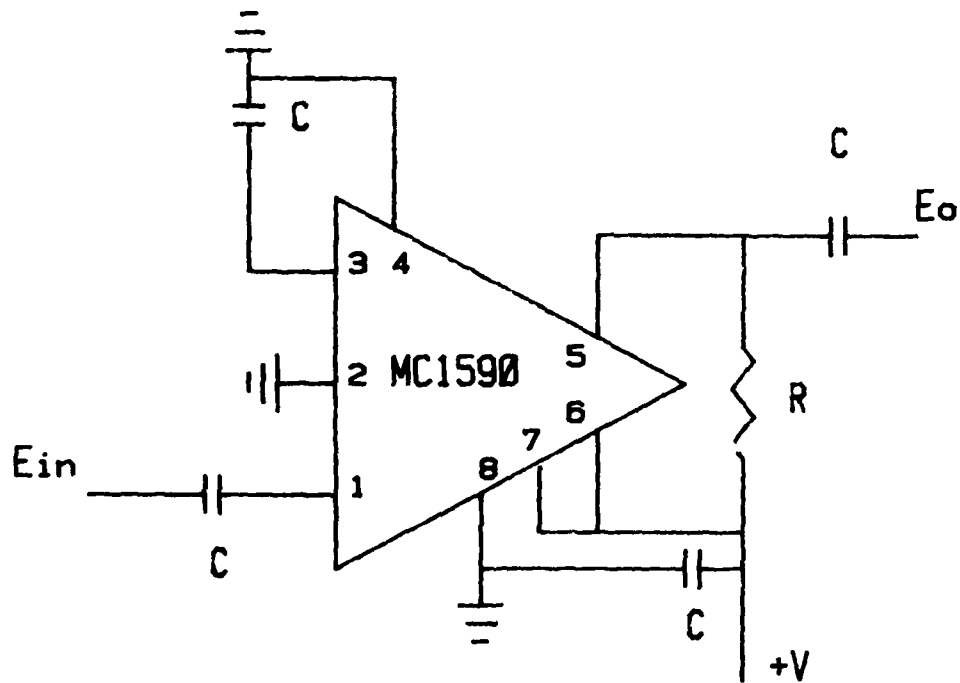
The amplifier's input RC time constant when the gate is "OFF" is given by $R_{in}C = 16$ nsec. Thus for a 10 MHz sampling rate, the input capacitor is fully discharged before the next sample is acquired. Conversely, the amplifier's output RC time constant when the switch is

"OFF" is given by $\frac{R_L R_o C_o}{R_L + R_o} = 2.6$ nsec and the output capacitor is fully

charged between samples for a 10 MHz sampling rate. Thus, in reality the practical filter impulse response as derived in Section 3 is of no consequence since interference from adjacent samples will not occur. This is because the input capacitor is discharged before the next sample is acquired. Indeed, the gain equation given in Section 3 may be used directly to compute the overall system gain.

4.6 Pulse Generation Devices

In order to provide suitable sampling pulses having picosecond pulse widths, specialized pulse generators and power splitters have been developed by Avtech Electrosystems Limited under the sponsorship of DREO. The larger units in Fig. 4.10 are impulse generators which provide 200 psec - 2 nsec pulse widths, 0-25 MHz pulse repetition rates and output pulse amplitudes to 15 volts (Fig. 4.11). The smaller units in Fig. 4.10 are special wideband power splitters which divide the input pulse into complementary positive and negative pulses (Fig. 4.12). These devices have exhibited risetimes of less than 60 picoseconds.



$R-1.0k$
 $C-1.0\mu F$

FIGURE 4.9 - VIDEO AMPLIFIER CIRCUIT

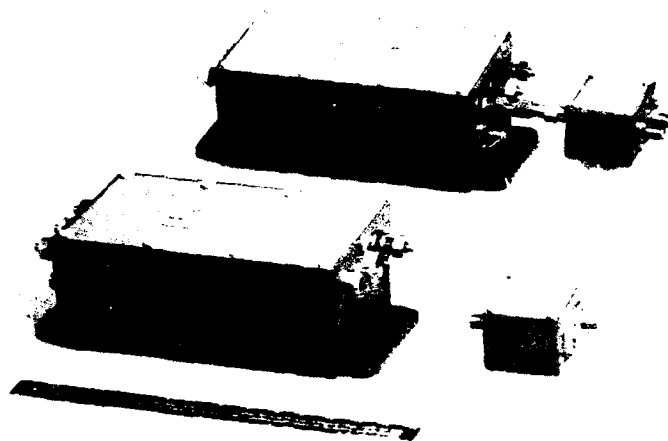


FIGURE 4.10 - PICOSECOND PULSE DEVICES

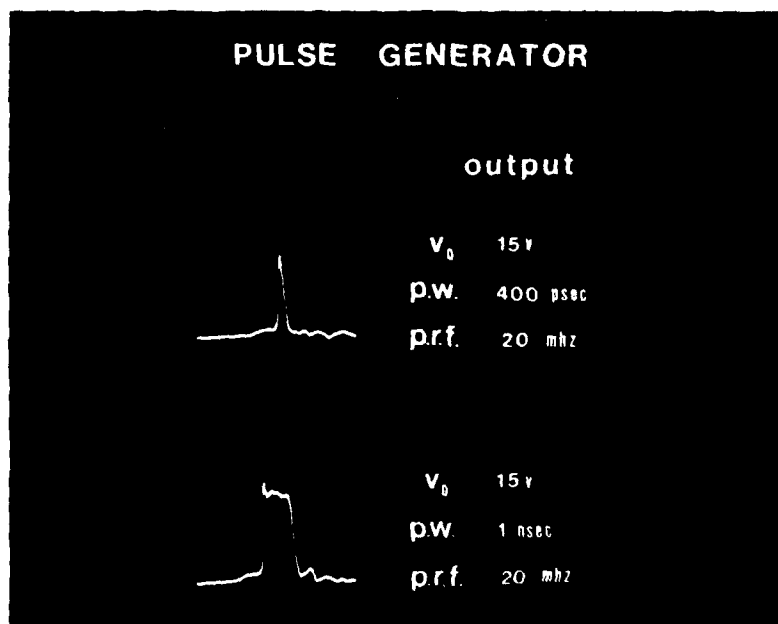


FIGURE 4.11 - TYPICAL PULSE GENERATOR OUTPUT WAVEFORMS

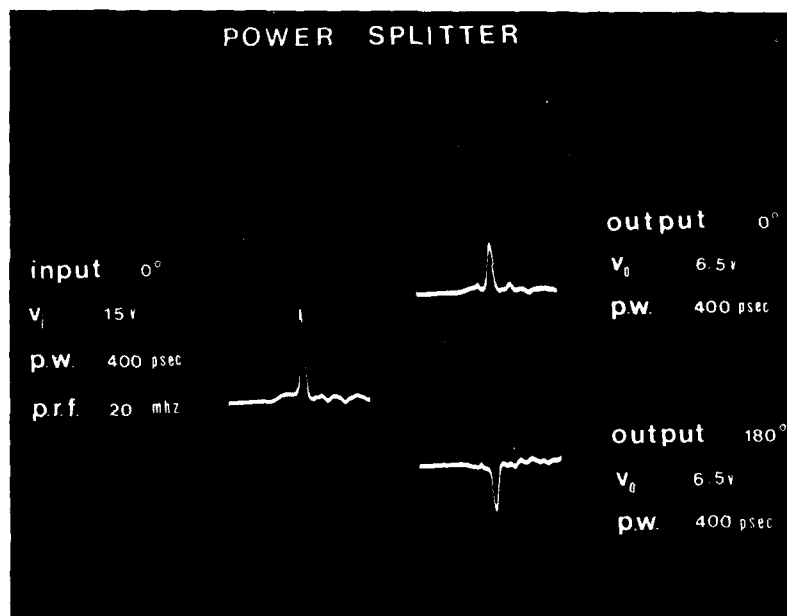


FIGURE 4.12 - COMPLEMENTARY OUTPUTS PRODUCED BY A POWER SPLITTER

5.0 EXPERIMENTAL RESULTS

5.1 Introduction

The results of the overall system performance are reported in this section. Basic subsystem parameter measurements are initially introduced in order to identify some of the system parameters and limitations. Overall system parameter measurements such as gain, frequency response and compression factor are subsequently described and compared with theoretical values.

5.2 Subsystem Parameter Measurements

5.2.1 Introduction

This section discusses a number of subsystem parameters including the insertion loss of the input and output meander delay lines for both the unassembled and assembled circuit board and the insertion loss, input to output feedthrough and "on" resistance of the sampling gate. The effect of the sampler units on the meander delay lines is also described.

5.2.2 Meander Delay Line Insertion Loss

An automated set-up was used to obtain the insertion loss for both input and output delay lines. The system set-up and programming are provided in Appendix F. The input and output insertion losses for the unassembled circuit board are shown in Fig. 5.1 and 5.2. The measured insertion losses for both input and output lines are essentially the same as the calculated insertion loss given in the previous section. There is, however, a band-reject filter characteristic present in both meander lines. The frequency at which this occurs corresponds to about one wavelength between adjacent channels (T_g). The frequency of operation is expected to be below 1.1 GHz (input) and therefore this filter-like effect will be of no consequence.

A second set of measurements were conducted on the assembled experimental circuit. These measurements were carried out with the sampler units reverse-biased to 2 volts. Fig. 5.3 and Fig. 5.4 show the insertion loss for the input and output meander delay line, respectively. Again, the measurements correspond to the calculated insertion loss given in Section 4. In addition however, there is a band-reject filter response within the expected range of operation. It will be shown that the sampler units contribute to the increase in insertion loss about the input frequency of 900 MHz. As a result of this increased insertion loss, the output frequency response of the experimental circuit will be limited to approximately 450 MHz. (The glitch in the response about 100 MHz is a result of the source being switched on.)

5.2.3 Sampler Characteristics

Measurements of insertion loss, input to output feedthrough and switch resistance were carried out on the sampling gate. Fig. 5.5

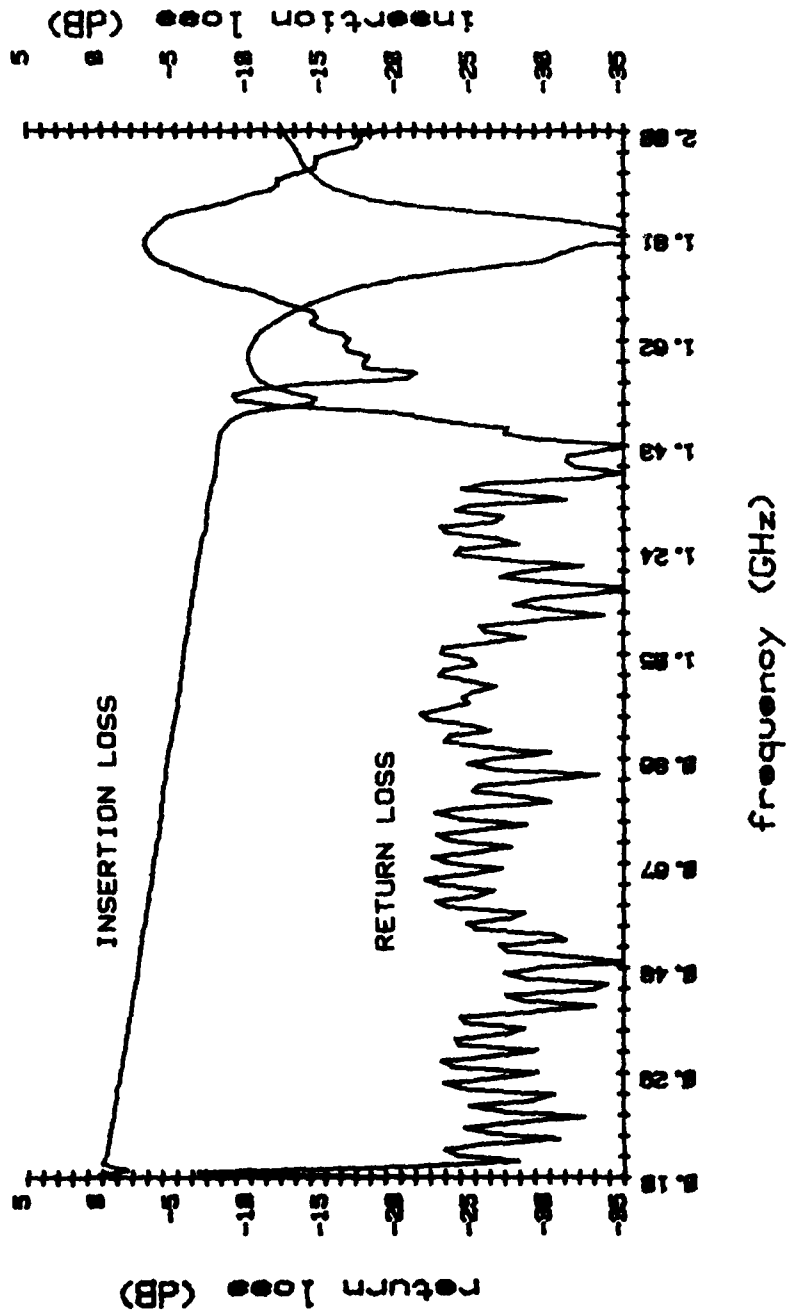


FIGURE 5.1 - INSERTION LOSS AND RETURN LOSS MEASUREMENTS OF THE INPUT MEANDER DELAY LINE FOR THE UNASSEMBLED BOARD

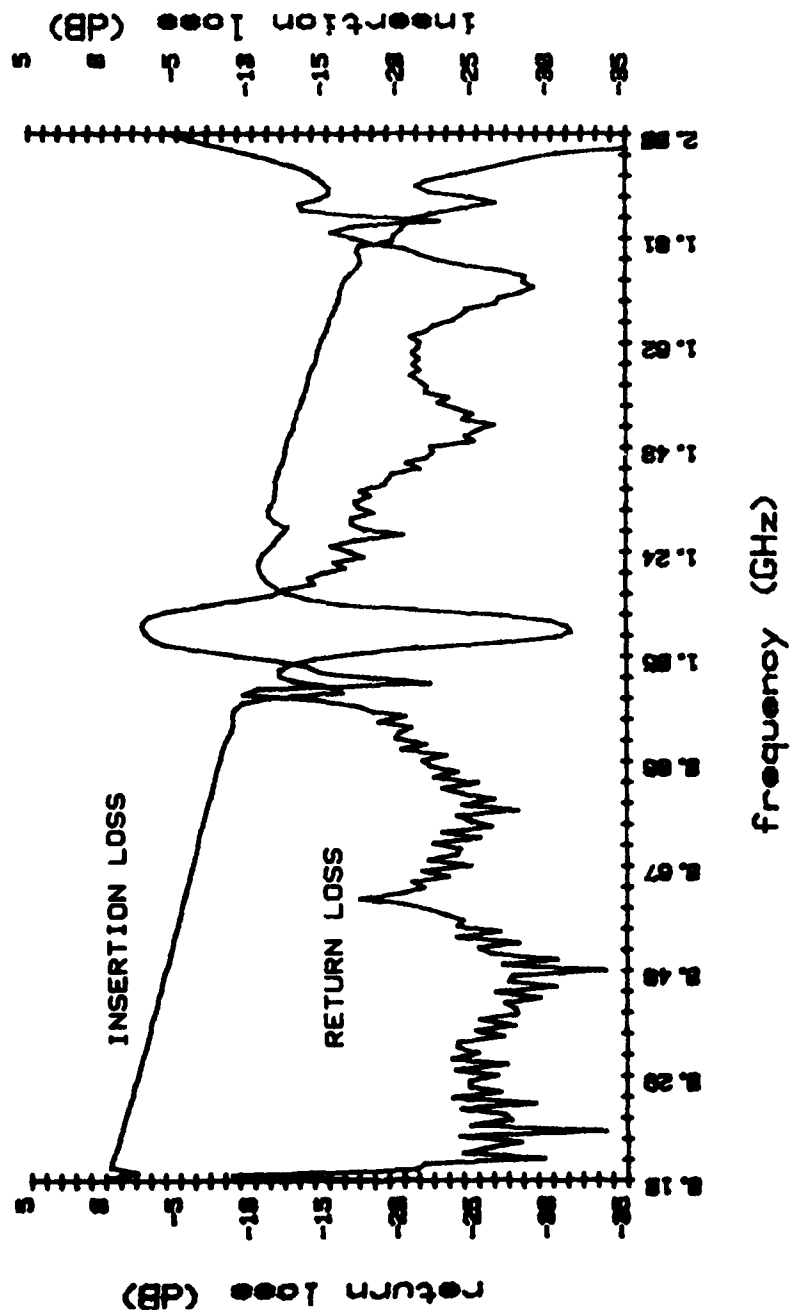


FIGURE 5.2 - INSERTION LOSS AND RETURN LOSS MEASUREMENTS OF THE OUTPUT MEANDER DELAY LINE FOR THE ASSEMBLED BOARD

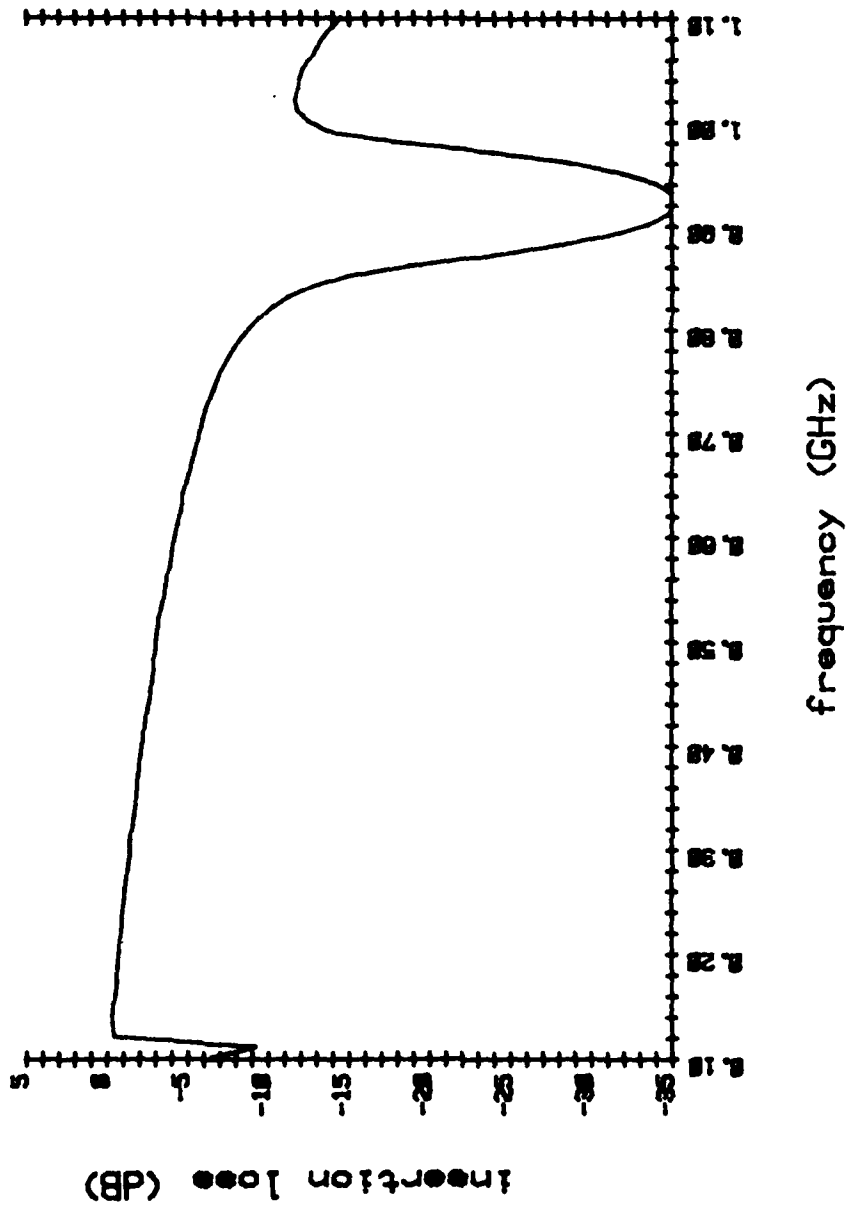


FIGURE 5.3 - INSERTION LOSS MEASUREMENT OF THE INPUT MEANDER DELAY LINE FOR THE ASSEMBLED BOARD

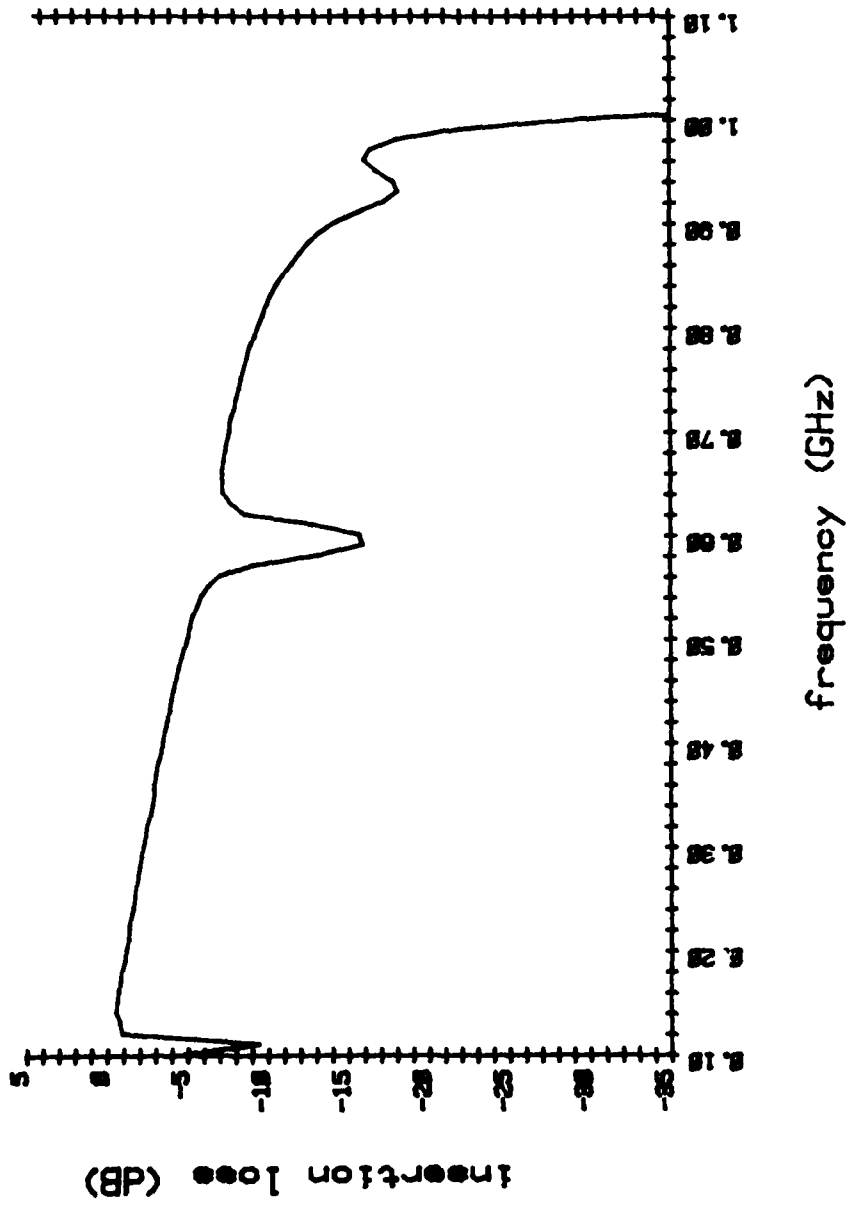


FIGURE 5.4 - INSERTION LOSS MEASUREMENT OF THE OUTPUT MEANDER DELAY LINE FOR THE ASSEMBLED BOARD

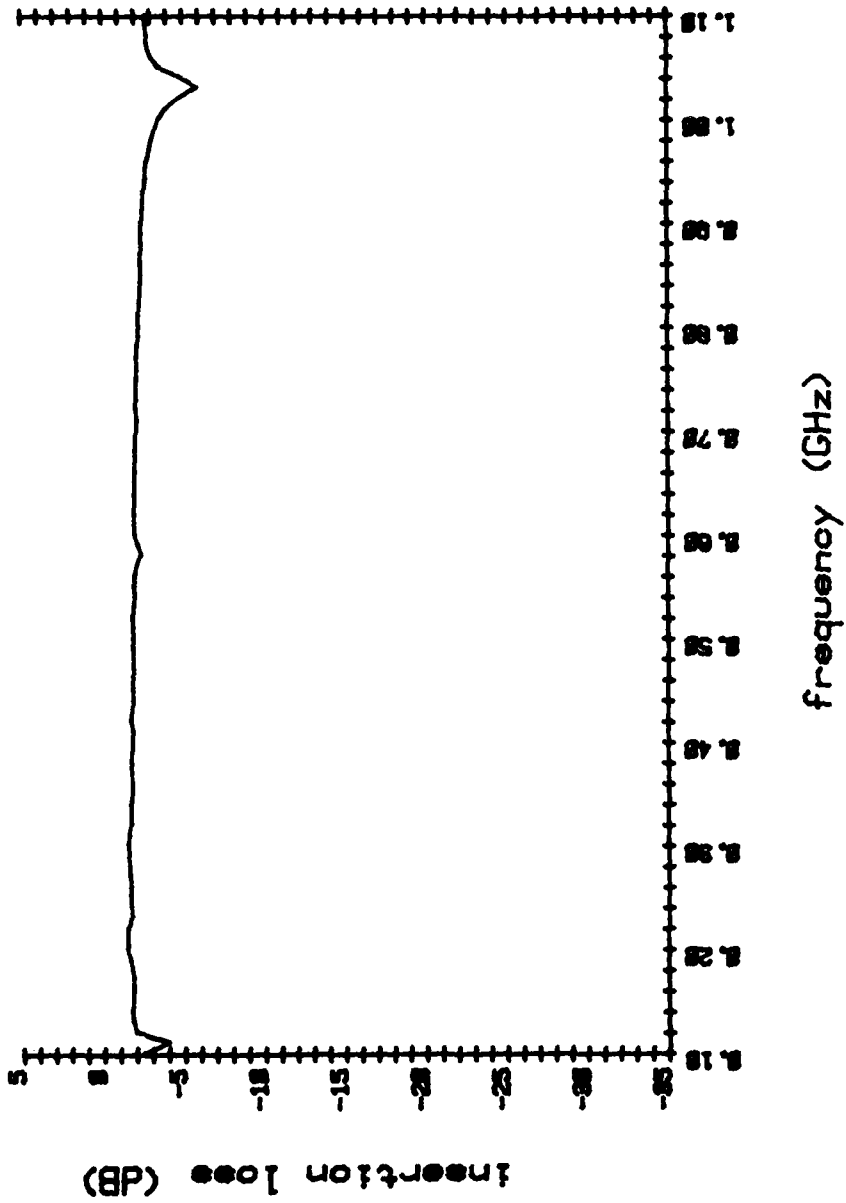


FIGURE 5.5 - INSERTION LOSS MEASUREMENT OF THE SAMPLER UNIT UNDER A FORWARD BIAS (ON) CONDITION

illustrates the insertion loss of the sampler under the forward bias ("on") condition. The response is reasonably flat over the 0-1 GHz range. The input to output feedthrough in the "off" state may be obtained by subtracting the sampler's "off" state insertion loss of Fig. 5.6 from the "on" state insertion loss of Fig. 5.5. The feedthrough component is less than -23 dB up to 800 MHz. It rises linearly from this point to 1 GHz where it reaches a maximum of -7 dB. This explains the increased insertion loss of the input meander delay line about 900 MHz.

The sampler's "on" resistance (R_s) when pulsed is different from the continuously-biased "on" condition. It is thus necessary to determine the "on" resistance of the sampler when it is pulsed with a 450 psec and 950 psec pulse. The experimental set-up of Fig. 5.7 was used to conduct this measurement. The switch resistances for the above two cases are 68 Ω (R_{si}) and 44 Ω (R_{so}) respectively.

5.3 System Measurements

5.3.1 Basic Experimental Set-up

The experimental frequency compression circuit is shown in Fig. 5.8. The input meander delay line, output meander delay line and input and output pulse lines are shown. The components (diodes, amplifiers, etc...) are situated on the back side of the board (Fig. 5.9).

Fig. 5.10 illustrates the basic experimental set-up used to measure and verify most of the system performance parameters. A frequency synthesizer served as the input signal source. All measurements were conducted with an input CW signal. A second synthesizer activated an assortment of pulse generators. Two final pulse generators provided the sampling pulses. Pulse splitters were used to provide the necessary complementary sampling pulses. Both input and output sampling pulse lines contained phase shifters. These devices aligned the sampling pulses thus insuring that their respective sampling gates were being activated by both pulses simultaneously. A sampling scope, a 1 GHz oscilloscope and a spectrum analyzer were used for conducting various measurements.

5.3.2 Sampling Pulses

The input and output sampling pulses were adjusted in accordance with the maximum pulse width criteria given in Section 4. Thus, the input and output sampling pulses were set to 450 psec and 950 psec (pulse width) about their bias points respectively (Fig. 5.11 and Fig. 5.12.). To afford maximum output power, the delay between input and output sampling pulses was set to the optimum value of 20 nsec.

5.3.3 Time Domain and Frequency Domain Responses

Fig. 5.13a shows the input and output time domain of the 20 channel frequency compression circuit. A synthesized input CW signal of 90 mv at 357 MHz translates into an output pulse signal of approximately 125 mv centered about 191 MHz. Fig. 5.13b illustrates both time domain and

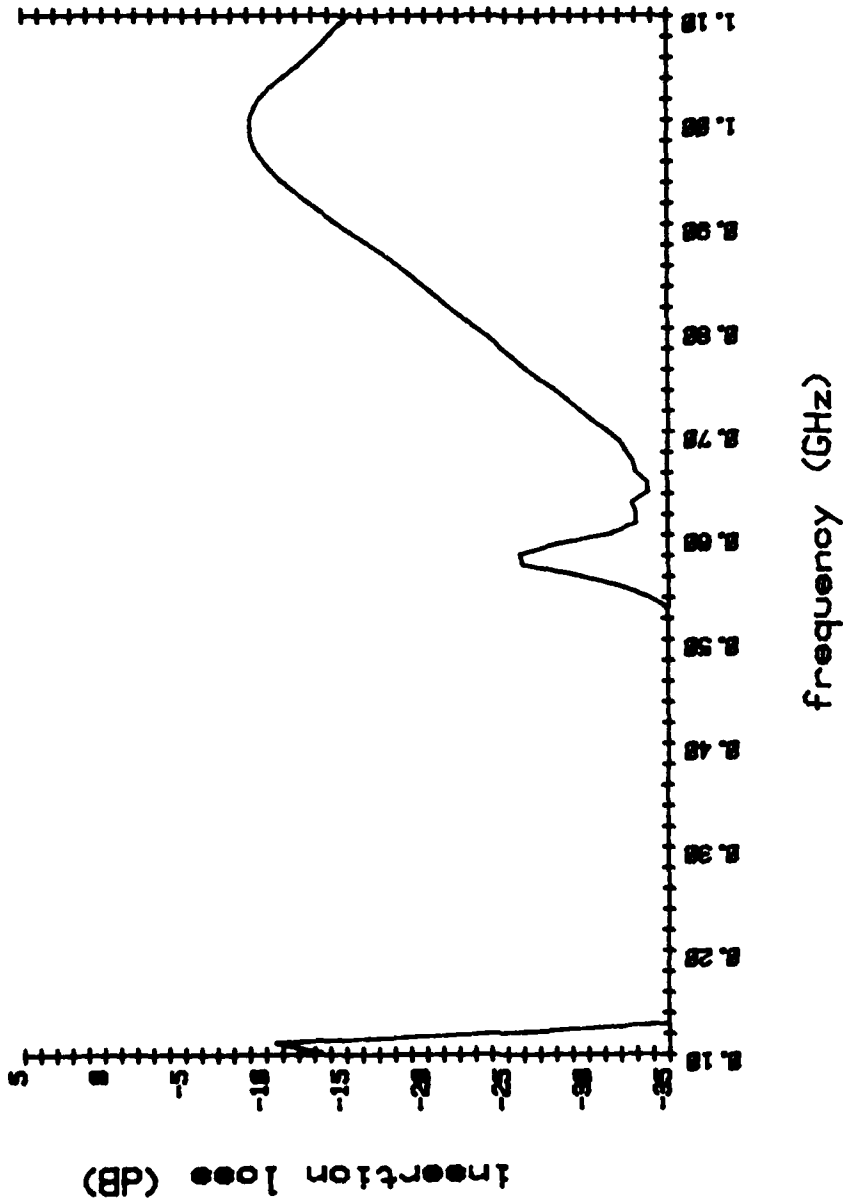
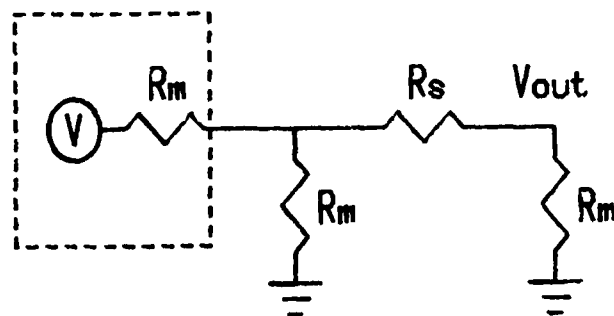
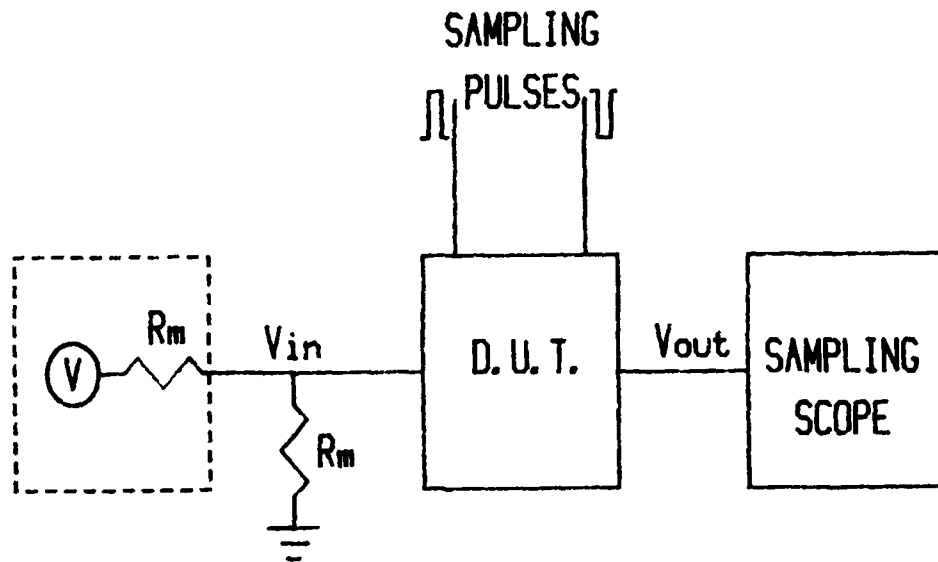


FIGURE 5.6 - INSERTION LOSS MEASUREMENT OF THE SAMPLER UNIT UNDER A REVERSE BIAS (OFF) CONDITION



$$R_s = R_m / 2 (V / V_{out} - 3)$$

(b)

FIGURE 5.7 - EXPERIMENTAL SET-UP FOR MEASURING THE SAMPLER'S ON RESISTANCE IN THE PULSED MODE

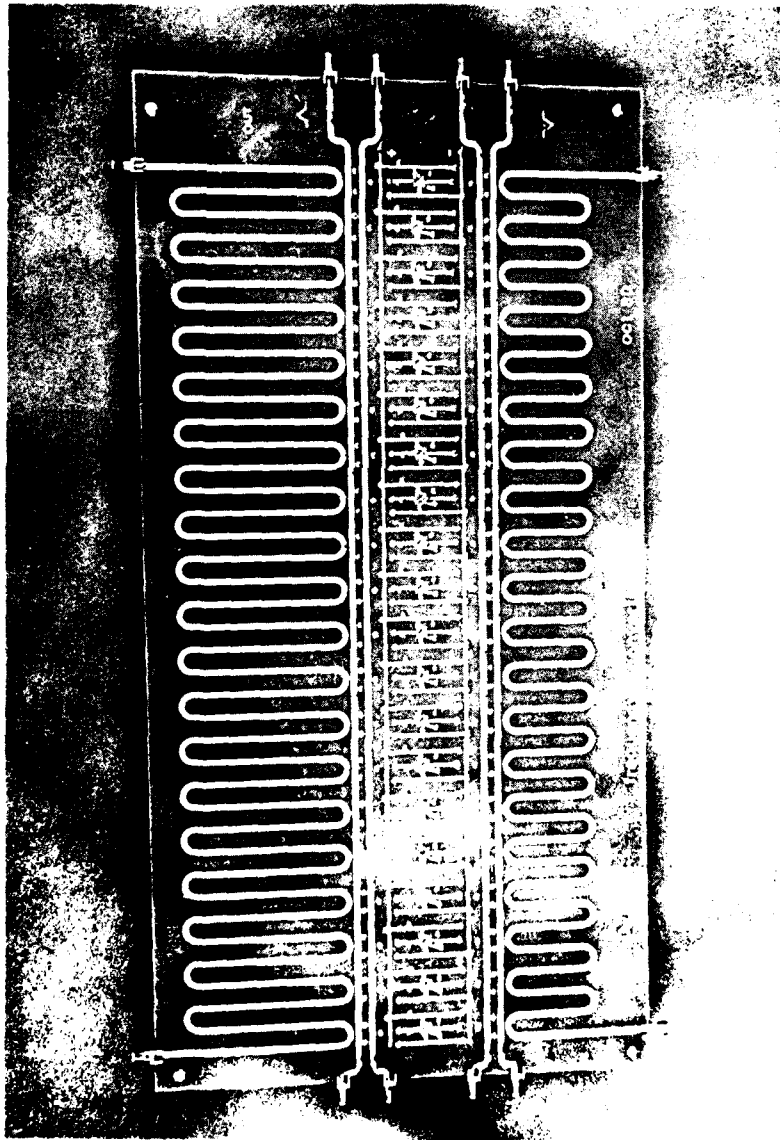


FIGURE 5.8 - EXPERIMENTAL FREQUENCY COMPRESSION CIRCUIT

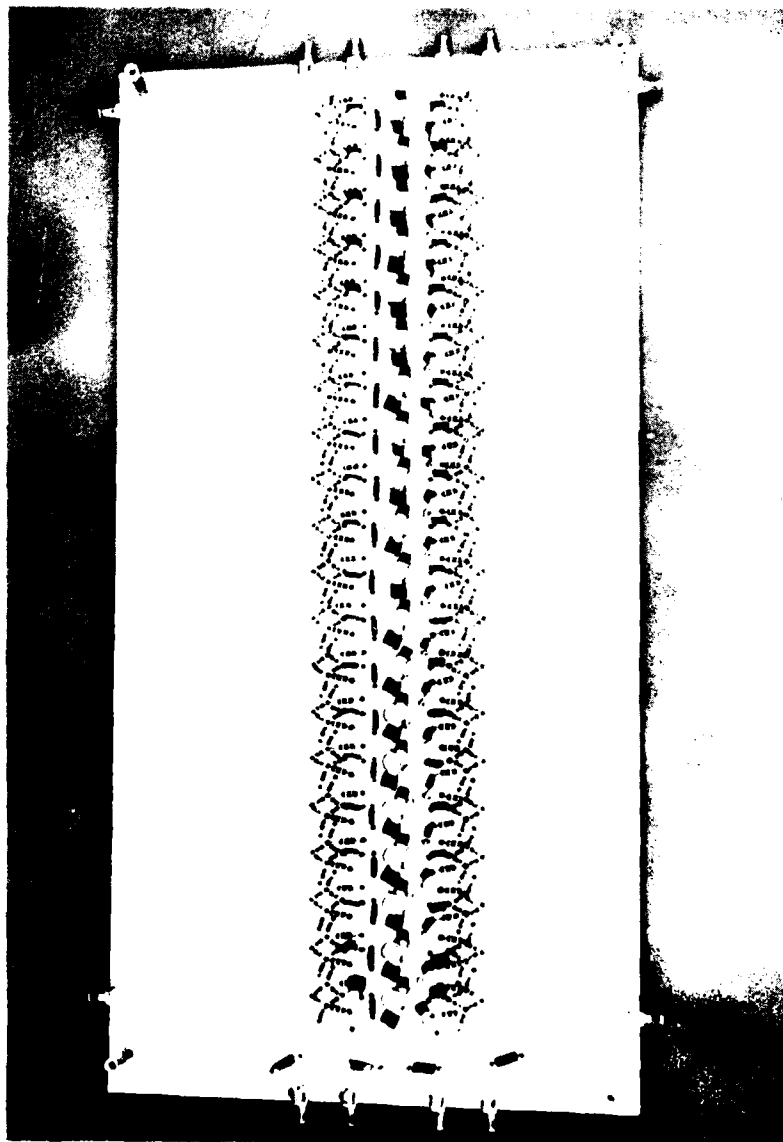


FIGURE 5.9 - COMPONENT SIDE OF THE EXPERIMENTAL
FREQUENCY COMPRESSION CIRCUIT

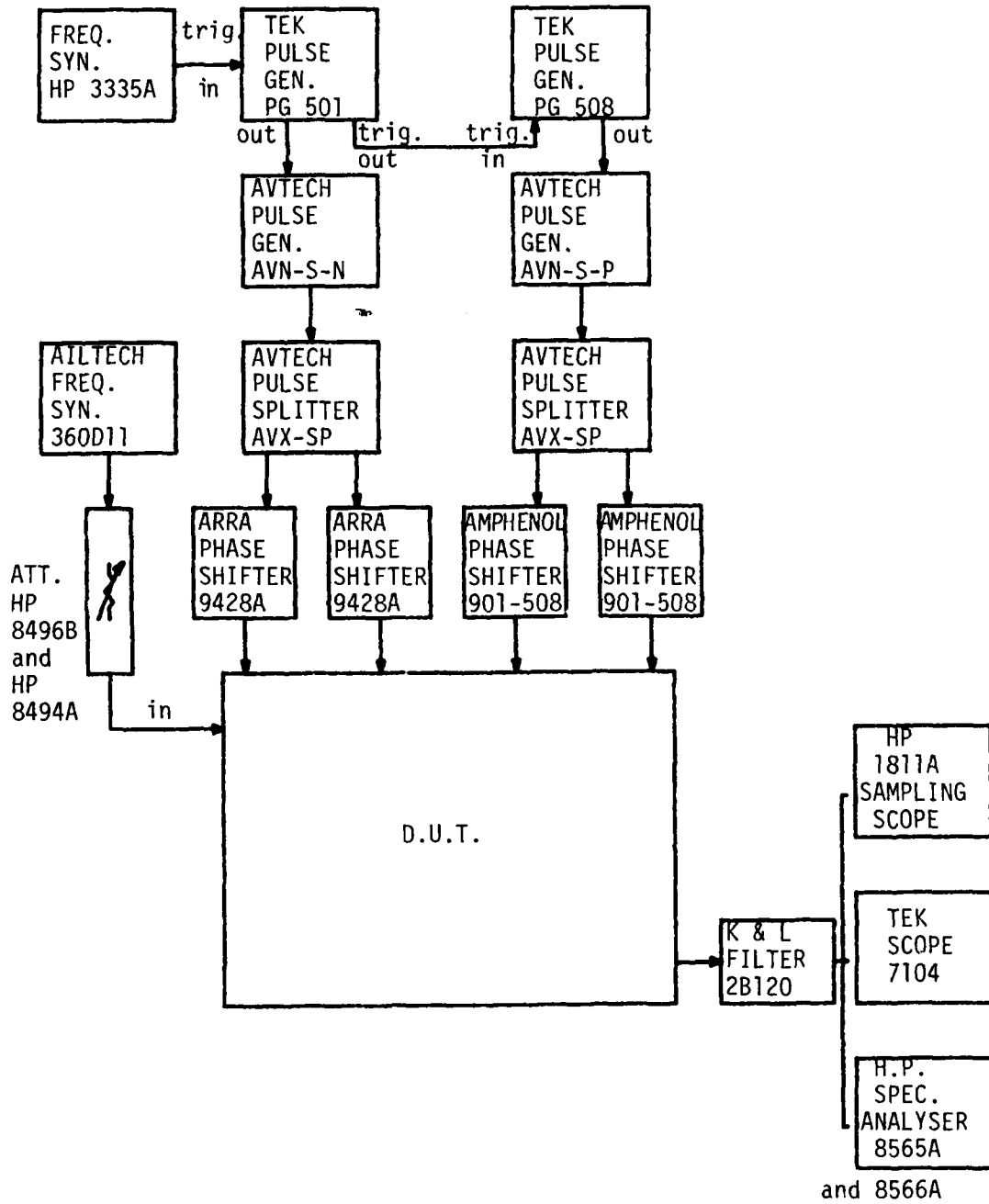


FIGURE 5.10 - BASIC EXPERIMENTAL SET-UP

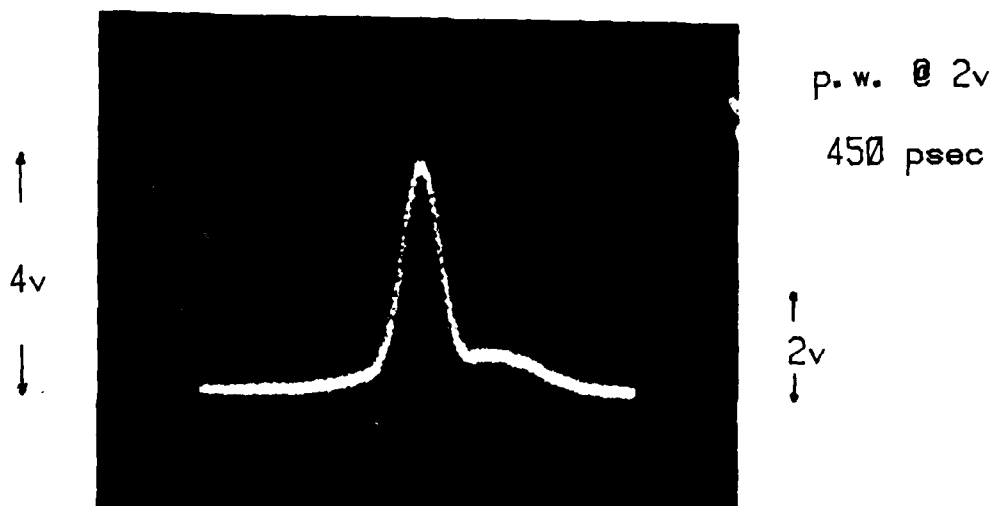


FIGURE 5.11 - INPUT SAMPLING PULSE

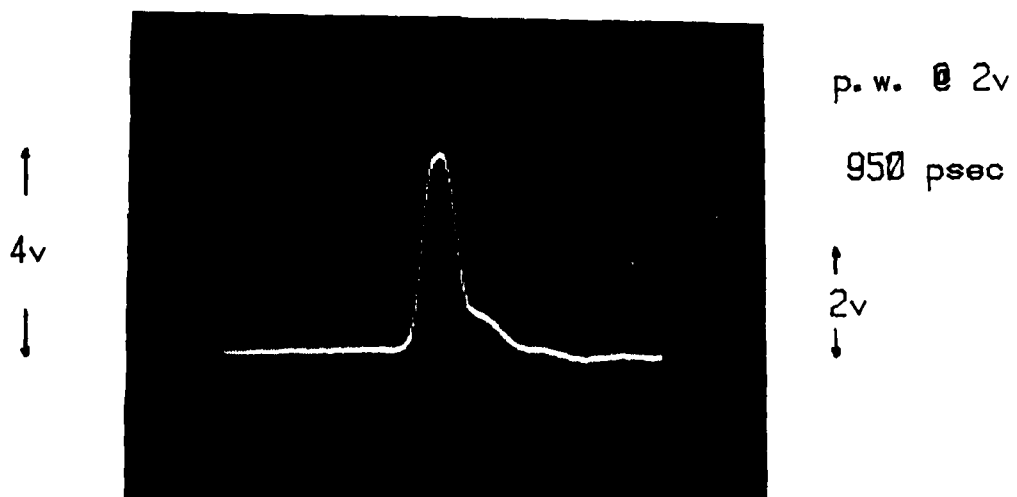
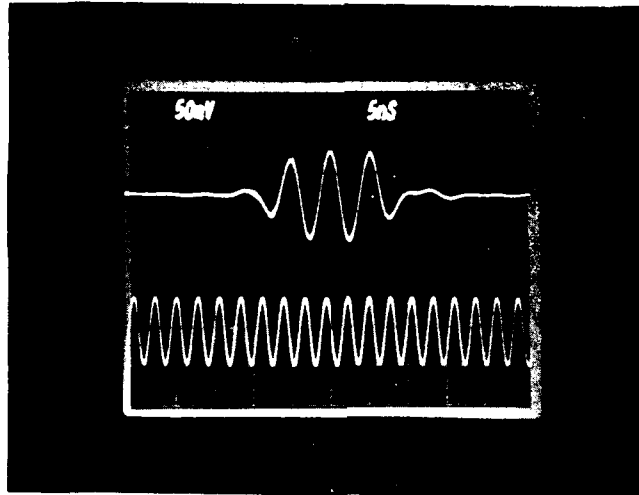
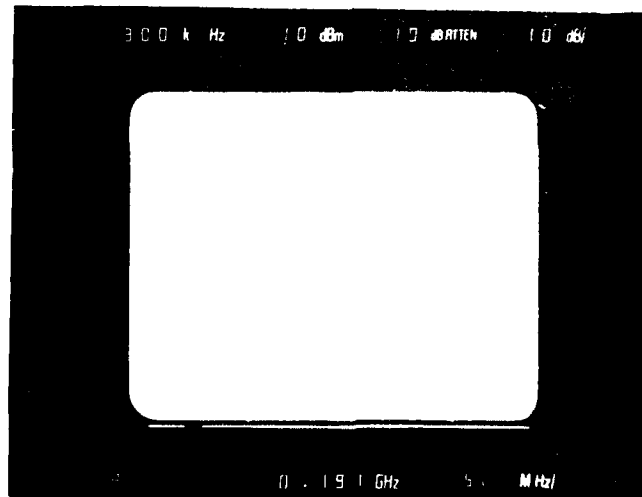


FIGURE 5.12 - OUTPUT SAMPLING PULSE



(a)



(b)

FIGURE 5.13 - (a) INPUT AND OUTPUT TIME DOMAIN WAVEFORMS
 (b) OUTPUT TIME DOMAIN AND FREQUENCY DOMAIN WAVEFORMS

frequency domain of the output signal. The output filter used in the set-up limits the $(\sin x)/x$ response of the output pulse to within its bandpass regime. The frequency domain of the input CW signal and its corresponding output pulse signal is illustrated in Fig. 5.14.

5.3.4 System Performance Measurements

Various measurements were conducted to determine the sensitivity, 1 dB compression point, dynamic range, gain and frequency response of the experimental circuit. Fig. 5.15a illustrates the output frequency spectrum of the device when an input CW signal of -17 dBm is applied. When no signal is applied, as in Fig. 5.15b, a noise spectrum is evident. These noise components result from a slight misalignment of the sampling diodes. Phase shifters were inserted to align the sampling pulses to avoid any pulse feedthrough, however, since the diodes are not accurately positioned some degree of noise is expected. Thus, the sensitivity S^* of the experimental circuit will be defined as the input signal level for which its corresponding output reaches the self induced noise level. An input signal level of -35 dBm at 357 MHz was measured for the sensitivity S^* . Accurate alignment of individual diodes would substantially decrease the self induced noise level thereby improving the sensitivity. For the unfiltered output of Fig. 5.16 no additional noise is introduced into the bandpass region.

The 1 dB compression point was measured using precision attenuators at the input to the circuit. The output was monitored on a spectrum analyzer as the input level was increased in 1 dB steps. An input of -17 dBm at 357 MHz was obtained for the 1 dB compression point.

The dynamic range defined as the difference between the 1 dB compression point and the sensitivity level S^* is therefore 18 dB.

The gain G_C given by equation 3-23 assumes the input signal is completely sampled. Since the input is a CW signal the gain of the system may be obtained by subtracting a representative "output CW" signal level from the input CW signal level. Hence, for an input CW signal of -21 dBm at 357 MHz an output pulse signal of -34 dBm about the center frequency of 186 MHz is obtained. Taking the pulse desensitization α_L [23] and the compression factor into account a representative "output CW" signal level is given by

$$-34 \text{ dBm} - 20 \log (\tau_{\text{eff}} \cdot \text{PRF}) - 20 \log a$$

where τ_{eff} is the effective pulse width of the output [15]. The effective pulse width τ_{eff} was calculated from the main frequency lobe width and has a value of

$$\tau_{\text{eff}} \approx \frac{2}{6.5 \times 20 \text{ MHz}} = 15.38 \text{ nsec.}$$

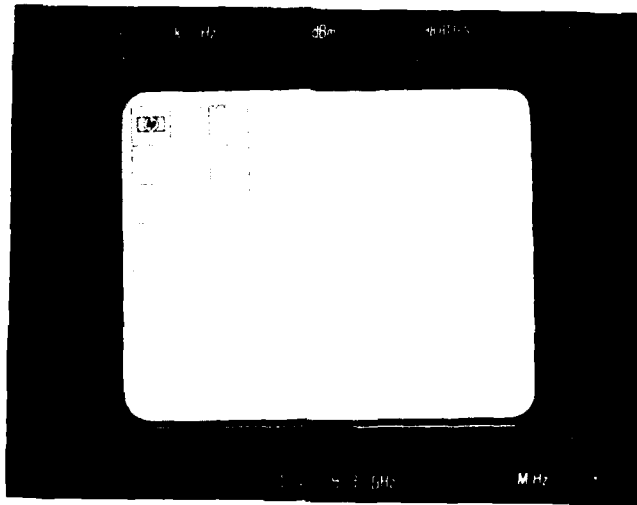
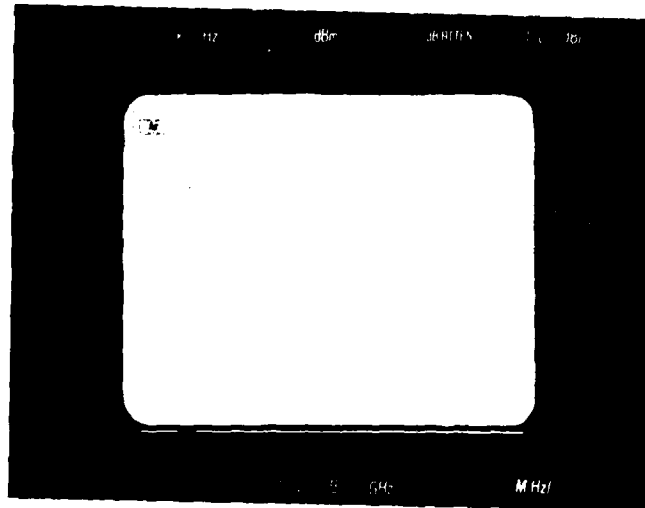
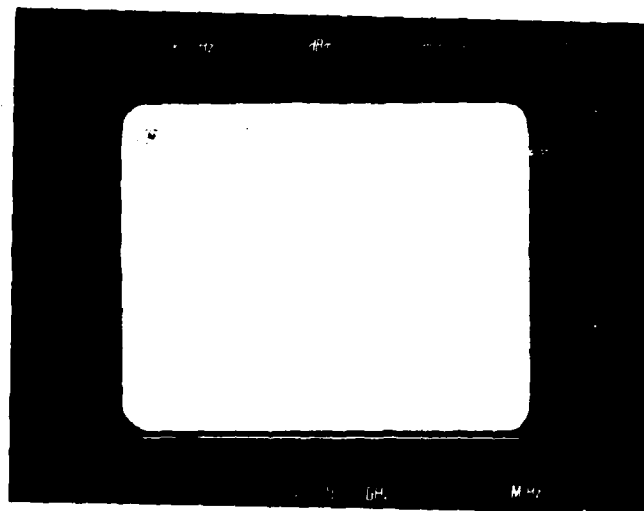


FIGURE 5.14 - FREQUENCY SPECTRUM OF THE INPUT CW SIGNAL ($f_{in} = 257$ MHz)
AND OUTPUT PULSE SIGNAL (CENTERED ABOUT 193 MHz)



(a)



(b)

FIGURE 5.15 - (a) OUTPUT COMPRESSED SIGNAL
(b) OUTPUT NOISE FREQUENCY SPECTRUM

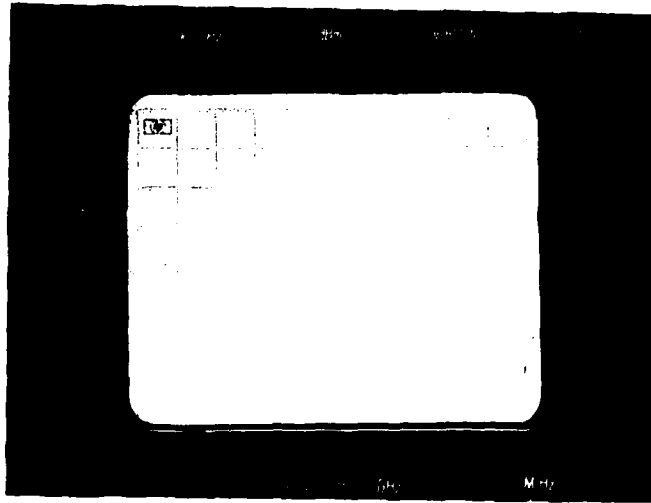


FIGURE 5.16 - UNFILTERED OUTPUT FREQUENCY SPECTRUM

Consequently, for $\tau_{\text{eff}} = 15.38$ nsec, PRF = 10 MHz and $a = .5191$ (this value is verified in a subsequent section), the representative "output CW" signal level is -12.05 dBm, resulting in a gain (G_C) of $[-12.05 \text{ dBm} - (-21 \text{ dBm})] \approx 9 \text{ dB}$. De-embedding the delay line insertion loss at the input frequency of 357 MHz produces a gain (G_C) of approximately 11 dB.

The theoretical gain (G_C) for $a = .5191$, $G_n = 3328$, $(2B/N) \cdot \tau_1 = 1$
 $2B \cdot \tau_2 = 1$, $G_o = 1$, $R_m = 50\Omega$, $R_{si} = 68\Omega$, $R_{in} = 2500\Omega$, $C = 6.4$ pf, $\tau_1 = 450$
 psec, $R_o = 20 \text{ K}\Omega$, $C_o = 2.7$ pf, $R_L = 1000\Omega$, $R_{so} = 44\Omega$ and $\tau_2 = 950$ psec
 is 12 dB.

The maximum output power level is

$$-18 \text{ dBm} + G = -14.7 \text{ dBm}$$

or -12.7 dBm for the de-embedded microstrip line. With the aid of equation 4-15, the theoretical maximum output power level for $V_b = 12\text{V}$, $R_s = 44\Omega$, $R_L = 25\Omega$ and $R_b = 3.9 \text{ K}\Omega$ is computed as -12.5 dBm.

The (output) frequency response of the system, for an output pulse width of 950 psec, is given in Fig. 5.17. The signal amplitude decreases linearly as the frequency is increased. By de-embedding the microstrip insertion loss, a 3 dB cutoff frequency of approximately 430 MHz is obtained. The cutoff frequency in this case is governed by the band-reject filter characteristic of the input meander delay line. Consequently, the theoretical cutoff frequency cannot be compared for an output pulse width of 950 psec. However, by increasing the output pulse width the cutoff frequency can be lowered enabling verification of the theoretical expression. For output pulse widths of 1.25 nsec and 1.5 nsec theoretical cutoff frequencies of $(1/2\tau_2 = B)$ 400 MHz and 333 MHz are predicted. By de-embedding the insertion loss of Fig. 5.18a and 5.18b, cutoff frequencies of 375 MHz and 300 MHz are obtained. Hence, the theoretical and experimental values closely agree. Given that present minimum pulse widths of 100 picoseconds can be generated frequency compression of signals to 5 GHz appears feasible. The perturbations in the frequency response for the wider pulse widths are a result of the sampling pulse widths being in excess of the propagation delay between adjacent output channels.

5.3.5 Frequency compression factor a

In conducting experiments on the frequency compression system with a CW signal, especially since the system is necessarily a pulse system, it is essential to interpret the results correctly. Such a situation arises in the case of an AM modulated signal. Fig. 5.19a shows a 1 KHz AM modulated CW signal applied at the input to the frequency compression circuit. The output produces a converted carrier frequency with the same 1 KHz sidebands (Fig. 5.19b). Clearly, since a major portion

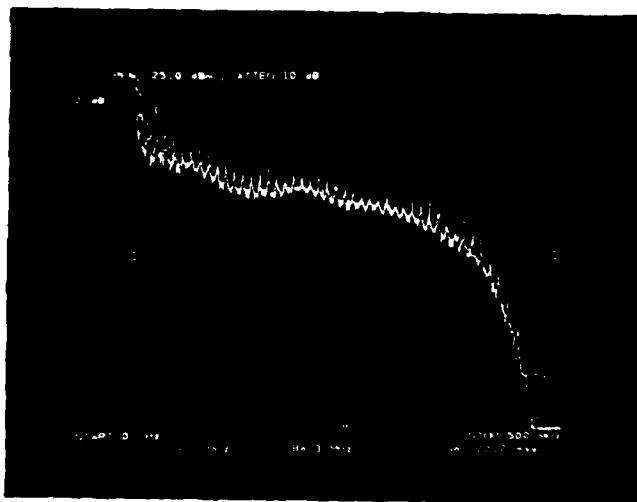
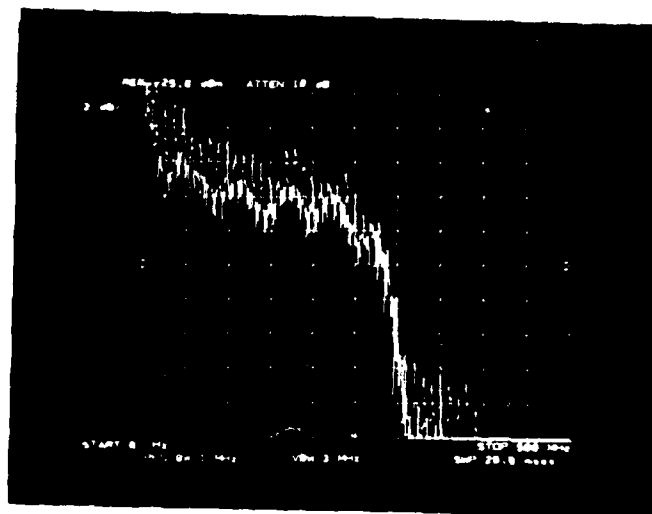
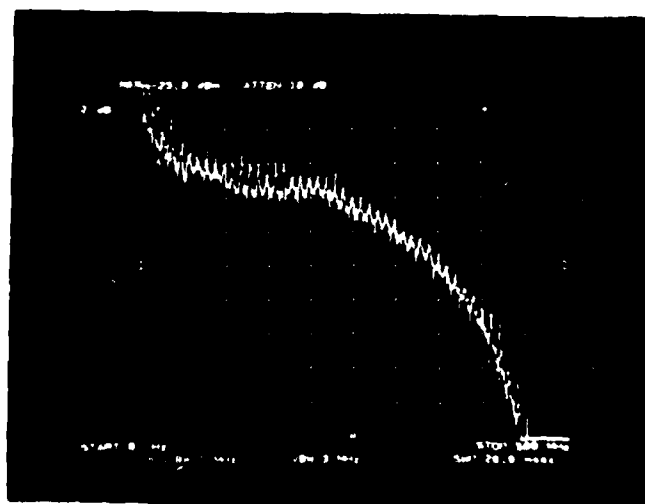


FIGURE 5.17 - OUTPUT FREQUENCY RESPONSE FOR AN OUTPUT SAMPLING PULSE WIDTH OF 950 psec

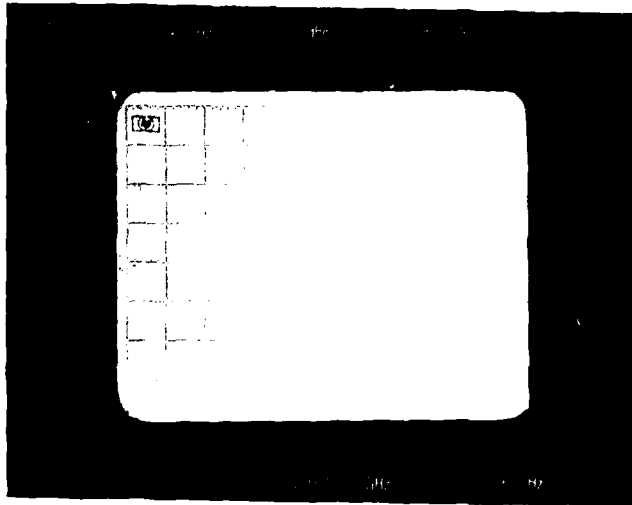


(a)

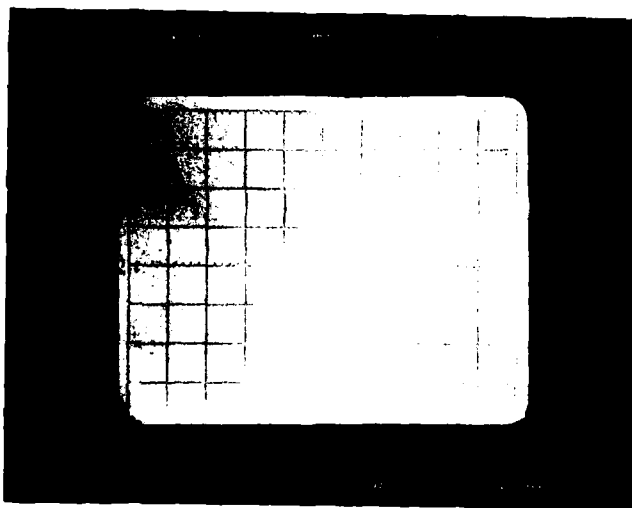


(b)

FIGURE 5.18 - OUTPUT FREQUENCY RESPONSE FOR AN OUTPUT SAMPLING PULSE WIDTH OF
(a) 1.25 nsec and
(b) 1.5 nsec



(a)



(b)

FIGURE 5.19 - (a) INPUT CW SIGNAL WITH 1 KHz 73% AM MODULATION
(b) OUTPUT CONVERTED PULSE SIGNAL

of the AM envelope is not contained within the input meander delay line, frequency compression of the 1 KHz AM modulation cannot be carried out. Consequently, the experimental frequency compression circuit has a lower frequency limit which is directly related to the delay of the input meander delay line. Indeed, this characteristic may be useful in providing carrier frequency conversion in communication systems.

A second difficulty arises when a CW signal is used for carrying out compression factor measurements on the system. It became apparent that the use of a CW signal to conduct compression factor measurements introduced a quantization effect. That is to say, only specific frequencies were being exactly compressed by the conversion factor. These frequencies had the usual and desired $(\sin x)/x$ spectrum. Other frequencies on the other hand, had uncharacteristic frequency spectrums. The top photo of Fig. 5.20a shows a properly converted signal with a correctly identified $(\sin x)/x$ dependence. Conversely, Fig. 5.20b shows an atypical frequency spectrum with two adjacent frequency components of equal amplitude with no clearly identifiable center frequency component.

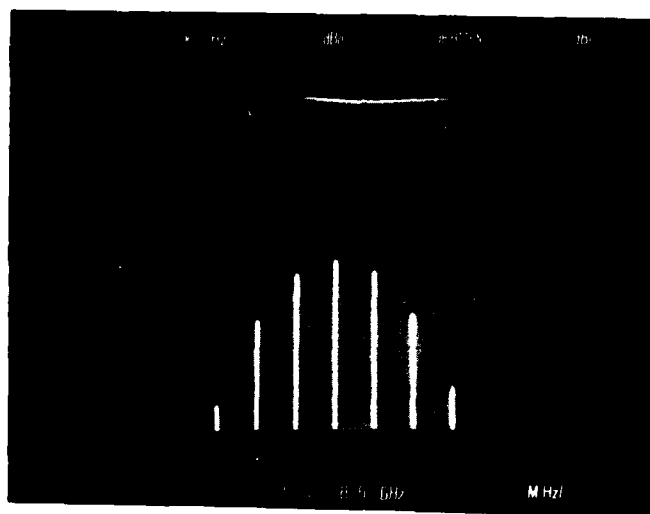
Table 5.1 indicates the experimentally determined frequencies for which a $(\sin x)/x$ dependence is clearly established for a 10 MHz PRF. The nature of this dependence appears to be related to the phase error introduced at the output for various input frequencies. For certain input frequencies a continuous output phase from pulse to pulse is established as shown in Fig. 5.21a. However, at most other frequencies a phase discontinuity (or error) is introduced, thereby altering the output frequency spectrum. The theoretical input frequencies which give a continuous phase relationship for the output converted signal for a compression factor of a $\approx .5191$ and PRF = 10 MHz are given in Table 5.2. Examination of Tables 5.1 and 5.2 suggest a strong correlation between experimental and theoretical values. Consequently, it is postulated that the phase error introduced by using a CW signal to carry out frequency compression causes the output to be uncharacteristic. It is further postulated that if an input pulse signal were completely sampled, frequency compression by a fixed factor would be possible at every frequency. Since the input meander delay line is relatively short (9 nsec) experimental verification of the above was not possible.

5.3.6 Multiple Signal Reconstruction

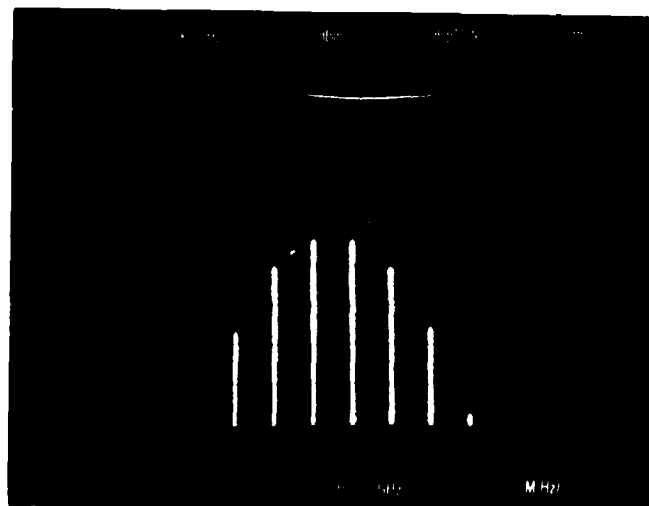
The frequency compression system is capable of handling multiple simultaneous signals. Fig. 5.22 shows a single output pulse signal centered at 268 MHz. Application of a second input signal at 307 MHz produces a corresponding output pulse signal centered at 159 MHz. No deterioration in amplitude or deviation of frequency is apparent indicating that the system is linear. The maximum input (and output) amplitude of individual signals will be further limited since the 1 dB compression point is a function of the combined signal levels.

5.3.7 Summary of Results

A summary of the results is given in Table 5.3. Both experimental and de-embedded experimental values are shown. Theoretical values which exclude the meander delay line's insertion loss are also given.



(a)



(b)

FIGURE 5.20 - (a) USUAL AND DESIRED $(\sin x)/x$ SPECTRUM
(b) ATYPICAL $(\sin x)/x$ SPECTRUM

TABLE 5.1

EXPERIMENTAL INPUT AND OUTPUT FREQUENCIES FOR THE
USUAL AND DESIRED OUTPUT $(\text{SIN } x)/x$ SPECTRUM

f_{in} MHz	f_{out} (center component) MHz	$\frac{f_{out}}{f_{in}} = a$
398	207	.520
377	196	.520
357	186	.521
334	173	.518
313	162	.518
293	152	.519
272	141	.518
252	131	.520
231	120	.520
211	110	.521
189	98	.519
168	87	.518

uncertainty ± 1 MHz

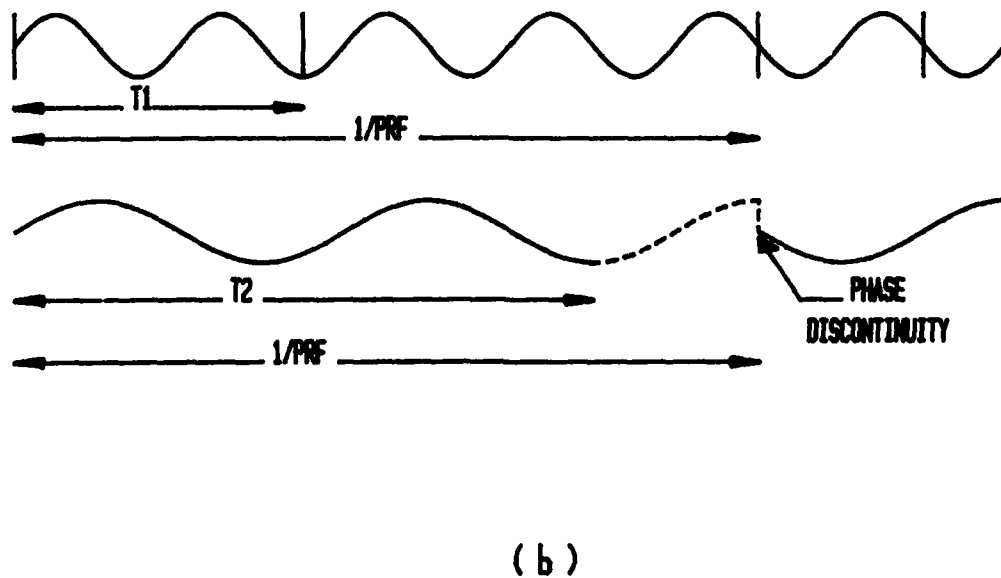
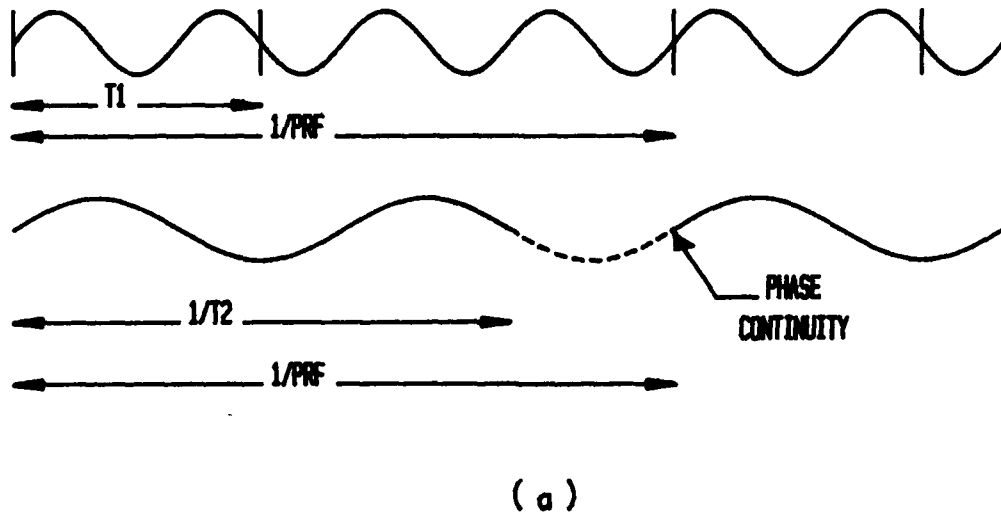
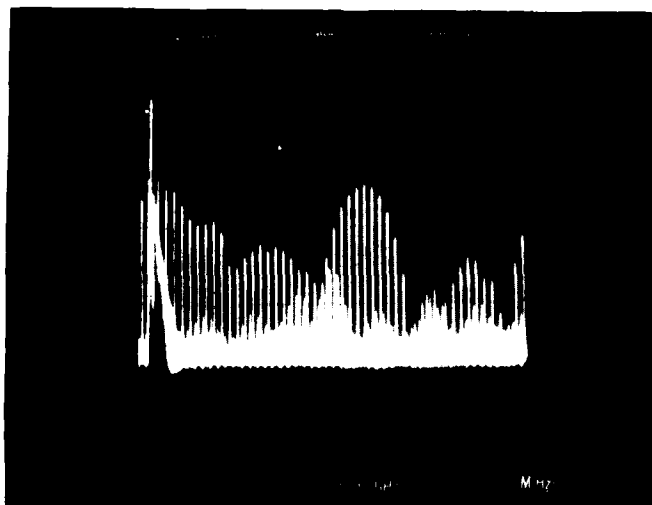


FIGURE 5.21 - (a) CONTINUOUS OUTPUT PHASE FOR A GIVEN INPUT FREQUENCY
 (b) DISCONTINUOUS OUTPUT PHASE FOR A GIVEN INPUT FREQUENCY

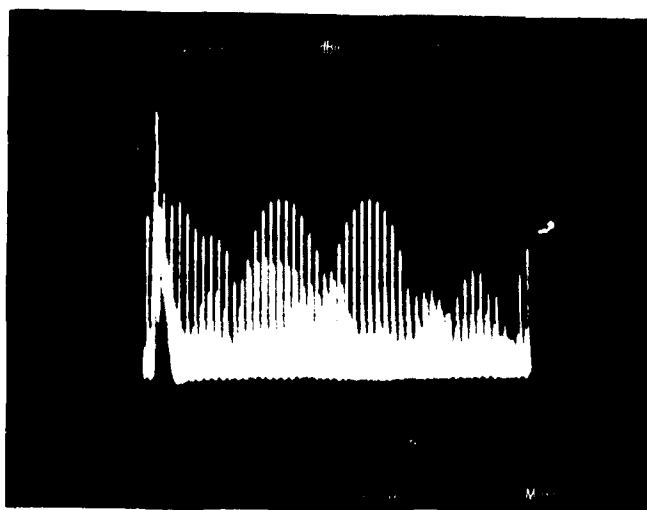
TABLE 5.2

THEORETICAL INPUT AND OUTPUT FREQUENCIES FOR A CONTINUOUS PHASE
RELATIONSHIP FOR A COMPRESSION FACTOR OF .5191 AND A PRF OF 10 MHz

$f_{in} \pm .5$ MHz	$f_{out} \pm .5$ MHz	$\frac{f_{out}}{f_{in}} = a$
395	205	.52
374	194	.52
354	184	.52
333	173	.52
312	161	.52
291	151	.52
270	140	.52
249	129	.52
229	119	.52
208	108	.52
187	97	.52
166	86	.52



(a)



(b)

FIGURE 5.22 - (a) UNFILTERED OUTPUT FOR A SINGLE INPUT SIGNAL
(b) UNFILTERED OUTPUT FOR TWO INPUT SIGNALS

TABLE 5.3

SUMMARY OF RESULTS

	SENSITIVITY	1 dB COMPRESSION POINT (INPUT)	MAX. PEAK OUTPUT POWER LEVEL	DYNAMIC RANGE	GAIN G_c	MAXIMUM FREQUENCY OF OPERATION (2)		COMPRESSION FACTOR α (3)
	S^0 (1)	dBm	dBm	dB	dB	MHz		
EXPERIMENTAL VALUES	-35	-17	-14.7	18	9	P.W. msec		.519 ± .001
						1.25	1.5	
DE-EMBEDDED EXPERIMENTAL VALUES	-33	-15	-12.7	18	11	375	300	-
THEORETICAL VALUES	-	-	-12.5	-	12	400	333	.5191

- (1) The sensitivity level is reduced for the de-embedded values since the noise level increases in this case.
- (2) The maximum operating frequency of 430 MHz was limited as a result of the filter-like characteristic of the input meander delay line. The above values are given for increased output pulse widths allowing verification of the theoretical values.
- (3) The value of α is given for a symmetrical $(\sin x)/x$ response.

6.0 CONCLUSIONS

6.1 Summary and Conclusions

In this report a system for carrying out frequency compression (expansion) of wideband pulsed r.f. signals has been proposed. The present methods of converting r.f. signals upward or downward in frequency are either by heterodyne conversion or by harmonic or sub-harmonic generation. Although in general limited to pulse systems, the frequency compression (expansion) system has certain advantages over these conventional methods. These include the ability to handle multiple simultaneous signals, retain the instantaneous bandwidth in the frequency compression (expansion) operation, convert signals over an infinite number of conversion factors and provide signal amplification.

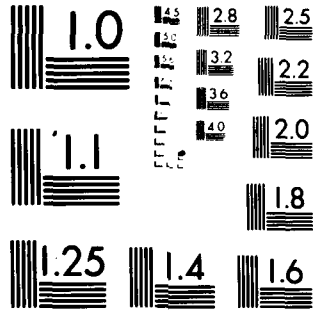
Sampling techniques permit frequency compression (expansion) and amplification of wideband pulsed r.f. signals using delay lines and lowpass narrowband amplifiers. Such a system allows the frequency compression (expansion) and amplification of signals at frequencies far above the cutoff frequencies of the amplifying devices used. The mathematical model presented is of sufficiently general nature that it may be used in designing frequency compression or expansion systems.

From the experimental results, it was concluded that it was possible to achieve frequency compression from 820 MHz to 427 MHz i.e. by a factor of 1.92, in the prototype circuit. The system overall performance was essentially as predicted. Output power level and frequency response limitations observed in the prototype circuit were primarily a result of the sampler characteristics. Additionally, sensitivity and dynamic range limitations were due to the misalignment of individual diodes in the sampler units. The maximum frequency of operation is directly dependent on the minimum pulse width achievable. Consequently, frequency compression of pulsed r.f. signals to 5 GHz is believed possible using the techniques outlined in this report.

6.2 Future Work Areas

It is recommended that some future efforts be devoted to extending the frequency of operation and output power level of the frequency compression system. This would incorporate improvements to alleviate some of the problems associated with the sampling gate. In particular, reduction of the sampling gate feedthrough and drive requirements are necessary. Additionally, development of impulse generation units having pulse widths of less than 100 psec and high drive capability could be carried out.

Some work could also be devoted to investigating a more compact format. This could include a single channel multiple memory cell arrangement referred to in Section 2. Another area of interest is the examination of frequency expansion of pulsed r.f. signals.



MICROCOPY RESOLUTION TEST CHART
NATIONAL BUREAU OF STANDARDS-1963-A

7.0 REFERENCES

- (1) Tucker, T.W., "Countermeasures System", U.S. Patent Application 924,446.
- (2) Cornish, W.D., "Microwave Frequency Dividers — Devices and Applications", 2nd Military Microwaves Conference Proceedings 1980, Microwave Exhibitions and Publishers Ltd., 1980, pp 13-18.
- (3) Spector, S.C., "A Coherent Microwave Memory using Digital Storage: the Loopless Memory Loop", Electronic Warfare, January/February, 1975, pp. 108-110.
- (4) Watson, H.A., "Microwave Semiconductor Devices and Their Circuit Applications", McGraw Hill, New York, 1969.
- (5) Harrison, R.G., "A Broadband Frequency Divider Using Varactors", IEEE Trans. on Microwave Theory and Techniques, Vol. MTT-25, No. 12, pp. 1055-1059, Dec. 1977.
- (6) Lathi, B.P., "Amplification of Wideband Signals Using Narrowband Amplifiers: The Sampling Amplifier", Conf. Rec., 7th Asilomar Conf. Circuits Systems and Computers.
- (7) Tucker, T.W., Conway, L.J., Bouchard, S.L., "Radio Frequency Signal Storage", Canadian Patent Application 342,527, 1980.
- (8) Stearns, S.D., "Digital Signal Analysis", Hayden Book Company Inc., New Jersey, 1975, pp. 37-40.
- (9) Lathi, B.P., "An Introduction to Random Signals and Communication Theory", International Textbook Company, Scranton, Pennsylvania, 1968.
- (10) Lathi, B.P., "Communications Systems", John Wiley & Sons Inc., New York, 1968.
- (11) Schwartz, M., "Information Transmission, Modulation and Noise", McGraw Hill, New York, 1970, pp. 122-123.
- (12) Hammerstad, E.O., "Equations for Microstrip Circuit Design", Proc. European Microwave Conference, Hamburg (Germany), pp. 268-272, September 1975.
- (13) Bahl, I.J., Trivedi, D.K., "A Designer's Guide to Microstrip Line", Microwaves, May 1977, pp. 174-182.
- (14) Blood, W.R., "MECL System Design Handbook", Motorola Semiconductor Products Inc., December 1972, pp. 27-30.

- (15) Pucel, R.A., Massé, D.J., Hartwig, C.P., "Losses in Microstrip", IEEE Trans. Microwave Theory and Techniques", Vol. MTT-16, No. 6, pp. 342-350, June, 1968. "Correction to Losses in Microstrip", Ibid., (Correspo.), Vol. MTT-16, p. 1064, December
- (16) Welch, J.D., Pratt, H.J., "Losses in Microstrip Transmission Systems for Integrated Microwave Circuits", NEREM Rec. Vol. 8, pp. 100-101, 1966.
- (17) Schneider, M.V., "Dielectric Loss in Integrated Microwave Circuits", Bell Syst. Tech. J. 48, No. 7, pp. 2325-2332, Sept. 1969.
- (18) Saul, P.H., "A GaAs MESFET Sample and Hold Switch", IEEE Trans. Journal of Solid State Circuits, Vol. SC-15, No. 3, June 1980.
- (19) Millman, J., Taub H., "Pulse, Digital and Switching Waveforms", McGraw Hill, New York, 1965, pp. 646-647.
- (20) Diode and Transistor Designer's Catalog, 1980, Hewlett Packard Components.
- (21) Grove, W.M., "Sampling for Oscilloscopes and Other rf Systems: dc Through X-band", IEEE Trans. Microwave Theory and Techniques, Vol. MTT-14, No. 12, December 1966.
- (22) Motorola, Volume 6 Linear Integrated Circuits Series A, Semiconductor Data Library, 1975.
- (23) Hewlett Packard, "Spectrum Analysis...Pulsed rf", Application note 150-2, November 1971, pp. 5-9.
- (24) Strum, R.D., Ward, J.R. "Electric Circuits and Networks", Quantum Publishers Inc., New York, 1973, pp. 86-87.
- (25) Hewlett Packard, "Hewlett-Packard 9825A Calculator Operating and Programming", H-P Calculator Products Division, Colorado, 1976.

APPENDIX A

INPUT AND OUTPUT MEANDER LINE-SAMPLER-AMPLIFIER MODELLING

The model used for the input meander delay line switch-amplifier network is shown in Fig. A-1. An equation for v_{ji} as a function of v , R_m , R_{si} , R_{in} and C is derived as follows:

$$i_o = i_1 + i_2 \quad (1)$$

and

$$i = i_3 + i_4. \quad (2)$$

Now,

$$i_o = \frac{v-v_1}{R_m}, \quad (3)$$

$$i_1 = \frac{v_1}{R_m}, \quad (4)$$

$$i_2 = \frac{v_1 - v_{ji}}{R_{si}}, \quad (5)$$

$$i_3 = C \frac{dv_{ji}}{dt} \quad (6)$$

and

$$i_4 = \frac{v_{ji}}{R_m}. \quad (7)$$

Substituting 3, 4, 5, 6 and 7 into 1 and 2 gives,

$$\frac{v-v_1}{R_m} = \frac{v_1}{R_m} + \frac{v - v_{ji}}{R_{si}} \quad (8)$$

and

$$\frac{v_1 - v_{ji}}{R_{si}} = C \frac{dv_{ji}}{dt} + \frac{v_{ji}}{R_{in}}. \quad (9)$$

From equation 9,

$$v = R_{si}C \frac{dv_{ji}}{dt} + \left(\frac{R_{si}}{R_{in}} + 1\right)v_{ji}. \quad (10)$$

Rearranging equation 8 gives,

$$v = \left(2 + \frac{R_m}{R_{si}}\right)v_1 - \frac{R_m}{R_{si}} v_{ji}. \quad (11)$$

Substituting equation 10 into 11 gives

$$v = \left(2 + \frac{R_m}{R_{si}}\right) R_{si}C \frac{dv_{ji}}{dt} + \left(2 + \frac{R_m}{R_{si}}\right)\left(\frac{R_{si}}{R_{in}} + 1\right)v_{ji} - \frac{R_m}{R_{si}} v_{ji}. \quad (12)$$

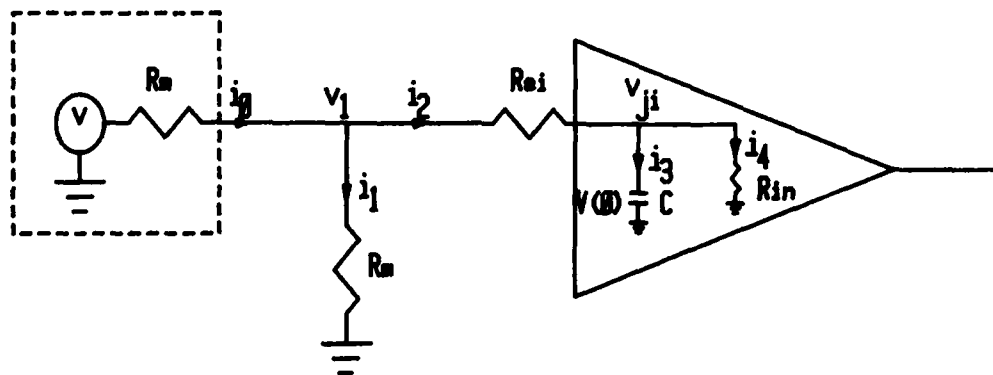


FIGURE A-1 - MODEL OF THE INPUT MEANDER LINE-SWITCH-AMPLIFIER NETWORK DURING THE SAMPLER'S BIAS ON CONDITION

This reduces to

$$v = (2R_{si} + R_m) C \frac{dv_{ji}}{dt} + \left(\frac{2R_{si} + R_m}{R_{in}} + 2 \right) v_{ji}, \quad (13)$$

or

$$\frac{dv_{ji}}{dt} + \left(\frac{2R_{si} + 2R_{in} + R_m}{R_{in}(2R_{si} + R_m)C} \right) v_{ji} - \frac{v}{(2R_{si} + R_m)C} = 0. \quad (14)$$

A total solution for this differential equation is given by

$$v_{ji} = v_{c_{ji}} + v_{p_{ji}} \quad (15)$$

where $v_{c_{ji}}$ is the complementary function which satisfies the source-free equation

$$\frac{dv_{ji}}{dt} + \frac{2R_{si} + 2R_{in} + R_m}{R_{in}(2R_{si} + R_m)C} v_{ji} = 0, \quad (16)$$

and $v_{p_{ji}}$ is the particular integral which satisfies the forced equation

[24]. A solution for equation 14 is given by

$$v_{c_{ji}} = C_1 \exp\left(-\frac{(2R_{si} + 2R_{in} + R_m)t}{R_{in}(2R_{si} + R_m)C}\right) \quad (17)$$

$$\text{and } v_{p_{ji}} = C_2. \quad (18)$$

Hence the total solution is given by

$$v_{ji} = C_1 \exp\left(-\frac{(2R_{si} + 2R_{in} + R_m)t}{R_{in}(2R_{si} + R_m)C}\right) + C_2. \quad (19)$$

At $t = \infty$, C is fully charged and

$$\frac{v - v_1}{R_m} = \frac{v_1}{R_m} + \frac{v_1 - v_{ji}}{R_{si}}, \quad (20)$$

and

$$\frac{v_1 - v_{ji}}{R_{si}} = \frac{v_{ji}}{R_{in}}. \quad (21)$$

Rearranging equation (21) gives

$$v_1 = \frac{R_{si} + R_{in}}{R_{in}} v_{ji}. \quad (22)$$

Substituting equation 22 into 20 and rearranging gives

$$v = \frac{2R_{si} + 2R_{in} + R_m}{R_{in}} v_{ji}, \quad (23)$$

or

$$v_{ji} = \frac{R_{in}}{2R_{si} + 2R_{in} + R_m} v, \quad (24)$$

therefore,

$$C_2 = \frac{R_{in}}{2R_{si} + 2R_{in} + R_m} v. \quad (25)$$

At $t = 0$

$$v_{ji} = V(0) = C_1 + C_2. \quad (26)$$

Hence

$$C_1 = V(0) - \frac{R_{in}}{2R_{si} + 2R_{in} + R_m} v \quad (27)$$

and

$$v_{ji} = \left[V(0) - \frac{R_{in}}{2R_{si} + 2R_{in} + R_m} v \right] \exp \left[- \frac{(2R_{si} + 2R_{in} + R_m)t}{R_{in}(2R_{si} + R_m)C} \right] + \frac{R_{in}}{2R_{si} + 2R_{in} + R_m} v. \quad (28)$$

Setting

$$K_1 = \frac{R_{in}}{2R_{si} + 2R_{in} + R_m},$$

$$K_2 = \frac{1}{K(2R_{si} + R_m)C},$$

and

$$t = \tau_1,$$

equation 28 reduces to

$$v_{ji} = [V(0) - K_1 v] \exp(-K_2 \tau_1) + K_1 v. \quad (29)$$

The model used for the output amplifier-switch-meander line configuration is shown in Fig. A-2. The model in Fig. A-2a shows the condition prior to sampling out. Fig. A-2b models the condition during sampling. An equation for v_o as a function of the open circuit voltage v_{oc} , the output resistance R_o , the output shunt capacitance C_o and the load resistance R_l is derived as follows:

$$i_o = i_1 + i_2 \quad (30)$$

$$i_o = \frac{v_{oc} - v_o}{R_o} \quad (31)$$

$$i_1 = C_o \frac{dv_o}{dt} \quad (32)$$

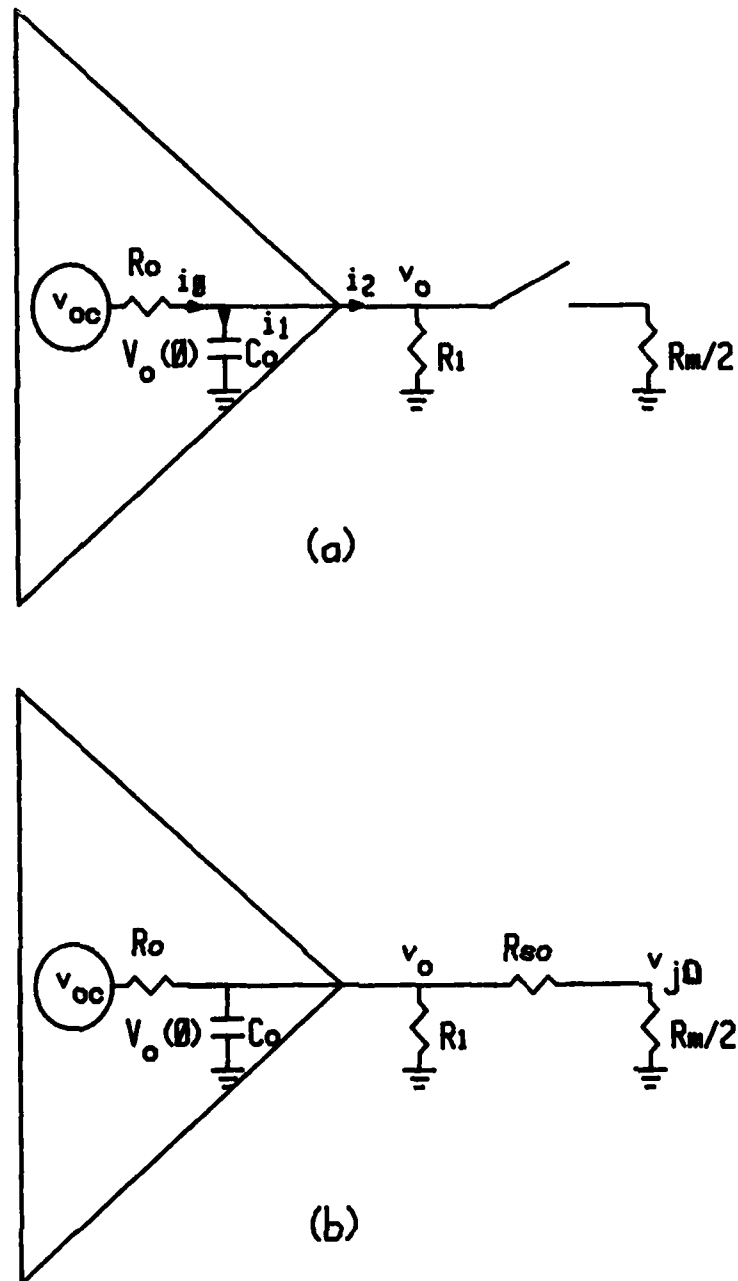


FIGURE A-2 - MODEL OF THE OUTPUT AMPLIFIER SWITCH
MEANDER LINE CONFIGURATION FOR THE
(a) OFF CONDITION AND
(b) ON CONDITION

and

$$i_2 = \frac{v_o}{R_1} . \quad (33)$$

Substituting equation 31, 32 and 33 into equation 30 gives,

$$\frac{v_{oc} - v_o}{R_o} = C_o \frac{dv_o}{dt} + \frac{v_o}{R_1} . \quad (34)$$

Rearranging equation 34 gives

$$\frac{dv_o}{dt} + \frac{(R_1 + R_o)}{C_o R_1 R_o} v_o - \frac{v_{oc}}{C_o R_o} = 0 . \quad (35)$$

A total solution for this differential equation is given by

$$v_o = v_{c_o} + v_{p_o} . \quad (36)$$

A solution for equation 35 is thus

$$v_{c_o} = C_1 \exp \left(- \frac{(R_1 + R_o)}{C_o R_1 R_o} t \right) \quad (37)$$

and

$$v_{p_o} = C_2 . \quad (38)$$

Hence the total solution is given by

$$v_o = C_1 \exp \left(- \frac{(R_1 + R_o)}{C_o R_1 R_o} t \right) + C_2 . \quad (39)$$

At $t = \infty$, $i_1 = 0$ and

$$v_o = \frac{R_1}{R_o + R_1} v_{oc} = C_2 . \quad (40)$$

At $t = 0$

$$v_o = V_o(o) = C_1 + C_2 . \quad (41)$$

Therefore,

$$C_1 = V_o(o) - \frac{R_1}{R_o + R_1} v_{oc} \quad (42)$$

and

$$v_o = \left[V_o(o) - \frac{R_1}{R_o + R_1} v_{oc} \right] \exp \left(- \frac{R_1 + R_o}{R_1 R_o C_o} t \right) + \frac{R_1}{R_o + R_1} v_{oc} . \quad (43)$$

Consequently, the second model is simply

$$v_o = \left[V_o(o) - \frac{R'_1}{R_o + R'_1} v_{oc} \right] \exp \left(- \frac{R'_1 + R_o}{R'_1 R_o C_o} t \right) + \frac{R'_1}{R_o + R'_1} v_{oc} \quad (44)$$

where

$$R_1' = R \parallel (R_{SO} + R_m/2) .$$

Setting

$$K_5 = \frac{R_1'}{R_o + R_1'} \quad (45)$$

and

$$K_6 = \frac{R_1' + R_o}{R_1' R_o C_o} \quad (46)$$

equation 15 reduces to

$$v_o = [V_o(o) - K_5 v_{oc}] \exp(-K_6 \tau_2) + K_5 v_{oc} . \quad (47)$$

since

$$\frac{v_o}{v_{jo}} = \frac{2R_{so} + R_m}{R_m} = \frac{1}{K_3}$$

equation 47 now becomes

$$v_{jo} = K_3 \{ [V_o(o) - K_5 v_{oc}] \exp(-K_6 \tau_2) + K_5 v_{oc} \} . \quad (48)$$

If the capacitor is fully charged before sampling out

$$V_o(o) = \frac{R_1}{R_o + R_1} V_{oc} = K_4 V_{oc} \quad (49)$$

Consequently, equation 48 reduces to

$$\frac{v_{jo}}{v_{oc}} = K_3 \{ [K_4 - K_5] \exp(-K_6 \tau_2) + K_5 \} . \quad (50)$$

APPENDIX B

MICROSTRIP DESIGN EQUATIONS,
PROGRAM LISTING AND DESIGN TABLE

Hammerstad's expressions [12] include useful relationships defining both characteristic impedance and effective dielectric constant:

For $W/h < 1$,

$$Z_0 = \frac{60}{\sqrt{\epsilon_{\text{eff}}}} \ln (8h/W + 0.25 W/h)$$

where:

$$\epsilon_{\text{eff}} = \frac{\epsilon_r + 1}{2} + \frac{\epsilon_r - 1}{2} [(1 + 12h/W)^{-\frac{1}{2}} + 0.04 (1 - W/h)^2] .$$

For $W/h > 1$,

$$Z_0 = \frac{120\pi \sqrt{\epsilon_{\text{eff}}}}{W/h + 1.393 + 0.667 \ln (W/h + 1.444)}$$

where:

$$\epsilon_{\text{eff}} = \frac{\epsilon_r + 1}{2} + \frac{\epsilon_r - 1}{2} (1 + 12h/W)^{-\frac{1}{2}} .$$

Hammerstad notes that the maximum relative error in ϵ_{eff} and Z_0 is less than ± 0.5 per cent and 0.8 per cent, respectively, for $0.05 < W/h < 20$ and $\epsilon_r < 16$.

If the conductor thickness is taken into account the strip width, W , is replaced by an effective strip width, W_e . Expressions for W_e are:

For $W/h > 1/2\pi$,

$$\frac{W_e}{h} = \frac{W}{h} + \frac{t}{\pi h} \left(1 + \ln \frac{2h}{t}\right) .$$

For $W/h < 1/2\pi$,

$$\frac{W_e}{h} = \frac{W}{h} + \frac{t}{\pi h} \left(1 + \ln \frac{4\pi W}{t}\right) .$$

Additional restrictions for applying the above are $t < h$ and $t < W/2$.

PROGRAM LISTING

```

"MICROSTRIP PARAMETERS":
"ε<sub>e</sub>/h→S, w/h→A, eff. dielectric→Q ":
"":
"MATHEMATICAL FORMULAS WERE OBTAINED FROM ":
"MICROWAVES MAY 1977 P-174 ":
"ALL CALCULATIONS INCLUDE THE EFFECTIVE WIDTH DUE TO THE ":
"LINE THICKNESS ":
"FURTHER INFO MAY BE OBTAINED FROM MICROWAVES MAY 1977 ":
"THE SOFTWARE LANGUAGE IS NPL":
"FURTHER INFO ON SOFTWARE PROGRAMMING MAY BE OBTAINED FROM REF. [25]":
  END 4
  "":
  ENT "dielectric constant",E
  ENT "line thickness",L
  ENT "dielectric thickness",A
  ENT "start w/h at ?",A
  ENT "stop w/h at ?",P
  ENT "SET PRINTER 4 LINES BELOW TOP OF FORM ",K
  A←.01→A
  "start":0→N
  WTD 0,27,04
  WTD 0,27,70,INT(928/04),INT(928)
  ENT 1,20X,"MICROSTRIP PARAMETERS",40,3X,"permittivity=",F5.2
  WRT 0.1,13,10,10,10,E
  ENT 2,3X,"line thickness=",F5.2,"mils",9X,"board thickness=",F5.2,"mils"
  WRC 0.2,F,A
  ENT 1,20,10X,"w/h",10X,"ZO",10X,"ε<sub>eff</sub>",10X,"w",10X,"ε<sub>e</sub>"
  WRT 0.1,13,10
  ENT 1,10
  WRT 0.1,13
  "one":A+.01→A
  A←A→A
  IF A<1/2π;GTO "first"
  A←1/πA*(1+ln(2h/r))→S
  S←h→C
  GTO "try"
  "first":A+(1/πA)(1+ln(4πw/r))→S
  S←A→C
  "try":if S>1;GTO "second"
  (E+1)/2+(E-1)/2*((1+12/S)^(-.5)+.04(1-S)^2)→Q
  (00/√Q)ln(0/S+.25S)→Z
  GTO "prin"
  "second":(E+1)/2+((E-1)/2)(1+12/S)^(-.5)→Q
  120π/√Q/(S+1.393+.007*ln(S+1.444))→Z
  "prin":A+1→A
  ENT 2,10X,F4.2,F13.2,F13.3,F12.2,F11.3
  WRT 0.2,A,Z,Q,W,C
  IF M=P;GTO "out"
  IF W>49;GTO "start"
  GTO "one"
  "out":END

```

MICROSTRIP DESIGN TABLE

MICROSTRIP PARAMETERS

permittivity= 4.70
line thickness= 1.50mils

board thickness=58.00mils

w/d	Z ₀	ε _{eff}	N	n _e
1.55	52.34	3.501	95.70	98.254
1.60	52.16	3.502	96.28	98.834
1.67	51.99	3.504	96.86	99.414
1.63	51.81	3.506	97.44	99.994
1.69	51.64	3.507	98.02	100.574
1.70	51.47	3.509	98.60	101.154
1.71	51.30	3.511	99.18	101.734
1.72	51.13	3.512	99.76	102.314
1.73	50.96	3.514	100.34	102.894
1.74	50.79	3.516	100.92	103.474
1.75	50.62	3.517	101.50	104.054
1.76	50.46	3.519	102.08	104.634
1.77	50.30	3.520	102.66	105.214
1.78	50.13	3.522	103.24	105.794
1.79	49.97	3.524	103.82	106.374
1.80	49.81	3.525	104.40	106.954
1.81	49.65	3.527	104.98	107.534
1.82	49.49	3.528	105.56	108.114
1.83	49.34	3.530	106.14	108.694
1.84	49.18	3.531	106.72	109.274
1.85	49.03	3.533	107.30	109.854
1.86	48.87	3.535	107.88	110.434
1.87	48.72	3.536	108.46	111.014
1.88	48.57	3.538	109.04	111.594
1.89	48.42	3.539	109.62	112.174
1.90	48.27	3.541	110.20	112.754
1.91	48.12	3.542	110.78	113.334
1.92	47.97	3.544	111.36	113.914
1.93	47.82	3.545	111.94	114.494
1.94	47.67	3.547	112.52	115.074
1.95	47.53	3.548	113.10	115.654

APPENDIX CMICROSTRIP CONDUCTOR LOSS EQUATIONS

Expressions for the conductor loss derived by Pucel [15] are given by

For $W/h < 1/2\pi$,

$$\frac{\alpha_c Z_0 h}{R_s} = \frac{8.68}{2\pi} \left[1 - \left(\frac{W_e}{4h} \right)^2 \right] \left\{ 1 + \frac{h}{W_e} + \frac{h}{\pi W_e} \left[\ln \left(\frac{4\pi W}{t} + \frac{t}{W} \right) \right] \right\}$$

For $1/2\pi < W/h < 2$,

$$\frac{\alpha_c Z_0 h}{R_s} = \frac{8.68}{2\pi} \left[1 - \left(\frac{W_e}{4h} \right)^2 \right] \left\{ 1 + \frac{h}{W_e} + \frac{h}{\pi W_e} \left[\ln \left(\frac{2h}{t} - \frac{t}{h} \right) \right] \right\}$$

For $2 < W/h$

$$\frac{\alpha_c Z_0 h}{R_s} = \frac{8.68}{\left\{ \frac{W_e}{h} + \frac{2}{\pi} \ln \left[2\pi e \left(\frac{W_e}{2h} + 0.94 \right) \right] \right\}^2} \left(\frac{W_e}{h} + \frac{W_e/\pi h}{\frac{W_e}{2h} + 0.94} \right) \cdot \left\{ 1 + \frac{h}{W_e} + \frac{h}{\pi W_e} \left[\ln \left(\frac{2h}{t} - \frac{t}{h} \right) \right] \right\}$$

where α_c is in dB/cm.

APPENDIX D

MOTOROLA MC1590 G AMPLIFIER SPECIFICATIONS

HIGH-FREQUENCY CIRCUITS

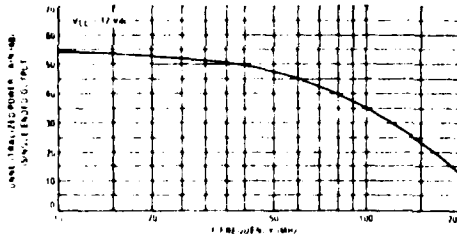
MC1590G

RF/IF/AUDIO AMPLIFIER

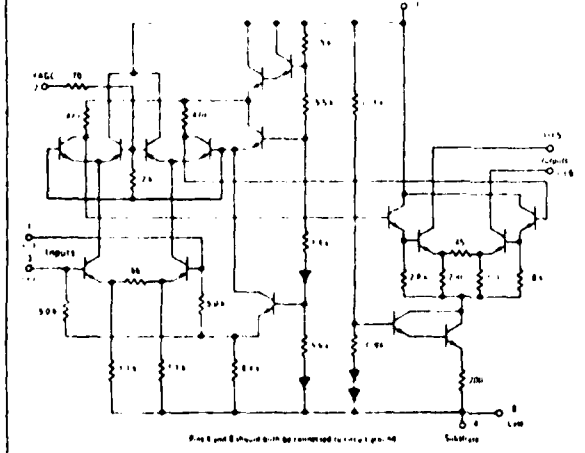
an integrated circuit featuring wide-range AGC for use in RF/IF amplifiers and audio amplifiers over the temperature range, -55 to +125°C. See Motorola Application Note AN 513 for design details.

- High Power Gain 50 dB typ at 10 MHz
45 dB typ at 60 MHz
35 dB typ at 100 MHz
- Wide Range AGC - 60 dB min, dc to 60 MHz
- Low Reverse Transfer Admittance < 10 μmhos typ at 60 MHz
- 6.0 to 15 Volt Operation Single Polarity Power Supply

FIGURE 1 - UNNEUTRALIZED POWER GAIN versus FREQUENCY
(Tuned Amplifier, see Figure 16)



CIRCUIT SCHEMATIC



See Packaging Information Section for outline dimensions
See MC1590, MC1590G for room temperature information

WIDEBAND AMPLIFIER WITH AGC

SILICON MONOLITHIC INTEGRATED CIRCUIT

METAL PACKAGE PIN CONNECTIONS
CASE 601

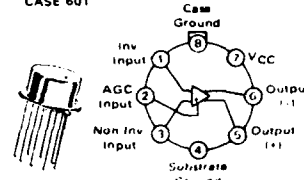


FIGURE 2 - VOLTAGE GAIN versus FREQUENCY
(Video Amplifier, see Figure 17)

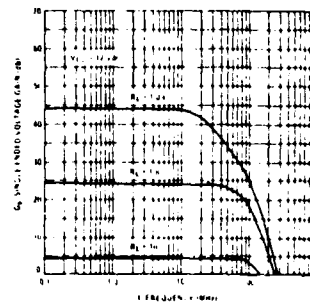
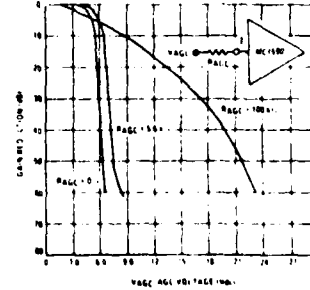


FIGURE 3 - TYPICAL GAIN REDUCTION versus AGC VOLTAGE



MAXIMUM RATINGS ($T_A = +25^\circ\text{C}$ unless otherwise noted)

Rating	Symbol*	Value	Unit
Power Supply Voltage	VCC	+18	Vdc
Output Supply Voltage (Pins 5 and 6)	V ₅ , V ₆	+18	Vdc
AGC Supply	VAGC	VCC	Vdc
Input Differential Voltage	VID	5.0	Vdc
Power Dissipation (Package Limitation) Derate above $T_A = +25^\circ\text{C}$	P _D	680 4.6	mW mW/°C
Operating Ambient Temperature Range	T _A	-55 to +125	°C
Storage Temperature Range	T _{stg}	-65 to +150	°C

ELECTRICAL CHARACTERISTICS (Unless otherwise noted, VCC = +12 Vdc, T_A = 25°C, f = 60 MHz, BW = 1.0 MHz. See Figure 16 for test circuit.)

Characteristic	Symbol	Min	Typ	Max	Unit
AGC Range (V _{AGC} = 5.0 Vdc to 7.0 Vdc) (V _{AGC} = 5.0 Vdc to 7.0 Vdc, -55°C ≤ T _A ≤ 125°C)	-	60 58	68	-	dB
Single Ended Voltage Gain (-55°C ≤ T _A ≤ 125°C)	A _{vs}	40 37	45	-	dB
Single Ended Power Gain (-55°C ≤ T _A ≤ 125°C)	G _p	40 37	45	-	dB
Noise Figure (R _S = 50 Ω)	NF	-	6.0	7.0	dB
Output Voltage Range (Pin 5) Differential Output 10 dB AGC 10 dB AGC, -55°C ≤ T _A ≤ 125°C 1-30 dB AGC 1-30 dB AGC, -55°C ≤ T _A ≤ 125°C Single Ended Output 10 dB AGC 10 dB AGC, -55°C ≤ T _A ≤ 125°C 1-30 dB AGC 1-30 dB AGC, -55°C ≤ T _A ≤ 125°C	V ₅	13 10 5.5 4.5	14 -	- -	V _{p-p}
Output Stage Current (Pins 5 and 6)	I ₅ , I ₆	4.0	5.6	7.5	mA
Power Supply Current (V _i = 0 V) (V _i = 0 V, -55°C ≤ T _A ≤ 125°C)	I _{CC}	-	14	17 20	mA

ADMITTANCE PARAMETERS (VCC = +12 Vdc, T_A = +25°C)

Parameter	Symbol	Typ		Unit
		f = 30 MHz	f = 60 MHz	
Single Ended Input Admittance	Y ₁₁ b ₁₁	0.4 1.2	0.75 3.4	mmhos
Single Ended Output Admittance	Y ₂₂ b ₂₂	0.05 0.50	0.1 1.0	mmhos
Forward Transfer Admittance (Pin 1 to Pin 5)	Y ₂₁ b ₂₁	150 -45	150 -105	mmhos degrees
Reverse Transfer Admittance*	Y ₁₂ b ₁₂	0 -5.0	0 -10	mmhos

*The value of Reverse Transfer Admittance includes the feedback admittance of the test circuit used in the measurements. The test feedback capacitance (including test circuit) is @ 0.25 pF and is a more practical value for design calculations than the internal feedback of the device alone. (See Figure 6)

SCATTERING PARAMETERS (VCC = +12 Vdc, T_A = +25°C, Z₀ = 50 Ω)

Parameter	Symbol	Typ		Unit
		f = 30 MHz	f = 60 MHz	
Input Reflection Coefficient	S ₁₁ θ ₁₁	0.95 -7.3	0.93 -16	degrees
Output Reflection Coefficient	S ₂₂ θ ₂₂	0.98 -3.0	0.98 -5.5	degrees
Forward Transmission Coefficient	S ₂₁ θ ₂₁	16.8 178	14.7 64.3	degrees
Reverse Transmission Coefficient	S ₁₂ θ ₁₂	0.00048 84.9	0.00062 79.2	degrees

TYPICAL CHARACTERISTICS
 (VCC = 12 Vdc, TA = +25°C unless otherwise noted)

FIGURE 4 - FIXED TUNED POWER GAIN versus TEMPERATURE
 (See test circuit, Figure 16)

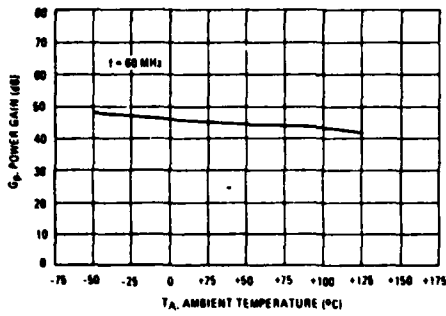


FIGURE 5 - POWER GAIN versus SUPPLY VOLTAGE
 (See test circuit, Figure 16)

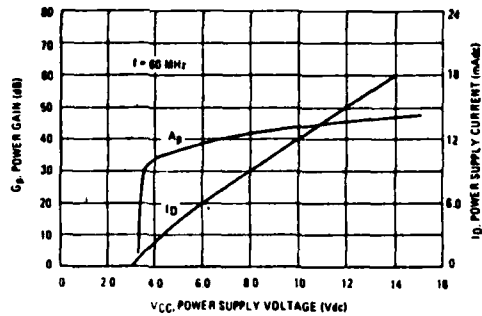


FIGURE 6 - REVERSE TRANSFER ADMITTANCE versus FREQUENCY
 (See Parameter Table, page 2 of MC 1590 specification)

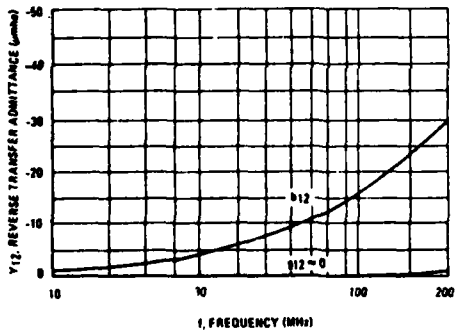


FIGURE 7 - NOISE FIGURE versus FREQUENCY

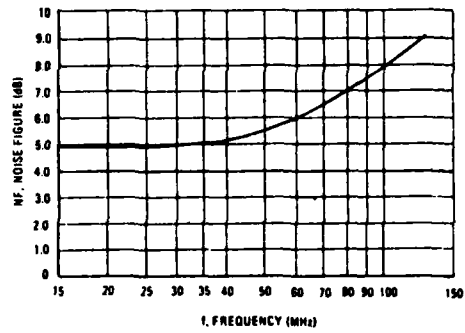


FIGURE 8 - SINGLE-ENDED OUTPUT ADMITTANCE

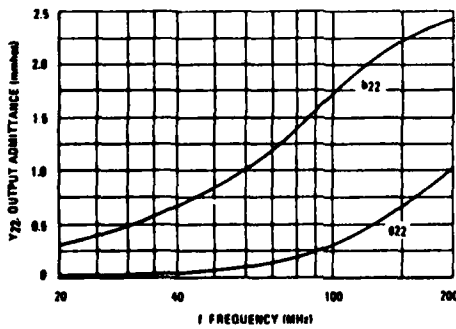
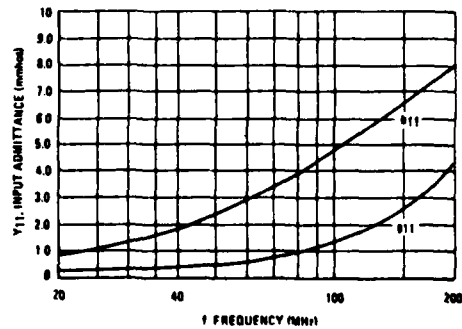


FIGURE 9 - SINGLE-ENDED INPUT ADMITTANCE



TYPICAL CHARACTERISTICS (continued)

FIGURE 10 - Y_{21} , FORWARD TRANSFER ADMITTANCE, RECTANGULAR FORM

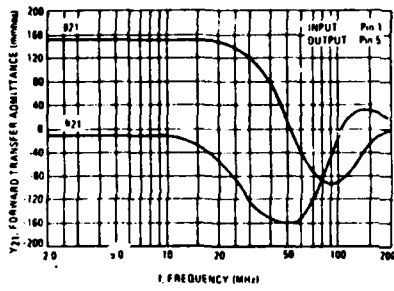


FIGURE 11 - Y_{21} , FORWARD TRANSFER ADMITTANCE, POLAR FORM

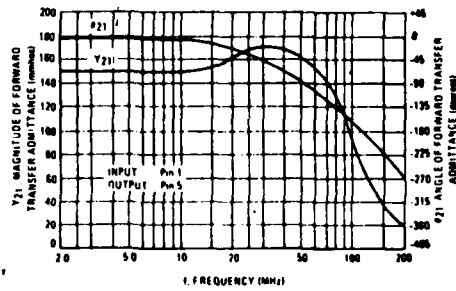


FIGURE 12 - S_{11} and S_{22} , INPUT AND OUTPUT REFLECTION COEFFICIENT

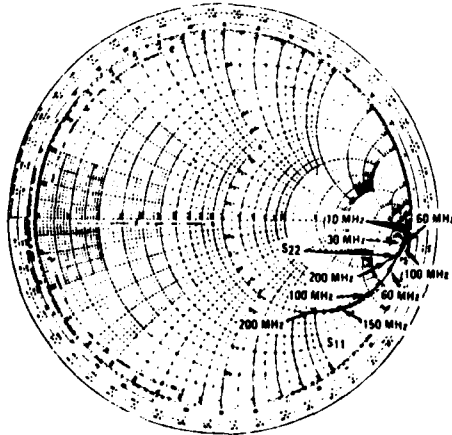
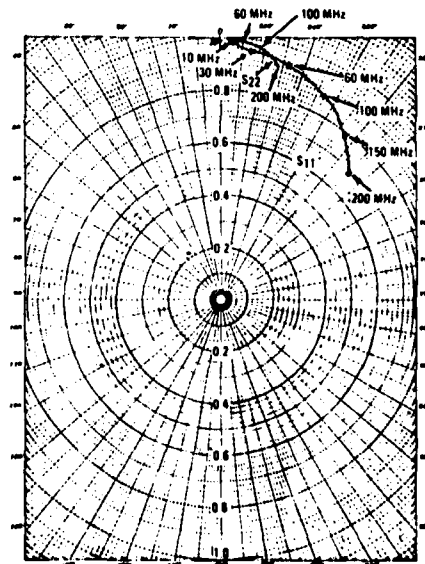


FIGURE 13 - S_{11} and S_{22} , INPUT AND OUTPUT REFLECTION COEFFICIENT



TYPICAL CHARACTERISTICS (continued)

FIGURE 14 - S_{21} , FORWARD TRANSMISSION COEFFICIENT (GAIN)

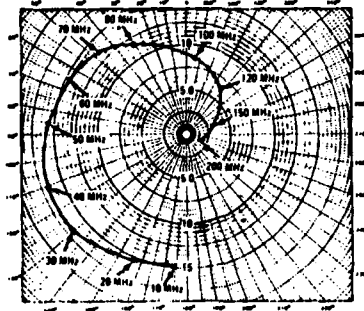
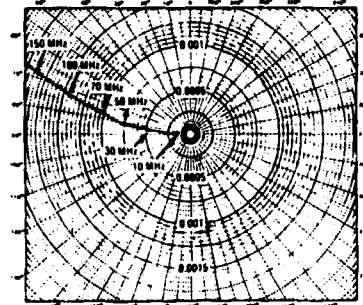


FIGURE 15 - S_{12} , REVERSE TRANSMISSION COEFFICIENT (FEEDBACK)



TYPICAL APPLICATIONS

FIGURE 16 - 60-MHz VOLTAGE AND POWER GAIN TEST CIRCUIT

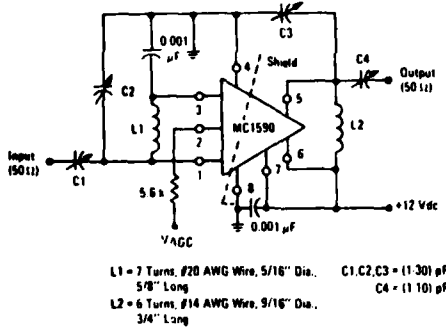


FIGURE 17 - VIDEO AMPLIFIER

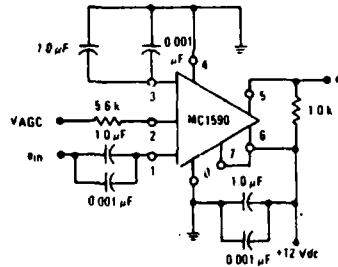


FIGURE 18 - 30-MHz AMPLIFIER (Power Gain = 50 dB, BW ≈ 1.0 MHz)

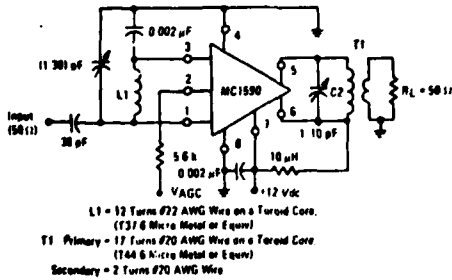
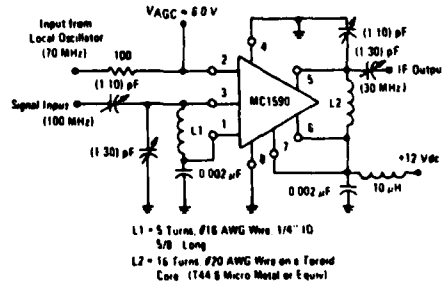


FIGURE 19 - 100-MHz MIXER



APPENDIX E

SAMPLING GATE VOLTAGE BIAS DERIVATION

The required voltages V_b and $-V_b$ of the diode sampling gate depend on the amplitude V_s of the signal and are determined by the condition that the current be in the forward direction in each of the diodes D1, D2, D3 and D4 [19]. The current in each diode consists of two components, one due to V_b (as indicated by Fig. E-1b) and the other due to V_s (as indicated by Fig. E-1c). In order to simplify the analysis, the forward diode resistance R_s in all four conducting diodes are assumed equal. The currents for Fig. E-1b are obtained as follows:

since no d.c. current flows in the load

$$i_1 = i_2 = i_3 = i_4 \quad (1)$$

and

$$i_5 = i_6 \quad (2)$$

Also from symmetry

$$V_2 = -V_1 \quad (3)$$

Now

$$i_5 = i_1 + i_3 \quad (4)$$

and since

$$i_5 = \frac{V_b - V_1}{R_b} \quad (5)$$

$$i_1 = \frac{V_1}{R_s} \quad (6)$$

and

$$i_3 = \frac{V_1}{R_s} \quad (7)$$

equation 4 is reduces to

$$\frac{V_b - V_1}{R_b} = \frac{2V_1}{R_s} \quad (8)$$

or

$$V_b = \frac{2R_b + R_s}{R_s} V_1 \quad (9)$$

or

$$V_1 = \frac{R_s}{2R_b + R_s} V_b \quad (10)$$

Therefore,

$$i_1 = \frac{V_1}{R_s} = \frac{V_b}{2R_b + R_s} = i_2 = i_3 = i_4 \quad (11)$$

The currents for Fig. E-1c are derived as follows:

From symmetry

$$V'_1 = V'_2 \quad (12)$$

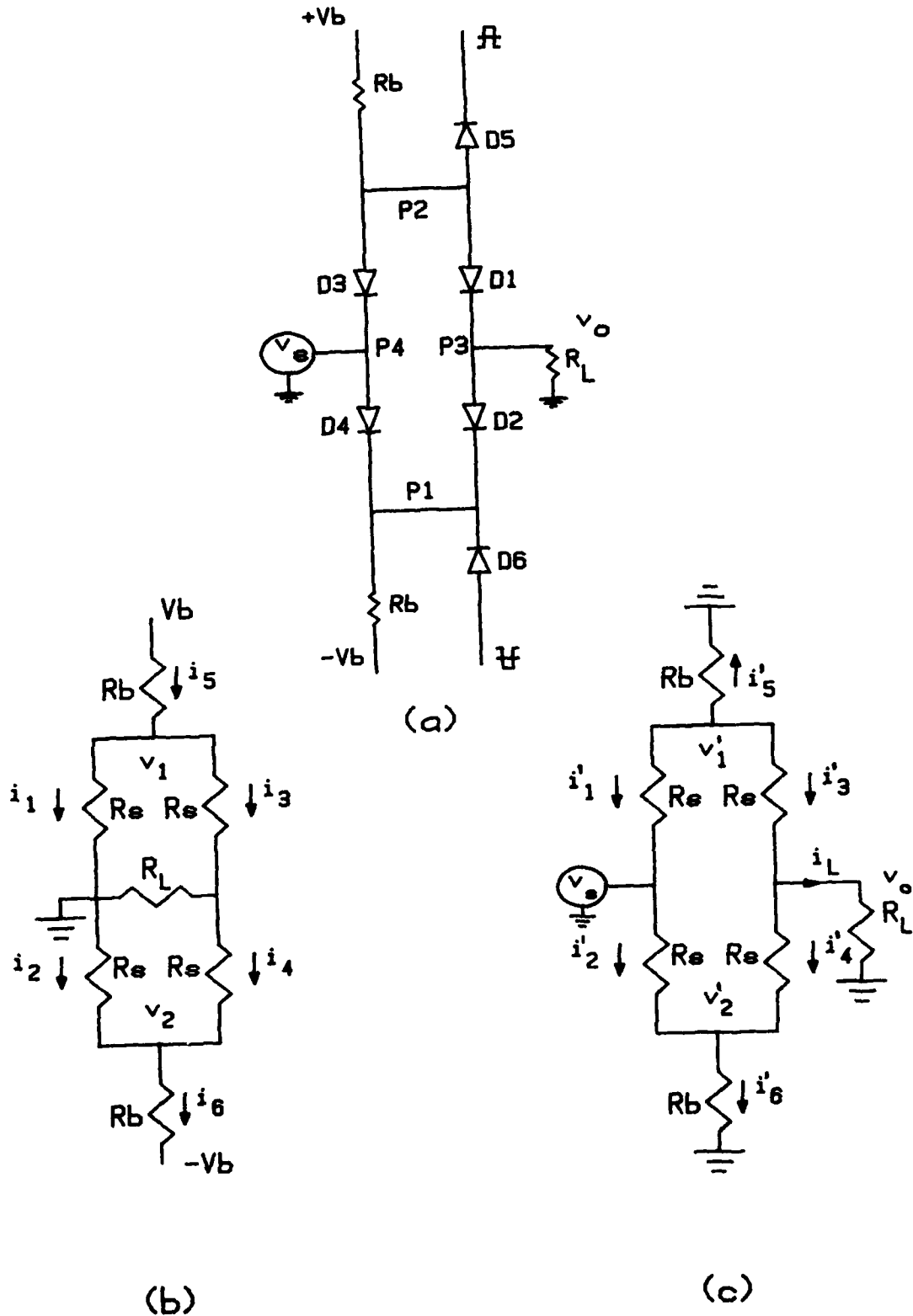


FIGURE E-1 - (a) SIX-DIODE SAMPLING GATE
 (b) CURRENT CONDUCTION DUE TO THE VOLTAGE BIAS
 (c) CURRENT CONDUCTION DUE TO THE INPUT SIGNAL

$$i'_1 = i'_2 \quad (13)$$

$$i'_3 = i'_4 \quad (14)$$

and

$$i'_5 = i'_6 \quad (15)$$

Now

$$i'_1 = i'_3 + i'_5 \quad (16)$$

$$i'_1 = \frac{V_5 - V'_1}{R_s} = i'_2 \quad (17)$$

$$i'_5 = \frac{V'_1}{R_b} = i'_6 \quad (18)$$

$$i'_3 = \frac{V'_1 - V_0}{R_s} = i'_4 \quad (19)$$

and

$$i_L = \frac{V_0}{R_L} \quad (20)$$

Substituting equations 17, 18 and 19 into 16 gives

$$\frac{V_s V'_1}{R_s} = V'_1 \left(\frac{1}{R_b} + \frac{1}{R_s} \right) - \frac{V_0}{R_s} \quad (21)$$

$$V_s = V'_1 \left(\frac{R_s}{R_b} + 2 \right) - V_0 \quad (22)$$

Also

$$i_1 = i'_3 + i'_4 = 2i'_3 \quad (23)$$

or

$$\frac{V_0}{R_L} = 2 \left(\frac{V'_1 - V_0}{R_s} \right) \quad (24)$$

Rearranging equation (24) gives

$$V_0 \left(\frac{R_s + 2R_L}{R_s R_L} \right) = \frac{2}{R_s} V'_1 \quad (25)$$

or

$$V_0 = \frac{2R_L}{R_s + 2R_L} V'_1 \quad (26)$$

Substituting equation 26 into 22 gives

$$V_s \left(\frac{R_s + 2R_b}{R_b} - \frac{2R_L}{R_s + 2R_L} \right) V'_1 \quad (27)$$

or

$$V_1' = \frac{R_b(R_s + 2R_L)}{(R_s + 2R_L)(R_s + 2R_b) - 2R_L R_b} V_s \quad (28)$$

Substituting equation 28 into equation 17 gives

$$i_1' = i_2' = \frac{1}{R_s} \left[1 - \frac{R_b(R_s + 2R_L)}{(R_s + 2R_L)(R_s + 2R_b) - 2R_L R_b} \right] V_s \quad (29)$$

The currents i_3' and i_4' are obtained by first substituting equation 26 into 19 which gives

$$i_3' = i_4' = \frac{V_1'}{R_s} - \frac{2R_L}{R_s(R_s + 2R_L)} V_1' = \frac{V_1'}{R_s + 2R_L} \quad (30)$$

Now substituting equation 28 into 30 gives

$$i_3' = i_4' = \frac{R_b}{(R_s + 2R_L)(R_s + 2R_b) - 2R_L R_b} V_s \quad (31)$$

The current due to V_b is $V_b/(2R_b + R_s)$ and is in the forward direction in each diode, but the current due to V_s is in the reverse direction in D3 (between P_1 and P_4) and in D2 (between P_3 and P_2). The larger reverse current is in D3 and equals

$$\frac{1}{R_s} \left[1 - \frac{R_b(R_s + 2R_L)}{(R_s + 2R_L)(R_s + 2R_b) - 2R_L R_b} \right] V_s$$

and hence this quantity must be less than $V_b/(2R_b + R_s)$. The minimum value of V_b is therefore given by

$$(V_b)_{\min} = \frac{2R_b + R_s}{R_s} \left[1 - \frac{R_b(R_s + 2R_L)}{(R_s + 2R_L)(R_s + 2R_b) - 2R_L R_b} \right] V_s \quad (32)$$

The maximum output voltage $(V_o)_{\max}$ in terms of V_b is derived as follows:

From equation 26

$$V_o = \frac{2R_L}{R_s + 2R_L} V_1' \quad (33)$$

or

$$V_1' = \frac{R_s + 2R_L}{2R_L} V_o \quad (34)$$

Substituting equation 34 into equation 22 gives

$$V_s = \left[\left(\frac{R_s + 2R_b}{R_b} \right) \left(\frac{R_s + 2R_L}{2R_L} \right) - 1 \right] V_o$$

$$= \frac{(R_s + 2R_b)(R_s + 2R_L) - 2R_L R_b}{2R_L R_b} V_o \quad (35)$$

Substituting equation 35 into equation 32 and reducing yields

$$(V_b)_{\min} = \frac{2R_b + R_s}{R_s} \left[\frac{(R_s + 2R_L)(R_s + R_b) - 2R_L R_b}{2R_L R_b} \right] V_o$$

or equivalently

$$(V_o)_{\max} = \frac{2R_s R_L R_b}{(2R_b + R_s)[(R_s + 2R_L)(R_s + R_b) - 2R_L R_b]} V_b \quad (36)$$

The maximum output power is simply

$$(P_o)_{\max} = \frac{(V_o)_{\max}^2}{R_L}$$

where R_L is the load which the sampling gate sees.

APPENDIX F

AUTOMATIC INSERTION LOSS AND RETURN
LOSS MEASUREMENT PROGRAM DESCRIPTION

AUTOMATIC MEASUREMENT

PROGRAM DESCRIPTION

"RETURN"

This program does an automatic measurement of insertion loss and return loss for any device under test. The frequency coverage is anywhere between .1 and 18 GHz. It first performs a calibration run without the D.U.T. The calibration results are stored into memory and subtracted from the measured value when the D.U.T. is in the circuit. This eliminates any errors caused by the R.F. source, connectors and test equipment. After the test run, a plot of the insertion loss and/or return loss versus input frequency is provided.

Operating Procedures

1. Connect the equipment as shown in Fig. F-2, place a sheet of paper on the plotter and enter points P1 and P2.
2. Prior to running this test, 59313A A/D converter's channel 1 and 2 must be adjusted for a full range of $\pm 5V$.
3. Insert the flexible disk in the disk drive, type GET "return" and press RUN.
4. "Device under test?" will then appear. Type in: device name, serial number and press CONTINUE.
5. "freq. start?" will then appear. Type in the desired starting test frequency in GHz and press CONTINUE.
6. "freq. stop?" will then appear. Type in the desired final test frequency and press CONTINUE.
7. "resolution in MHz?". Type in the desired frequency increment between test points and press CONTINUE.

NOTE

This program is limited to 800 frequency points. If more than 800 points are chosen, the program automatically assigns the number of frequency points to 800.

8. "test?: 1 INS-LOS, 2 RET-LOS, 3 BOTH" will then appear. Type in: "1" for an insertion loss measurement only, "2" for a return loss measurement only or "3" for both tests.
9. "dB/div on channel A" will appear if a return loss measurement is desired. Type in the number of dB per division selected on the swept amplitude analyser's channel A push buttons.
10. "connect short at test port" will then appear. Connect a short at the reflectometer bridge test port and press CONTINUE. The program will now do its calibration run for the return loss measurement.

11. "dB/div on channel B" will appear if an insertion loss measurement is required. Type in the number of dB per division selected on the swept amplitude analyser's channel B push buttons.
12. "connect detector at test port" will then appear. Connect the 11664A detector at the reflectometer bridge test port and press CONTINUE. The program will now do its calibration run for the insertion loss measurement.
13. "make connection with D.U.T." will then appear. Connect everything as in Fig. F-1 and press CONTINUE. The program will now do its test run.

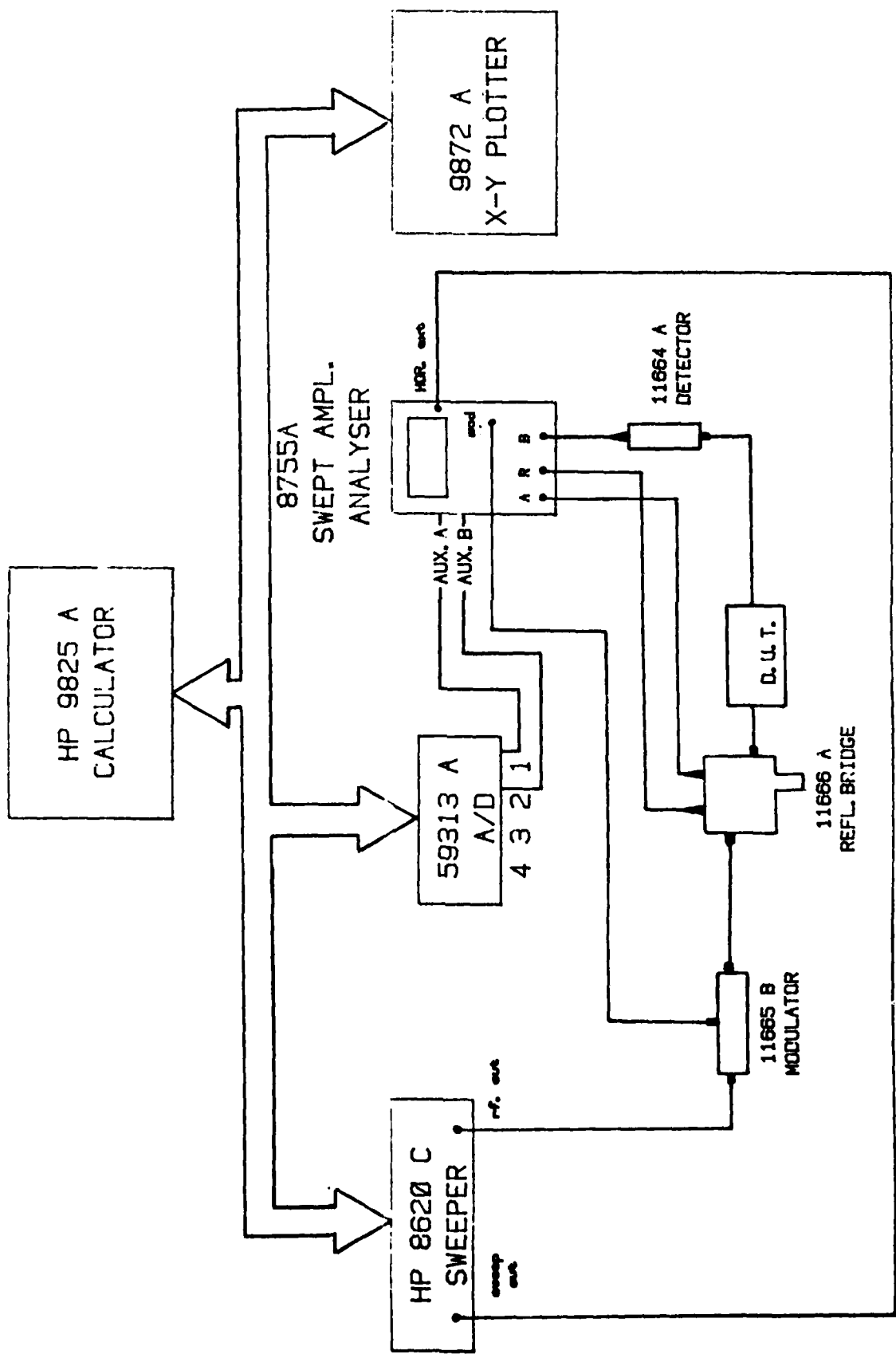


FIGURE 1-1 - AUTOMATIC INSERTION LOSS AND RETURN LOSS MEASUREMENT SET-UP

PROGRAM LISTING

```

"INFO ON THE MPL PROGRAMMING LANGUAGE MAY BE OBTAINED FROM REF.[25]":
"INSERTION & RETURN LOSS TEST":
dim A$(20);dim A$(3)
dev "sweep",710,"a/d",700
beep;ent "nr plug-in used: 86290 or 8621 ?",D
beep;ent "device under test ?",A$
if D=8621;goto "8621"
"low lmts of bands":2+r1;5+r2;12+r3
"width of bands":4.2+r4;0.4+r5;0+r6
"switch pts":0.1+r7;12.2+r8;goto "check"
"8621":.1+r1;1.7+r2;8+r3;1.9+r4;2.4+r5;4.4+r6;1.8+r7;4.3+r8
"check":beep;ent "freq. start in GHz?",L
beep;ent "freq. stop in GHz?",A;A+P
L+r10;A+r11
if r1>L;r1+r10
if 1>r3+r8;r3+r8+r11
beep;ent "resolution in MHz?",Q
lxa 3;(r11-r10)/(Q/1000)+C
if C>800;800+C
dim K(C+1);dim S(C+1);dim F(C+1)
beep;ent "test?:1=INS-LOS,2=REF-LOS,3=BOTH",D
if D=1;L+P;1+0;goto "chan.a"
beep;ent "db/div on channel A",A;-1+0
beep;asp "connect snort at test port";stp
call 'sweper'(1)
for J=1 to C+1
K(J)+S(J)
next J
"chan.a":if D=2;goto "axes"
beep;ent "db/div on channel B",B
beep;asp "connect detector at test port";stp
call 'sweper'(2)
for J=1 to C+1
K(J)+F(J)
next J
"axes":pcir;ent# 1
scl L=(A-B)*.1,A+(A-L)*.1,-9,3
lxa 2;xax -1,(A-L)/50,L,H,5
yax L,.2,-1,1
yax A,.2,-1,1
plt L+(A-L)/3,-9,-1;csiz 2.5,2,1,0
lbl "frequency (GHz)"
plt L+(A-B)/3,2,-1;lbl A$
if D=1;goto "INS-LOS"
"REF-LOS":beep;asp "make connection with D.U.T";stp
call 'sweper'(1)
pcir;ent# 2;lxa 2

```

Copy available to DTIC does not
 permit fully legible reproduction

PROGRAM LISTING

```

40: scl d-(a-l)*.1,d+(a-l)*.1,-9A,3A
41: if a>=1;ixd 0
42: yax d,a/3,-7A,x,-3
43: plt d-(a-l)*.1,-3A,-1;csiz 2.5,2,1,90
44: lbr "return loss (db)"
45: lln r10,r11,-7A,A
46: for j=1 to c+1
47: (x[j]-s[j])/100*A+Y
48: plt r10+(j-1)*(r11-r10)/C,Y
49: next j
50: pen# ;pcir
51: if j=3;gto "1-3-LOS"
52: beep;ent "do you want another test?";NS
53: if cap(NS)="Y";gto "again"
54: end
55: "1-3-LOS":beep;usp "make connection with D.U.T";stp
56: cil 'sweper'(2)
57: lxd 2
58: pcir;pen# 3
59: scl d-(a-l)*.1,d+(a-l)*.1,-9B,3B
60: if a>=1;ixd 0
61: plt d-(a-l)*.11,-3B,-1;csiz 2.5,2,1,90
62: lbr "insertion loss (db)"
63: pcir
64: yax d+(a-l)*.09,b/3,-7B,b,-3
65: lln r10,r11,-7B,B
66: for j=1 to c+1
67: (x[j]-r[j])/100*B+Y
68: plt r10+(j-1)*(r11-r10)/C,Y
69: next j
70: pen# ;pcir
71: beep;ent "do you want another test?";NS
72: if cap(NS)="Y";jto "again"
73: end
74: "again":beep;ent "device under test?";AS
75: jto "axes"
76: end
77: "sweper":
78: lnt 1,"MIS",11.0,"V",f3.3,"E"
79: for j=1 to c+1
80: r10+(j-1)*(r11-r10)/C+r
81: z+a;r3+a;r0+a
82: if r<r3;2+a;r2+a;r3+a
83: if r<r7;1+a;r1+a;r3+a
84: (r-a)*10/A+v
85: wrt "sweep.1",e,v
86: lxd 0
87: wrt "a/d","n",01,01,"AU"
88: for (ent(rdb(70j),-3),rdb(70j))+r[j]
89: next j

```

UNCLASSIFIED

Security Classification

DOCUMENT CONTROL DATA - R & D		
(Security classification of title, body of abstract and indexing annotation must be entered when the overall document is classified)		
1. ORIGINATING ACTIVITY DEFENCE RESEARCH ESTABLISHMENT OTTAWA NATIONAL DEFENCE HEADQUARTERS OTTAWA, ONTARIO, CANADA K1A 0Z4		2a. DOCUMENT SECURITY CLASSIFICATION UNCLASSIFIED
		2b. GROUP ██████████
3. DOCUMENT TITLE FREQUENCY COMPRESSION OF WIDEBAND SIGNALS USING A DISTRIBUTED SAMPLING TECHNIQUE (U)		
4. DESCRIPTIVE NOTES (Type of report and inclusive dates) DREO REPORT		
5. AUTHOR(S) (Last name, first name, middle initial) CONWAY, L.J.		
6. DOCUMENT DATE November 1981	7a. TOTAL NO OF PAGES 130	7b. NO OF REFS 25
8a. PROJECT OR GRANT NO. 31D20	9a. ORIGINATOR'S DOCUMENT NUMBER(S) DREO REPORT #852	
8b. CONTRACT NO.	9b. OTHER DOCUMENT NO.(S) (Any other numbers that may be assigned this document)	
10. DISTRIBUTION STATEMENT UNLIMITED		
11. SUPPLEMENTARY NOTES	12. SPONSORING ACTIVITY	
13. ABSTRACT Present methods of frequency conversion include heterodyne conversion and harmonic or subharmonic generation. These methods have inherent limitations which restrict their usefulness in a number of applications. A novel frequency compression/expansion system which makes use of sampling techniques is not confined to the same limitations as these conventional frequency conversion systems. The unique integration of delay lines, sampling gates and amplifiers permits frequency compression or expansion as well as amplification of wideband pulsed r.f. signals at frequencies far above the cut-off frequencies of the amplifying devices used. The theory and design of the frequency compression/expansion system is presented in this report. The theoretical results are compared with those obtained from an experimental system and good agreement is demonstrated.		

DSIS

77-865

UNCLASSIFIED

Security Classification

KEY WORDS

DISTRIBUTED SAMPLING

DEVICE TECHNOLOGY

FREQUENCY CONVERSION

MICROWAVE

INSTRUCTIONS

1. **ORIGINATING ACTIVITY** Enter the name and address of the organization issuing the document.
- 2a. **DOCUMENT SECURITY CLASSIFICATION** Enter the overall security classification of the document including special warning terms whenever applicable.
- 2b. **GROUP** Enter security reclassification group number. The three groups are defined in Appendix "M" of the DRB Security Regulations.
3. **DOCUMENT TITLE** Enter the complete document title in all capital letters. Titles in all cases should be unclassified. If a sufficiently descriptive title cannot be selected without classification, show title classification with the usual one-capital-letter abbreviation in parentheses immediately following the title.
4. **DESCRIPTIVE NOTES** Enter the category of document, e.g. technical report, technical note or technical letter. If appropriate, enter the type of document, e.g. interim, progress, summary, annual or final. Give the inclusive dates when a specific reporting period is covered.
5. **AUTHOR(S)** Enter the name(s) of author(s) as shown on or in the document. Enter last name, first name, middle initial. If military, show rank. The name of the principal author is an absolute minimum requirement.
6. **DOCUMENT DATE** Enter the date (month, year) of Establishment approval for publication of the document.
- 7a. **TOTAL NUMBER OF PAGES** The total page count should follow normal pagination procedures, i.e., enter the number of pages containing information.
- 7b. **NUMBER OF REFERENCES** Enter the total number of references cited in the document.
- 8a. **PROJECT OR GRANT NUMBER** If appropriate, enter the applicable research and development project or grant number under which the document was written.
- 8b. **CONTRACT NUMBER** If appropriate, enter the applicable number under which the document was written.
- 9a. **ORIGINATOR'S DOCUMENT NUMBER(S)** Enter the official document number by which the document will be identified and controlled by the originating activity. This number must be unique to this document.
- 9b. **OTHER DOCUMENT NUMBER(S)** If the document has been assigned any other document numbers (either by the originator or by the sponsor), also enter this number(s).
10. **DISTRIBUTION STATEMENT**: Enter any limitations on further dissemination of the document, other than those imposed by security classification, using standard statements such as
 - (1) "Qualified requesters may obtain copies of this document from their defence documentation center."
 - (2) "Announcement and dissemination of this document is not authorized without prior approval from originating activity."
11. **SUPPLEMENTARY NOTES**. Use for additional explanatory notes.
12. **SPONSORING ACTIVITY**. Enter the name of the departmental project office or laboratory sponsoring the research and development. Include address.
13. **ABSTRACT**: Enter an abstract giving a brief and factual summary of the document, even though it may also appear elsewhere in the body of the document itself. It is highly desirable that the abstract of classified documents be unclassified. Each paragraph of the abstract shall end with an indication of the security classification of the information in the paragraph (unless the document itself is unclassified) represented as (TS), (S), (C), (R), or (U).

The length of the abstract should be limited to 20 single-spaced standard typewritten lines, 7½ inches long.
14. **KEY WORDS**: Key words are technically meaningful terms or short phrases that characterize a document and could be helpful in cataloging the document. Key words should be selected so that no security classification is required. Identifiers, such as equipment model designation, trade name, military project code name, geographic location, may be used as key words but will be followed by an indication of technical context.

DATE
ILME